

RAPID ASSESSMENT OF HYDROLOGIC CONTROLS ON MOUNTAIN WATER  
RESOURCES

by

ALICE FRANCES HILL

B.S., Rice University, 2002

M.S., University of Colorado, 2012

A thesis submitted to the  
Faculty of the Graduate School of the  
University of Colorado in partial fulfillment  
of the requirement for the degree of  
Doctor of Philosophy  
Department of Geography  
2017

This dissertation entitled:  
Rapid assessment of hydrologic controls on mountain water resources  
written by Alice Frances Hill  
has been approved for the Department of Geography

---

Dr. Noah Molotch, committee chair

---

Dr. Waleed Abdalati

---

Dr. Richard Armstrong

---

Dr. Fengjing Liu

Date\_\_\_\_\_

The final copy of this thesis has been examined by the signatories, and we find that both the content and the form meet acceptable presentation standards of scholarly work in the above mentioned discipline.

Hill, Alice Frances (Ph.D., Geography)

Rapid assessment of hydrologic controls on mountain water resources

Dissertation directed by Associate Professor Noah P. Molotch

## **ABSTRACT**

The water stored in mountain snowpacks and glaciers provides an important water resource, seeding river systems that serve major populations centers and globally important ecosystems downstream. Mountain river systems are facing potential hydrologic changes imposed from a warming climate and hundreds of recent hydropower development proposals. The melt-dominated hydrologic regimes of mountain river systems are prone to a gradual shift due to change imposed by increasing temperatures as glacier masses decline and snowpack accumulation is altered, whereas dam development in remote mountain basins would impose a more abrupt transformation. Since these river systems play an important role in water supply and provide key ecosystem services, it is important to clarify their governing hydrologic processes.

Despite their high societal value, we know little about many remote mountain rivers and they are notoriously data scarce. To advance our understanding of remote mountain hydrologic processes over regional scales, this research develops a hybrid field-satellite methodology called Rapid Hydro Assessment (RHA) for data scarce mountain regions facing imminent change. This method 1) clarifies the role of climate-sensitive snow and ice source waters to river flow and 2) characterizes regional hydrologic controls within a study timescale of months-to-years, not decades. RHA uses targeted water chemistry and isotope data to elicit hydrologic insights not available from, but complemented by, remote sensing imagery. RHA methodology is initially

informed by headwater scale streamflow separation work at the Niwot Ridge Long Term Ecological Research site in the Colorado Rocky Mountains, and is further developed via two case studies in Kyrgyzstan's Tien Shan mountains and in the Peruvian Andes.

Results of the case studies demonstrate the complex and varied role of meltwater across scales and sites. Meltwater plays a critical role in surface flow and groundwater recharge in arid mountain areas like Colorado and Central Asia where snow makes up the vast majority of inputs. In contrast, in the more hydro-climatically variable Andes and Amazon, melt's role is less directly important to river flow. High storage capacity in alpine wetlands provides a reservoir for wet season rain that appears to source baseflow through the dry season, and Amazon moisture systems deliver lower lying tributaries with major rain inputs. The importance of melt in the Andes is instead indirectly connected to river flow, with the diminishing extent (size) of alpine wetland reservoirs connected to declining melt inputs as tropical glaciers melt out. The case studies demonstrate the ability for the overarching RHA framework to be applied across diverse sites with varying levels of data availability, field access, sampling configurations and mixing model techniques. This work serves as an example of the creative approaches needed to address mountain hydrologic knowledge gaps that will allow us to better anticipate future water vulnerabilities, and to inform holistic, basin-wide development strategies.

## ACKNOWLEDGEMENTS

*“Grad school is a team sport.”*

Sincere thanks go to my supportive and patient committee for helping me in diverse ways throughout this academic journey. I have felt empowered by Richard Armstrong’s consistent and quiet confidence in me, and by his trust in my vision for fieldwork and research with the CHARIS project. Fengjing Liu answered my cold call for hydro-chemistry expertise later in my graduate studies, and I am extremely thankful for his willingness to jump wholeheartedly on board to my committee. I am truly appreciative of Fengjing’s accessibility, constructive suggestions and consistent patience with my mixing model questions. Bob Stallard’s wacky enthusiasm for field work, mapping wild places, and his commitment to the Amazon were critical energy sources for me in the deep depths of writing this dissertation. Bob deserves a gold medal for giving me much of his time and attention throughout my Peruvian Andes field work preparation and data analysis. Waleed Abdalati has shown me the gold standard in humble leadership and effective pedagogy – no doubt interrelated – that I seek to achieve. I thank Waleed for igniting my interest in remote sensing, and for always making time for me no matter how full his schedule. I owe Mark Williams thanks for access to the rich dataset on Niwot Ridge, for connecting me to the CHARIS project, and for teaching me more about myself in graduate school than I ever expected to learn. Finally, immense thanks to Noah Molotch, who selflessly took me on as a student in a time of need and provided me with an academic home, timely motivation, a renewed spark, and critical guidance to make it down the homestretch. I hope some day to juggle as many balls with the grace and patience that Noah does.

I am indebted to the Mountain Hydrology Group as a community of peers and friends, always willing to lend a hand, provide feedback, or spark new ideas. I feel very fortunate to work

with, and be mentored by, the American and Asian scientists that make up the CHARIS team, learning much from them about collaborative cross-disciplinary project work. Thanks to my close friends in my Geography graduate student cohort who confirmed my shift from engineering because I felt I finally found my people. A special thanks to Holly Miller, not only for her stellar lab analyses but also for her friendship, to Katya Hafich and Cholpon Minbaeva for their support in and out of the research world, and of course to Alana Wilson who has been an absolutely invaluable lifeline and partner in crime on this roller coaster ride.

Last but certainly not least, I am swollen with gratitude for the unwavering support and love I have always felt from my parents, sister and especially Christian who was disproportionately the receiving ear of frustrations and challenging moments. Thanks for hanging in there with me. This accomplishment is as much yours as it is mine.

## CONTENTS

### CHAPTER

<b>1. INTRODUCTION</b> .....	1
1.2 Research Objectives and Experimental Design .....	4
1.3 Summary of research motivation and scope .....	9
<b>2. THE FATE OF AN ALPINE SNOWPACK: GEOLOGIC INFLUENCE ON THE TRANSPORT MECHANISMS OF MELT TO STREAMFLOW</b> .....	10
2.1 Introduction.....	11
2.2 Site .....	13
2.3 Methods.....	18
2.3.1 Field Methods .....	18
2.3.2 Laboratory analyses .....	20
2.3.3 Data analyses .....	21
2.4 Results.....	23
2.4.1 Climatology.....	23
2.4.2 Groundwater table height.....	24
2.4.3 Isotopes and chemistry.....	26
2.4.4 End Member Mixing Analysis (EMMA).....	34
2.5 Discussion.....	48
2.5.1 What is geology’s impact on how and when the water stored in seasonal snowpacks is routed downstream from the point of melt on Niwot Ridge? .....	48
2.5.2 How does geology affect streamflow generation mechanisms in the alpine? .	50

2.5.3 Confounding factors.....	51
2.6 Conclusions.....	54
2.7 Appendices.....	55
2.7.1 Appendix 1: Frozen soil dynamics .....	55
<b>3. HYDROLOGIC CONTROLS AND WATER VULNERABILITIES IN THE NARYN RIVER BASIN, KYRGYZSTAN: A SOCIO-HYDRO CASE STUDY OF WATER STRESSORS IN CENTRAL ASIA.....</b>	<b>56</b>
Abstract.....	56
3.1. Introduction.....	57
3.2 Materials and Methods.....	59
3.2.1 Quantifying the hydrologic setting .....	59
3.2.2 Synoptic sample design.....	60
3.2.3 Water sample collection and analysis .....	63
3.2.4 Mixing models and source water separations .....	64
3.3. Results.....	66
3.3.1. Hydrologic setting.....	66
3.3.2. Hydro chemistry elevation gradient.....	68
3.3.3 EMMA diagnostics and mixing model results.....	71
3.4. Discussion .....	81
3.4.1 Use of EMMA over regional scales.....	81
3.4.2 Hydrologic controls on river flow.....	82
3.5 Conclusion .....	83



#### 4. CLARIFYING REGIONAL HYDROLOGIC CONTROLS OF THE MARAÑÓN RIVER, PERU THROUGH RAPID ASSESSMENT TO INFORM SYSTEM-WIDE BASIN

PLANNING APPROACHES .....	85
4.1 Introduction.....	86
4.2 Study site.....	90
4.3 Methods.....	95
4.3.1 Sample design .....	95
4.3.2 Field sampling.....	96
4.3.3 Laboratory analysis.....	97
4.3.4 Two-end-member mixing models.....	98
4.3.5 Discharge data.....	101
4.3.6 Precipitation .....	102
4.3.7 Meltwaters.....	103
4.4 Results.....	104
4.4.1 Hydro-climatology.....	104
4.4.2 Isotopes .....	109
4.4.3 Hydrochemistry.....	114
4.4.4 Principal component analysis (PCA).....	115
4.4.5 Tributary volumes.....	117
4.4.6 Errors due to low sample density over a large domain.....	124
4.5 Discussion.....	126
4.5.1 Hydrologic controls on discharge .....	126
4.5.2 Discharge sensitivity to climate.....	128

4.6 Conclusions.....	131
4.7 Acknowledgments.....	133
4.8 Appendices.....	134
4.8.1 Appendix 4.1: Geologic map of the Marañón basin.....	134
4.8.2 Appendix 4.2: Piper diagram for all water samples.....	135
4.8.3 Appendix 4.3: Sampled sub-basin attributes .....	136
4.8.4 Appendix 4.4: Water sample data and mixing model components .....	138
4.8.5 Appendix 4.5: Laboratory equipment specifications .....	140
<b>5. FINAL THOUGHTS .....</b>	<b>141</b>
5.1 Synthesis of Results .....	141
5.2 Implications for future research .....	142
<b>REFERENCES .....</b>	<b>144</b>

**TABLES**

Table 1.1: Research design and progression of case studies .....	6
Table 2.1: Instruments and methods used for laboratory analysis.....	20
Table 2.2: Euclidean distances for all possible end members in the Saddle.....	39
Table 2.3: Euclidean distances for all possible end members in the Martinelli .....	39
Table 2.4: Summary of end member selection criteria and evaluation metrics.....	40
Table 2.5: Relative end member contributions to streamflow.....	41
Table 2.6: Summary of overall proportions of sources to annual river flow .....	46
Table 3.1: Methodology and rationale for end member selection. ....	75
Table 3.2: Summary of concentration reconstructions for model validation.....	78
Table 4. 1: Error-weighted mean mixing model results .....	120
Table 4. 2: Evaluating the impact of uncertainty on mixing fraction .....	122
Table 4. 3: Sampled sub-basin topographic, climatic and geologic attributes.....	136
Table 4. 4: Water chemistry and isotopic data, and mixing model components .....	138
Table 4. 5: Laboratory analysis instruments and specifications. ....	140

## FIGURES

Figure 2.1: Saddle-Martinelli site location .....	15
Figure 2.2: Subsurface geology characterization.....	16
Figure 2.3: Climatology on Niwot Ridge .....	24
Figure 2.4: Groundwater fluctuations in the Saddle and Martinelli basins .....	25
Figure 2.5: Isotopic value boxplots for all sampled waters .....	26
Figure 2.6: Ion and isotope pulse observed in multi-year groundwater patterns.....	27
Figure 2.7: Isotope variations in groundwater in 2010 .....	29
Figure 2.8: Ion concentration boxplots for all sampled waters.....	31
Figure 2.9: Ion variations in groundwater in 2010. ....	33
Figure 2.10: EMMA diagnostics for conservative tracer selection .....	35
Figure 2.11: Bi-plots of tracers using principal components.....	37
Figure 2.12: EMMA U-space diagrams.....	38
Figure 2.13: Concentration reconstructions for conservative tracers driving EMMA ....	43
Figure 2.14: Euclidean “S” distances for all groundwater samples.....	45
Figure 2.15: Hydrograph separations.....	47
Figure 2.16: Thermal-infrared drone imagery of the Saddle basin as a hydrologic tool ..	53
Figure 2.17: Soil and air temperature data on Niwot Ridge .....	55
Figure 3.1: Naryn basin site location and sampling sites.....	62
Figure 3.2: Naryn River hydrographs at the three gauge locations .....	67
Figure 3.3: MODIS derived snow cover probability across the Naryn basin.....	68

Figure 3.4: Hydro-chemical trends over the study domain elevation gradient.....	70
Figure 3.5: EMMA diagrams including mainstem Naryn River and tributary samples..	73
Figure 3.6: Source water separation results .....	77
Figure 3.7: Concentration reconstructions of modeled results vs. observed values. ....	80
Figure 4. 1: The Marañón River study site .....	91
Figure 4. 2: Study domain zonal designation and river sampling elevation transect.. ....	92
Figure 4. 3: Water sampling configuration utilized for mixing analysis .....	96
Figure 4. 4: Precipitation patterns across the Marañón basin .....	105
Figure 4. 5: Marañón River gage locations and discharge records.....	106
Figure 4. 6: Cryospheric inputs to the Marañón basin.....	108
Figure 4. 7: Stable isotope and deuterium excess progression .....	110
Figure 4. 8: $\delta\text{O}^{18}$ - $\delta\text{D}$ relationship of Marañón surface waters.....	113
Figure 4. 9: Variation of ion concentrations in tributaries and the mainstem.....	115
Figure 4. 10: Principal component analysis of hydrochemistry data across zones.....	117
Figure 4. 11: Mixing model results for tributary discharge contributions.....	119
Figure 4. 12: Error analysis of mixing model results.....	123
Figure 4. 13: Geologic map of the Marañón basin. ....	134
Figure 4. 14: Piper diagram of constituents of Marañón waters.....	135

## CHAPTER 1

### 1: INTRODUCTION

The water stored in mountain snowpacks and glaciers provides an important water resource, sourcing river systems that serve major populations centers and globally important ecosystems downstream. These river systems provide key ecosystem services and play an important role in water supply, storing winter precipitation and slowly releasing it to downstream populations through summer months. Mountain river systems are facing potential hydrologic change imposed from a warming climate and hundreds of recent hydropower development proposals.

In the context of a changing climate – and especially in relation to warming temperatures – much concern has been raised regarding the future and fate of mountain water resources because snow and ice are especially sensitive to temperature. Temperature affects not only the volume of frozen water storage (precipitation that falls as rain versus snow) (Knowles et al., 2006) but also its delivery of water downstream by changing when and how fast it arrives (Musselman et al., 2017). Embedded in these effects are secondary impacts to meltwater volume available for human consumption as historical eco-hydrologic regimes respond to changes in the availability of melt (e.g., Barnhart et al., 2016; Goulden & Bales, 2014).

Increasing water demands from growing desert cities of the Western US, together with prolonged drought periods (Cayan et al., 2010) including multi-year historically low snowpacks

in the Sierras (Griffin & Anchukaitis, 2014) emphasize the fragility of water resources in the American west, and the heavy reliance on snow to meet water needs. Many downstream areas also rely on rivers sourced by mountain glaciers. Since glacier mass balances are declining across all continents on the globe (IPCC, 2007), we need to identify and anticipate changes to global mountain water resources in a warming climate, and to better understand the role of meltwater in international water supplies.

Aside from climate, new river development projects may also impose major hydrologic change in mountain areas. In recent decades resource development like hydropower and mining projects are looking to remote, mountain river systems for new development sites. Historically remote basins have presented challenges with access and energy transmission, but remote mountain areas are pursued today given limited viable alternative sites and persistent energy and mineral demands. Hydropower and riverside mining can impose major hydrologic change to mountain river systems. Dams truncate the river continuum (Vannote et al., 1980) that is critical for biodiversity, sediment transport and erosion control. Integrated basin planning that aims to mitigate the abrupt impacts from hundreds of newly proposed dams holds promise as a smarter approach to hydropower development, but it requires basic environmental knowledge of subject basins that are relatively unstudied (Winemiller et al., 2016). Mountain streamflow dictates sediment, biologic and social patterns within the river corridor, so clarifying governing mountain hydrological processes in these basins is an obvious priority.

Central challenges to characterizing mountain hydrologic processes include accounting for high heterogeneity in mountain environments, from the headwater to the cordillera scale. Mountains are constantly changing in time and space: physically (topography, aspect, steepness, geology, vegetation), climatically (precipitation, temperature, humidity, snowpack depth and

density, energy fluxes, wind), and socially (land use, water withdrawals and returns, access and infrastructure, reservoir storage, hydropower needs). Few people live in headwater catchments, creating little water demand at that scale and necessitating the focus towards larger basins.

Agriculture and larger population centers occupy the lower lying areas of regional river domains, imposing a greater need for knowledge about hydrologic processes, and thus water vulnerability, at these elevations. Understanding the various sources to river flow is a useful first step in water vulnerability assessments because the potential for changing water inputs varies across sources.

Streamflow partitioning, the separation of river flow into its various source waters, has been studied at the headwater scale (Racoviteanu et al., 2013; Wilson et al., 2016), and these studies show flow composition to change rapidly with distance downstream even at high elevations. These spatial changes to streamflow composition suggest a clear need to improve river flow partitioning knowledge further downstream, where water requirements are much greater.

Exacerbating the challenges of heterogeneity and scale is data scarcity. Historically, field datasets relevant to snowpacks, glaciers and rivers were relied on to intuit mountain hydrologic processes, but the sparse spatial and temporal data network is largely unable to accommodate representativeness of the continuously changing mountain environment. Field measurement records in mountain headwaters are also limited due to difficult access and work conditions in places prone to high winds and hostile weather. Rapidly evolving satellite data products provide more accurate and higher resolution data over regional scales, allowing us profoundly improved data sets to tackle water resource questions across entire cordilleras. Having said that, remote sensing data has its own shortfalls and is not entirely sufficient for hydrologic study: ground surfaces are obscured by clouds common to mountain regions, signal saturation in snowpacks



and forests prevents information acquisition in some areas, mixed pixel problems yield uncertainty in land cover designation, to name a few. Also, subsurface information such as groundwater movement or geologic boundaries cannot be well-tracked at the basin scale because spectral satellite data only provides information at the earth's surface. *In situ* measurements complement satellite datasets because they identify issues not apparent from satellites and they ground-truth satellite information to improve interpretation and accuracy. So, the combination of remotely sensed data and targeted field measurements provide a way forward for clarifying mountain hydrology over regional scales.

The need for developing robust methods for regional field-satellite hydrologic studies is clear and urgent. Impending water stress from cryospheric (snow and ice) hydrologic shifts due to a changing climate are producing heightened international tension on trans-boundary rivers (Groll et al., 2015; The Economist, 2014). Impacts from major hydropower development in ecologically and socially important basins may be mitigated with thoughtful basin-wide planning informed by governing environmental processes (Winemiller et al., 2016). Little-to-no existing environmental data records in remote mountain river basins subject to these concerns and the short timescale upon which hydrologic controls need to be clarified calls for creative and new hydrologic methods.

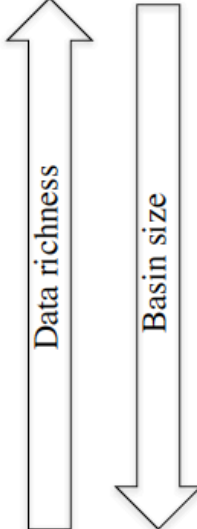
## **1.2 Research Objectives and Experimental Design**

In this dissertation, my goal is to respond to the need for large scale hydrologic characterization of poorly studied mountain basins. I develop a hybrid field-satellite methodology called Rapid Hydro Assessment (RHA) for data scarce mountain regions facing imminent change. This method will 1) clarify the role of climate-sensitive snow and ice source

waters to river flow and 2) characterize regional hydrologic controls within a study timescale of months-to-years, not decades. I aim to identify novel ways to use targeted water chemistry and isotope data to elicit hydrologic insights not available from, but complemented by, remote sensing imagery that allows for better understanding of these poorly-studied water systems. To achieve this, the research objectives shown in Table 1.1 were explored, and each is the subject of its own main body chapter.

**Table 1.1:** Research design via a progression of objectives and case studies en route to RHA development.

Research Objective	Case study	Data resolution	River reach length
Objective 1: How does geology affect the transport of meltwater downstream, and how does it impact local streamflow generation mechanisms? Lessons learned used to develop RHA.	Niwot Ridge sub-basins	Rich	< 1km
Objective 2: Can traditional hydrologic mixing models be adapted to identify streamflow composition changes through space? What role does melt play in regional groundwater recharge and surface flow over a 4,000m gradient in Central Asia's Tien Shan Mountains? RHA application of end member mixing model methods to identify spatial variation in streamflow partitioning.	Naryn River, Kyrgyzstan	Limited	440km
Objective 3: Can surface water hydrochemistry datasets alone be used to infer meltwater influence and hydrologic controls of a remote mountain hydrologic system in the Andean Marañón River? RHA application using Lagrangian surface water sample set to identify governing processes.	Maranon River, Peru	Scarce	620km



*Research objective #1: How does geology affect the transport of meltwater downstream, and how does it impact local streamflow generation mechanisms?*

While it is clear that geology has a strong control on meltwater flowpaths and streamflow generation, relatively little is known about the intricacies of this process because it transpires underground. The physical path that meltwater takes en route to downstream users is important because it impacts groundwater reservoir recharge, responsiveness of streamflow to melt onset, and the delay in meltwater accessibility due to longer residence times.

In a heavily instrumented and monitored headwater site on Niwot Ridge in the Rocky Mountains of Colorado, this research objective aims to use an extensive isotope and hydro-chemical time series to interpret the influences of geology on the pathways of meltwater as it

moves downstream, as well as its impact on streamflow generation sources throughout an average water year.

Key results from this long term, data-rich headwater study guides RHA method development.

We found:

- 1) Streamflow generation at the headwater scale is mostly a mixture of lateral subsurface interflow and overland melt run-off, emphasizing the need to sample the interflow end member. The relative proportions of these sources to alpine streamflow are a function of the depth of colluvium overlying bedrock.
- 2) This study provides insight into the variables and samples giving the most explanatory information to teasing out alpine and melt hydrologic process. This is a critical lesson for honing sample design to only the most essential locations over larger scales and condensed timeframes.
- 3) Fracture flow through bedrock is not relevant to streamflow generation at the headwater spatial scale on Niwot Ridge. This prompted questions about capturing information about non-local melt transport (deep flowpaths) in mountain bedrock environments over larger scales.

*Research objective #2, case study 1: Can traditional hydrologic mixing models be adapted to identify streamflow composition changes through space? What role does melt play in regional groundwater recharge and surface flow over a 4,000m gradient in Central Asia's Tien Shan Mountains?*

Research objective 1 evaluates the influence of meltwater to an alpine stream at a single point throughout a water year. In objective 2, we investigate the ability to adapt this approach

and apply a similar hydrochemistry-based mixing model method over a 440km spatial domain to determine the importance of meltwater to Naryn River discharge. This research objective aims to evaluate the sufficiency of minimal field sample numbers for addressing the role of snow and ice in river discharge over regional scales. In this study we also assess the feasibility of modifying traditional end member mixing models to accommodate classifications of continuously changing end members over the study domain. The robustness of EMMA applications across a wide spectrum of hydrologic regimes within the basin is also evaluated.

*Research objective 3, case study 2: Can surface water hydrochemistry datasets alone be used to infer meltwater influence and hydrologic controls of a remote mountain hydrologic system in the Andean Marañón River?*

In truly austere mountain environments, access to desired sampling sites and end members is not always achievable. Research objective 3 tests the ability to tease out meltwater influence and basic hydrologic understanding in basins without access to end member samples, or where sampling timeframes and/or access prescribes only a limited surface water sampling campaign. The case study spans 620km of Peru's mostly inaccessible Marañón River, headwater stem to the Amazon. It moves one-step further from data richness than in research objective 2 and tests the thresholds of targeted but minimal field sampling aspects of RHA.

Research objective 3 is an important aspect of the RHA methodology because of the realities of field work limitations, and the need for adaptability to accommodate limited access to data within the expedited study timeframe imposed by development proposals.

### **1.3 Summary of research motivation and scope**

Climate change (specifically its impact on melt waters) and other means of disturbance can impose hydrologic change in mountain basins. Our ability to anticipate water supply changes or inform water resource development projects requires an understanding of hydrologic controls over regional scales. This knowledge is more critical in poorly studied areas with few data records, as these areas are increasingly subject to development and/or have little water supply infrastructure in place to buffer hydrologic shifts.

This dissertation research develops and tests new methods for quickly gaining first order understanding of major river system controls fed by climate sensitive snowpack and glacier waters. I utilize remote sensing products combined with hydrochemistry and isotope tracer datasets to identify the stream discharge sources and meltwater influence in basins over varying scales and data richness. Three study basins are subject to this research: Niwot Ridge, Colorado; Naryn River basin, Kyrgyzstan; Marañón River basin, Peru.

The results of this work not only shed light on the hydrology of the subject basins, but more significantly it provides a contribution to the hydrology field by offering a tool for efficient characterization of globally important but unstudied basins. In these places the stakes are high when it comes to water resources. Through the research process I also hope to reiterate the value of field measurements and human observation, even amidst the power of satellite perspectives.

## CHAPTER 2

### **2: THE FATE OF AN ALPINE SNOWPACK: GEOLOGIC INFLUENCE ON THE TRANSPORT MECHANISMS OF MELT TO STREAMFLOW**

#### **Abstract**

Snow is the principal water input into the alpine regions of Colorado's Rocky Mountains. Shifts in climate are changing the mountain energy balance which in turn affects snow accumulation and melt patterns, and thus the hydrographs of melt-sourced waterways downstream. While climate principally impacts the timing and amount of meltwater, the underlying geology of alpine snowfields has the potential to affect the downstream hydrograph response because it largely dictates the flowpaths from point of melt to stream channel. Mountain geology is a constantly changing condition, made even more difficult to characterize because it lies subsurface and so is challenging to differentiate from one hillslope to the next. Our ability to predict subsurface flow paths is not only limited by difficulty in identifying changing geologies, but also by not having a firm grasp on *how* geology controls when and where water moves downslope.

This research utilizes two adjacent but contrasting headwater geologic environments, a colluvial and bedrock aquifer, at the Long Term Ecological Research Site on Niwot Ridge, Colorado Rocky Mountains to identify how geology controls flowpaths from meltwater to streamflow. We use hydrochemical and isotope tracers found in groundwater, snowpack,

meltwater and rain, together with a groundwater table depth record and mixing model methods, to calculate stream flow separations over an average water year.

We find that streamflow generation at the headwater scale is mostly a mixture of lateral subsurface interflow and overland melt run-off, and that the relative proportions of these sources to alpine streamflow are a function of the depth of colluvium overlying bedrock. Fracture flow through bedrock is not relevant to streamflow generation at the headwater spatial scale on Niwot Ridge but may transport meltwater further afield through deep flowpaths in mountain bedrock environments. Utilizing a multi-year data record, this work raises questions about the size of alpine groundwater reservoirs, and the time buffer they may provide for maintaining streamflow in the case of multi-year drought periods.

## **2.1 Introduction**

Mountains are natural "water towers" because they provide a disproportionate amount of essential water resources as well as a steep hydraulic gradient to lower-lying valleys and plains (Viviroli et al., 2003). Their snow packs and alpine aquifers provide natural water reservoirs to downstream populations and agriculture, providing water to low elevations during drier seasons. When and how much snow water is available has implications for downstream flood prediction, water resource planning, temperature and chemical considerations for surface water (Taylor et al., 2001). Regional groundwater systems, particularly in the western U.S., also rely on melt inputs (eg, *Clow et al.*, 2003; *Liu et al.*, 2004). Climate forecasts suggest an increase in temperature as well as a change to the amount and nature of hydrologic inputs in alpine areas (Barnett et al., 2005; Hamlet et al., 2005; N. Knowles et al., 2006; Mote, 2003; Mote et al., 2005; Regonda et al., 2005), with changes to snowpack accumulation not only affecting the amount of



water available but also how fast and when it melts (Musselman et al., 2017). The uncertainty involved in all of these climate-related factors embeds additional complexity to clarifying poorly understood hydrologic processes that dictate the behavior of groundwater-surface water systems in mountain regions.

The route that water takes from point of melt to end user depends on both the climate and hydrogeology of the basin. *Safeeq et al.*, [2013] suggest that geologic differences in aquifer systems are as important to climate change induced streamflow vulnerabilities as differences between rain and snow dominated catchments. Geo-climatic frameworks to address mountain water resource issues are needed (Tague & Grant, 2009) and a central challenge to this task is forecasting water movement from snowpacks to lower lying areas. We lack a holistic understanding of the water balance in alpine regions over large scales in part because a) several black box processes including groundwater flow and sublimation losses likely play a large role in hydrologic partitioning of snow water and b) snow-driven groundwater flow paths and recharge rates are poorly understood due to mountains' high spatial heterogeneity of snowpacks, topography, and geology (Blasch & Bryson, 2007).

Clarification of mountain hydrologic processes and meltwater flow pathways is crucial for evaluating the vulnerability of surface and groundwater systems to climate change (Uhlenbrook et al., 2002). Intensive field-based and modeling studies are needed to evaluate the impact of geologic factors on snowmelt-groundwater-surface water interactions. Such studies may be lacking due to logistical difficulty of conducting field work and installing groundwater monitoring sites in often inaccessible and remote alpine areas. The Niwot Ridge Long Term Ecological Research (LTER) site in the Rocky Mountain foothills outside Boulder, Colorado, is

one of few global research programs and data sets that affords high temporal and spatial monitoring of groundwater, surface water and snowmelt in a true alpine environment.

The objective of this study is to differentiate how contrasting geologies affect the transport of snow melt downstream as well as how subsurface variation impacts the groundwater response to snowmelt, and we do this by comparing two adjacent but distinct aquifer geologies on Niwot Ridge. Specifically, we ask: How do differences in catchment geology affect how and when snowmelt is routed from hillslopes to streams? To address this question we investigate the chemical and isotopic composition of groundwater and surface water, water table height and stream flow over the 2008 to 2012 water years on Niwot Ridge, Colorado. We utilize 14 alpine piezometers (groundwater monitoring wells) and an exhaustive source water sampling suite to identify snowmelt partitioning and melt water flow paths based on geochemical and isotopic tracers. Field data is further utilized in established mixing model methods (End Member Mixing Analysis (EMMA) (Christophersen et al., 1990; Hooper et al., 1990; Hooper, 2003a)) to clarify meltwater-groundwater-surface water interactions over a spectrum of high-to-low water years.

## **2.2 Site**

This study was conducted on Niwot Ridge, Colorado within the Saddle and Martinelli catchments. These two adjacent catchments have similar climate but have contrasting geologies (Figure 2.1). I adopt the geologic characterization of King (2012) which utilizes the drilling logs from the piezometer installation in 2008, geophysical studies conducted on Niwot Ridge, and historical mapping studies (Figure 2.2).

The Saddle catchment is considered a bedrock aquifer because it has only a thin (~1-2m) layer of material overlying the basement rock so most of the aquifer capacity is hypothesized to

be stored in bedrock fractures. Water flow through bedrock aquifers is dominated by fracture networks that act as preferential flowpaths for infiltrating waters. Colluvial aquifers such as the Martinelli are made up of porous, unconsolidated material often deposited in gullies or at the base of hillslopes due to slope creep and water driven mass wasting. Colluvial aquifers are generally assumed to be porous mediums that transport water via traditional Darcy flow. While the Martinelli catchment is also underlain by bedrock at depth, the overlying colluvium is of significantly thicker than in the Saddle (variable, but up to 5-8m in some areas) and is anticipated to serve as the major water storage mechanism in this catchment.

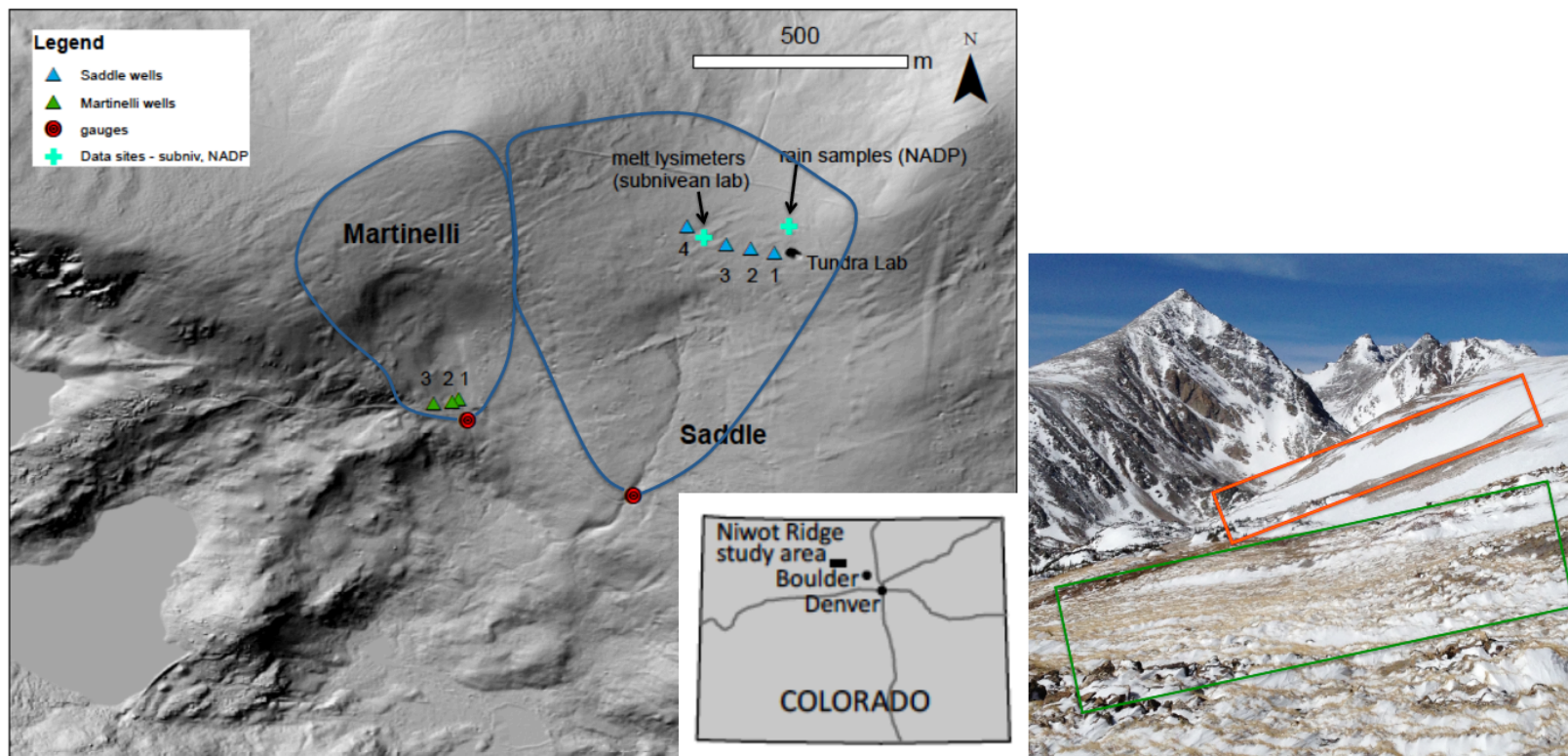


**Figure 2.1:** Left: Saddle-Martinelli site displayed on LTER 2m digital surface model imagery, including sampling site locations for end members and surface water (both stream samples and discharge measurements taken at gauge locations). The numbered groundwater well markers indicate the location of the piezometer pair (one shallow, one deep). Inset indicates Niwot Ridge LTER site in Colorado. Right: The adjacent Saddle (green box in photo) and Martinelli (red box in photo) basins lie on the south facing slopes of Niwot Ridge.

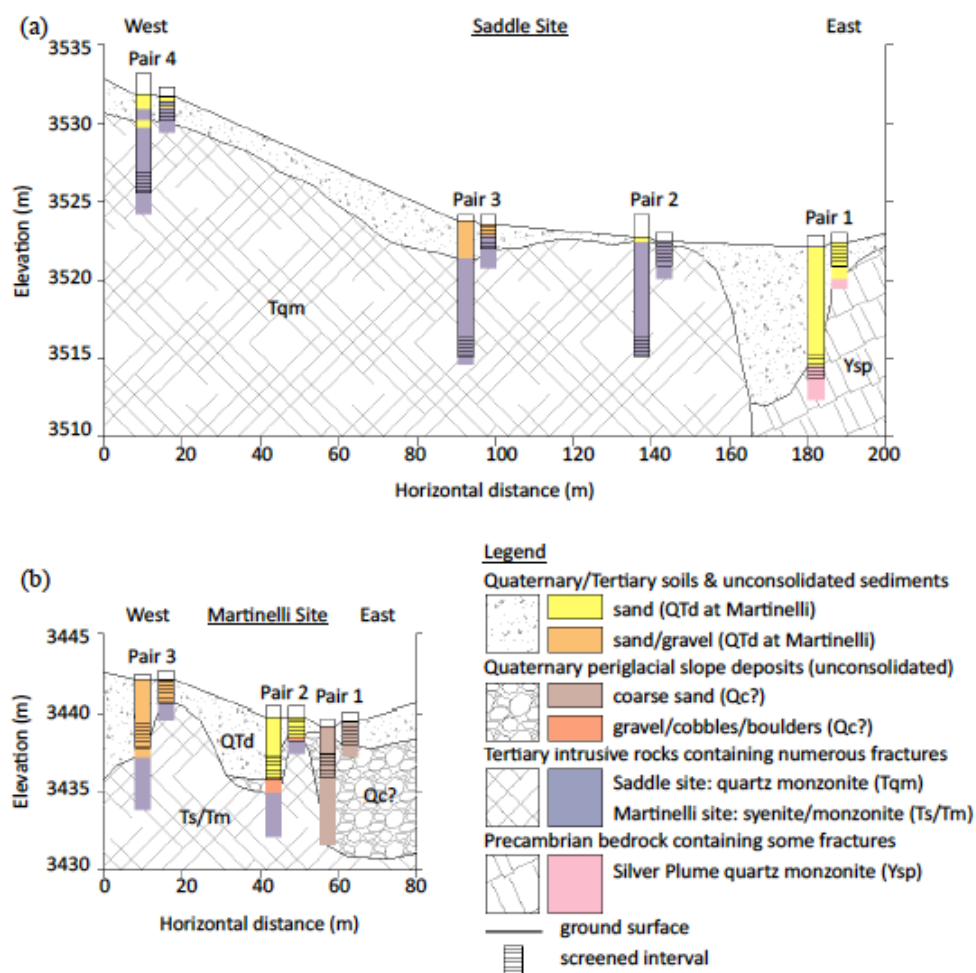


**Figure 2.2:** Subsurface geology characterization for the Saddle (a) and Martinelli (b) is based predominantly on reconstructing the core material excavated during the installation of groundwater monitoring piezometers in 2008. Credit: Jessica King.

The 0.24km<sup>2</sup> Saddle catchment spans from the crest of Niwot Ridge downslope to the southwest. The catchment has a 166° southerly aspect and ranges in steepness from 0.1° to 30.4° with a mean slope of 10° (Hanmann, 2002). The upper catchment has vegetation characteristic of alpine tundra such as communities of gramminoids and forbs, and little exposed bedrock. The

hydro-geologic setting of the Saddle is generally characterized by shallow unconsolidated surficial materials predominantly composed of sand and gravel. Underlying bedrock units are known to contain extensive fracture networks (Leopold et al., 2008; Pearson & Johnson, 1980) although fractures have not been mapped. Groundwater sampling sites within the basin are located at 3528m ASL. Snow accumulation in the Saddle is variable in part due to the strong west-northwesterly winds at the Saddle that aid in sublimation and re-distribution of snow from the north and east portions of the catchment to the south and west. Maximum snow depth is on the order of 4m in the western part of the basin. A 1.7 km intermittent stream flows from the beginning of snowmelt through early fall with a 2008-2012 average annual discharge of 53,062  $\text{m}^3\text{yr}^{-1}$ .

The 162° south-facing Martinelli catchment is smaller (0.14 $\text{km}^2$ ) and steeper than Saddle with an average slope of 20.5°, ranging from 4.5-39.2° (Hanmann, 2002). Martinelli is geologically dominated by unconsolidated material and 2-3m of diamicton (Leopold et al., 2008) composed of coarse sand, gravel, cobble and possible boulders underlain by crystalline bedrock. Due to deposition of wind-transported snow a semi-permanent snow field covers 45% of the basin in most years under which a 10-20cm basal ice layer has been known to form at the snow-soil interface (Caine, 1989). Groundwater monitoring sites are located at 3425m ASL in the Martinelli catchment. Overland flow and artesian conditions in piezometers is common during snowmelt. A 0.35 km length ephemeral stream drains the snow field to the basin outlet with an average annual flow of 79,477  $\text{m}^3\text{yr}^{-1}$  over 2008-2012. Climate data is not specifically recorded at the Martinelli site, however its proximity to the Saddle site suggests the Saddle climate data (temperature, precipitation) is also applicable to Martinelli. Wind conditions are often different at Martinelli than at the Saddle because Martinelli lies in the lee of the east knoll and is

considerably more protected.

Both basins are located above treeline within the Niwot Ridge Long Term Ecological Research (LTER) network site 35 kilometers outside of Boulder, Colorado in the front range of the Rocky Mountains (40°03'N, 105°35'W). Niwot Ridge is an alpine tundra ecosystem extending eastward from the Continental Divide with treeline at approximately 3400m ASL. It is generally characterized by high temperature and precipitation gradients, low annual temperatures, and high solar radiation. Strong winds from the west contribute to significant snow redistribution and water losses to sublimation on Niwot Ridge. Calculated losses range from 15% at the Saddle (Hood et al., 1999), one-third at the 3740m elevation D-1 site on Niwot Ridge (Greenland, 1989), and up to 72% of winter precipitation is lost to the atmosphere within 10 km downwind from the site (Knowles et al., 2012).

## **2.3 Methods**

### **2.3.1 Field Methods**

#### ***2.3.1.1 Groundwater***

Seven pairs of piezometers (groundwater monitoring wells) were installed in 2008. This monitoring network includes 4 pairs of wells in Saddle and 3 wells in Martinelli, with each pair including a deep and shallow well. The deep well depths range from 6.3-8.4m in Saddle to 3.3-4.3m in Martinelli. Wells are aligned east to west approximately perpendicular to the streams draining each basin (Figure 2.1) and were used for groundwater sampling. Extensive field sampling and monitoring was conducted year round from 2008-2012 except when excessive snow accumulation (i.e. > 4m) prohibited sampling due to inaccessibility of the piezometers.

Depth-to-water table (DTW) was monitored by hand concurrently with weekly hydrochemical sample collection using a weighted tape measure. Pressure transducers (In-Situ Inc. Level Troll 100, non-vented) were installed in SD3 & SD4 in January 2010 and collected groundwater data twice daily. Groundwater samples were collected for chemical and isotopic content using a PVC bailer and latex/nitrile gloves to prevent contamination.

### ***2.3.1.2 Surface Water***

Weekly to daily surface water grab samples were collected at the gauging locations on the Martinelli and Saddle streams (Figure 2.1). Sampling at the Saddle headwater site occurred during snow-free months and during the snowmelt season when stream channel access was achievable via digging through the snowpack. For both ground and surface water, sample bottles were soaked overnight then rinsed five times with de-ionized water. At the study site bottles were rinsed three times with the subject water before collecting triplicates of water samples. Bottles were kept cool and stored at 4 °C before being transported to the laboratory for analysis.

### ***2.3.1.3 Precipitation***

Weekly precipitation samples were acquired at the Saddle National Atmospheric Deposition Program site (NADP, site CO02, Figure 2.1) within a wet precipitation collector as well as at a co-located Belfort (5-780) precipitation gauge. Winter precipitation was adjusted for 61% over catch resulting from wind redistribution of snow [Williams *et al.*, 1998].

### ***2.3.1.4 Snow***

Snowpack physical and chemical properties were measured weekly at the Saddle site adjacent to the subnivean laboratory (Figure 2.1) using standard snow pit protocols (Williams *et al.*, 1999). Snow samples were stored frozen at -20 °C for 1-2 months prior to analysis and then



melted in sealed containers at room temperature. Twenty meters from the snowpit location, 1m<sup>2</sup> snowmelt lysimeters funneled snowmelt to the subnivien laboratory for meltwater grab sampling on a daily to weekly basis following protocols described in *Williams et al.* [1996b].

### 2.3.1.5 Soil Water

Soil water was collected monthly to bi-monthly in zero-tension (ZT) soil lysimeters at both the Saddle and Martinelli catchments (Figure 2.1). When single lysimeter water yields were too small for laboratory analysis, lysimeter samples were bulked.

### 2.3.2 Laboratory analyses

All water samples (groundwater, surface water, snow, snow melt, soil water) were analyzed at the Niwot LTER wet chemistry laboratory, the Kiowa Lab, in Boulder, Colorado. Analytes include pH, acid neutralizing capacity (ANC), conductance, major ions, dissolved silica, dissolved organic matter,  $\delta^{18}\text{O}$  and  $\delta\text{D}$ . Samples were filtered through pre-rinsed 47-mm Gelman A/E glass fiber filters with an approximate 1- $\mu\text{m}$  pore size. Instruments and methods for the analytes are shown in Table 2.1. Analytical precision for all solutes is less than 2%.

Table 2.1: Instruments and methods used for laboratory analysis of all water samples.

Analyte	Instrument	Method Detection Limits (MDL)
cations ( $\text{Ca}^{2+}$ , $\text{Mg}^{2+}$ , $\text{Na}^+$ , $\text{K}^+$ )	Perkin Elmer AAnalyst 200	0.09-0.49 $\mu\text{eq L}^{-1}$
anions ( $\text{Cl}^-$ , $\text{NO}_3^-$ , $\text{SO}_4^{2-}$ )	Metrohm 930 Compact IC	0.02 – 0.17 $\mu\text{eq L}^{-1}$
Si	Lachat QC 8500 FIA	0.2 $\mu\text{eq L}^{-1}$
ANC	Gran Titration	n/a
Stable isotopes	Picarro L1102-I	n/a

Stable water isotopes are reported as a  $\delta$  (per mil) ratio of the sample to Vienna Standard Mean Ocean Water (VSMOW), calculated as:

$$\delta^{18}\text{O}, \delta\text{D} = \left[ \left( \frac{R_{\text{sample}}}{R_{\text{VSMOW}}} \right) - 1 \right] * 10^3 \quad (1)$$

where R is the ratio of  $^{18}\text{O}/^{16}\text{O}$  or  $^2\text{H}/^1\text{H}$ . Precision on stable isotope measurements was 0.020 1- $\sigma$  for  $\delta^{18}\text{O}$  and 0.158 1- $\sigma$  for  $\delta\text{D}$  based on replicate samples, where  $\sigma$  is the standard deviation of the replicates.

### **2.3.3 Data analyses**

#### ***2.3.3.1 Isotopic and chemical tracers***

Temporal and spatial trends of isotopes and ions in groundwater and surface water were evaluated to aid in parsing out sources and flow paths of water inputs to the study basins. Stable isotopes are well recognized as being naturally occurring conservative tracers useful for determining source waters. Groundwater recharge periods that change seasonally can be defined by changes in groundwater isotopic signatures in relation to new water events (Abbott et al., 2000; Maule et al., 1994; O'Driscoll et al., 2005). Ion concentrations are traditionally considered products of water-rock interaction (Mast et al., 1990) thereby providing information on subsurface residence times and flow paths.

#### ***2.3.3.2 Hydrograph separation***

Hydrograph separation was calculated using Principal Component Analysis (PCA) and End Member Mixing Analysis (EMMA) (Christophersen et al., 1990; Christophersen & Hooper, 1992; Hooper, 2003b; Hooper et al., 1990). The methods of EMMA are well established and have been used to identify end-members of alpine surface water hydrochemistry by many researchers (e.g., Burns et al., 2001; Frisbee et al., 2011) including work in the adjacent Green Lakes Valley and its sub-catchments (Liu et al., 2004; Williams et al., 2006, 2007).

Tracer and end member selection follows Hooper (2003). Tracers utilized in EMMA must not violate the assumptions of standard mixing models, that is to say tracers must be conservative (not vanish into the environment via some other process). Conservative behavior is

identified by randomness among residuals (de-standardized projected concentration minus observed concentration) when plotted against the observed concentration. Correlation among residuals suggests the tracer is non-conservative, but there is no strict or prescribed  $R^2$  threshold for determining randomness, and thus conservativeness. I selected  $R^2 > 0.5$  as the threshold. Tracer selection is also aided by calculating residual root mean square error (RRMSE), whereby low RRMSE indicates a better tracer fit to the n-dimensional space. In 2-dimensions, selection of tracers should minimize the change in RRMSE between 1-D and 2-D.

End member selection is generally determined via two metrics:

1) visual geometric inspection of U-space plots whereby stream samples and end member median concentrations are projected into a transformed space dictated by principal components. In the case of a 2-dimensional projection (3 end members), the geometry of the U-space plot will ideally allow for 3 end members to form a triangle that encapsulates all stream samples.

2) Calculated Euclidean distances that describe the extent of transformation from actual-to-projected space as a percent of original observed value. Lower Euclidean distances suggest more appropriate end member selection insofar as their re-projection is more actually represented by the 2-D U-space plot. End member selection is a somewhat subjective process using these metrics and they need to be balanced to find the most suitable solution.

Further, end member selection may be iteratively refined using sample concentration reconstructions that provide feedback on model performance. Poorly performing models suggest that either tracer or end member selection has gone awry, and these steps should be re-evaluated.

## 2.4 Results

### 2.4.1 Climatology

Long term climate data has been recorded continuously at the Saddle site since 1981 [eg, *Humphries et al.*, 2008]. The study period affords the ability to compare hydrologic behaviors across average annual cumulative precipitation water years (October 1-September 30) in 2008-2010 with a record wet (2011) and record dry (2012) year over the period of record (Figure 2.3). 2011 had a total precipitation of 3.317m and 1.697m of SWE which is greater than the 2008-2012 average (0.8871m) by nearly a factor of two. In 2012 Niwot Ridge experienced a record low snow year with peak SWE less than a quarter of the previous year's at 0.4088m. Despite a wet summer in 2012, total cumulative precipitation over the study period was lowest in 2012 at 1.789m. An unusually early melt onset occurred on March 2 in 2012 while 2011 experienced an especially late melt onset on June 7. In average years such as 2008-2010, melt began between April 28 and May 27. Mean daily temperatures follow a traditional seasonal cycle, with the 2008-2012 maximum daily mean temperature of 15 degrees C and the anomalously low minimum daily mean of -29 degrees C. The long-term (WY 1982-2012) mean daily temperature is -2.16°C.

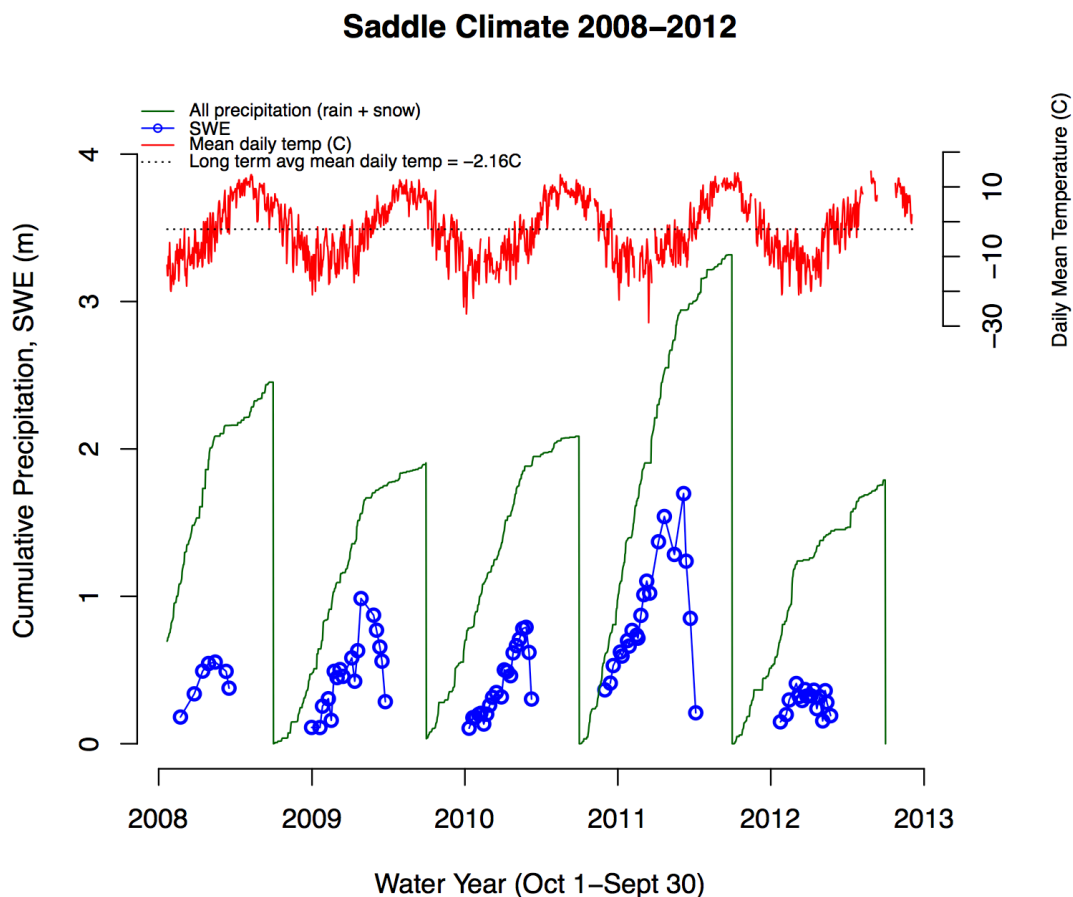


**Figure 2.3:** Climatology on Niwot Ridge over WY2008-2012. SWE and precipitation were measured at the Saddle snowpit and Saddle NADP site (CO02), respectively. Temperature is measured at the Tundra Lab site.

#### 2.4.2 Groundwater table height

Water table monitoring demonstrates that the major annual groundwater recharge event in both basins occurs in response to snowmelt influx in late spring (Figure 2.4). The Saddle wells show a higher maximum recharge but more recharge variability than Martinelli. Martinelli piezometers often experience artesian conditions with the water table at or near the ground surface. The water table in the Saddle basin, on the other hand, hovers between 2-8m below the surface for deep wells during average water years.

Groundwater fluctuations in Martinelli over the study period were similar across all wells with

average annual water table rises of 3.14m (MD1), 3.06m (MD2) to 3.17m (MD3). The permanent snow patch in Martinelli likely contributes to the consistency in behavior of all wells across all years except for smaller recharges in MD2 and MD3 in 2012. In contrast to the spatially consistent behavior in Martinelli, the average change in the water table height in the Saddle piezometers ranged from 2.22 (SD1) to 4.63m (SD4) with SD1 consistently experiencing the lowest water table. Interestingly, depth to peak water table height is significantly related to peak SWE only in MD2 ( $p=0.01$ ) and SD3 ( $p=0.03$ ).

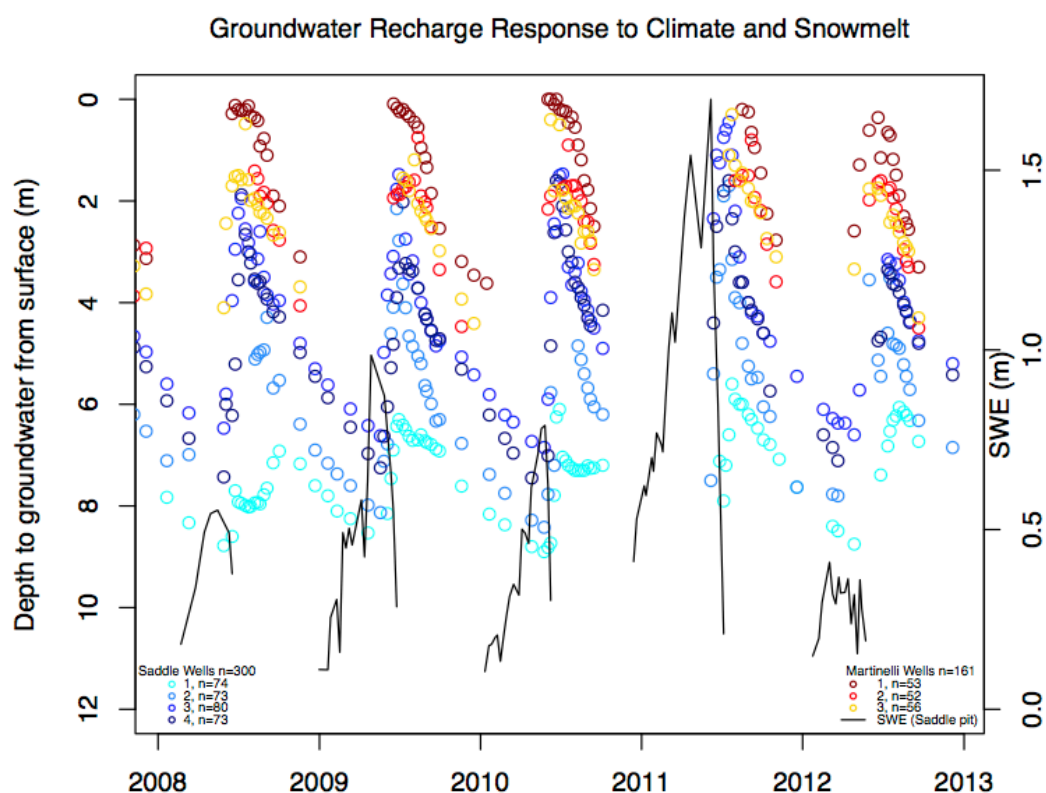


**Figure 2.4:** Groundwater fluctuations in the Saddle basin (4 wells ranging from 6.3-8.4 m deep) and the Martinelli basin (3 wells ranging from 3.3-4.3m deep) over WY2008-WY2012. Groundwater recharge is measured in piezometers by changes in the depth to the water table from the ground surface. Gaps in DTW measurements are due to the water table falling below the bottom of the well, or when deep snow packs prevented locating the piezometers for measurement. SWE at the Saddle pit is shown. Melt onset is indicated by the annual dramatic fall from peak SWE.

### 2.4.3 Isotopes and chemistry

Source water isotopes range from highly enriched summer precipitation (rain,  $\delta^{18}\text{O}$  median 10‰) to more depleted sources including snowpack, lysimeter meltwater, and winter precipitation (Figure 2.5). Receiving aquifers (represented by groundwater as measured in piezometers) and streamflow isotopic profiles indicate various mixing of source waters, with all isotopic values encapsulated by the range of isotopic values measured at the site.

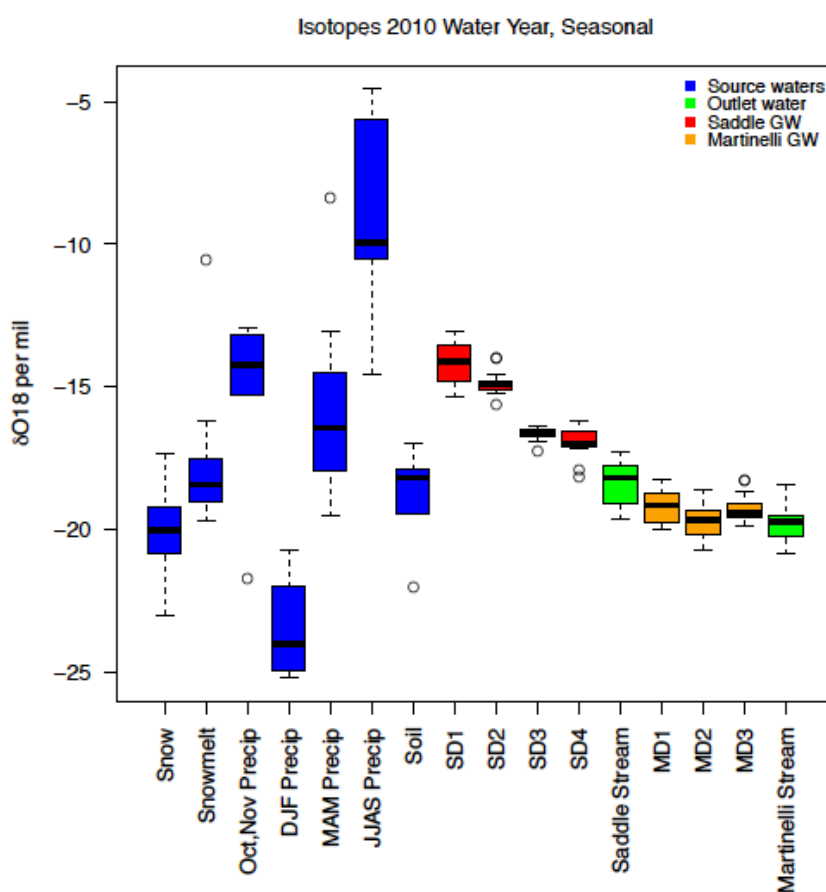


**Figure 2.5:** The range of  $\delta\text{O}18$  values in WY2010 across all sampled waters in both basins. Boxes relate to interquartile range, with whiskers identifying data falling within 1.5 times the interquartile range.

Across climate variations, snowmelt drives an isotope depletion and ion dilution pulse in

all groundwater wells over all years in the study period (Figure 2.6). Martinelli groundwater tracer composition is similar across all snow years (Figure 2.6, top panel) with the permanent snow field in Martinelli buffering changes to inter-annual climate variation by providing a consistent melt water source regardless of the seasonal snowpack.

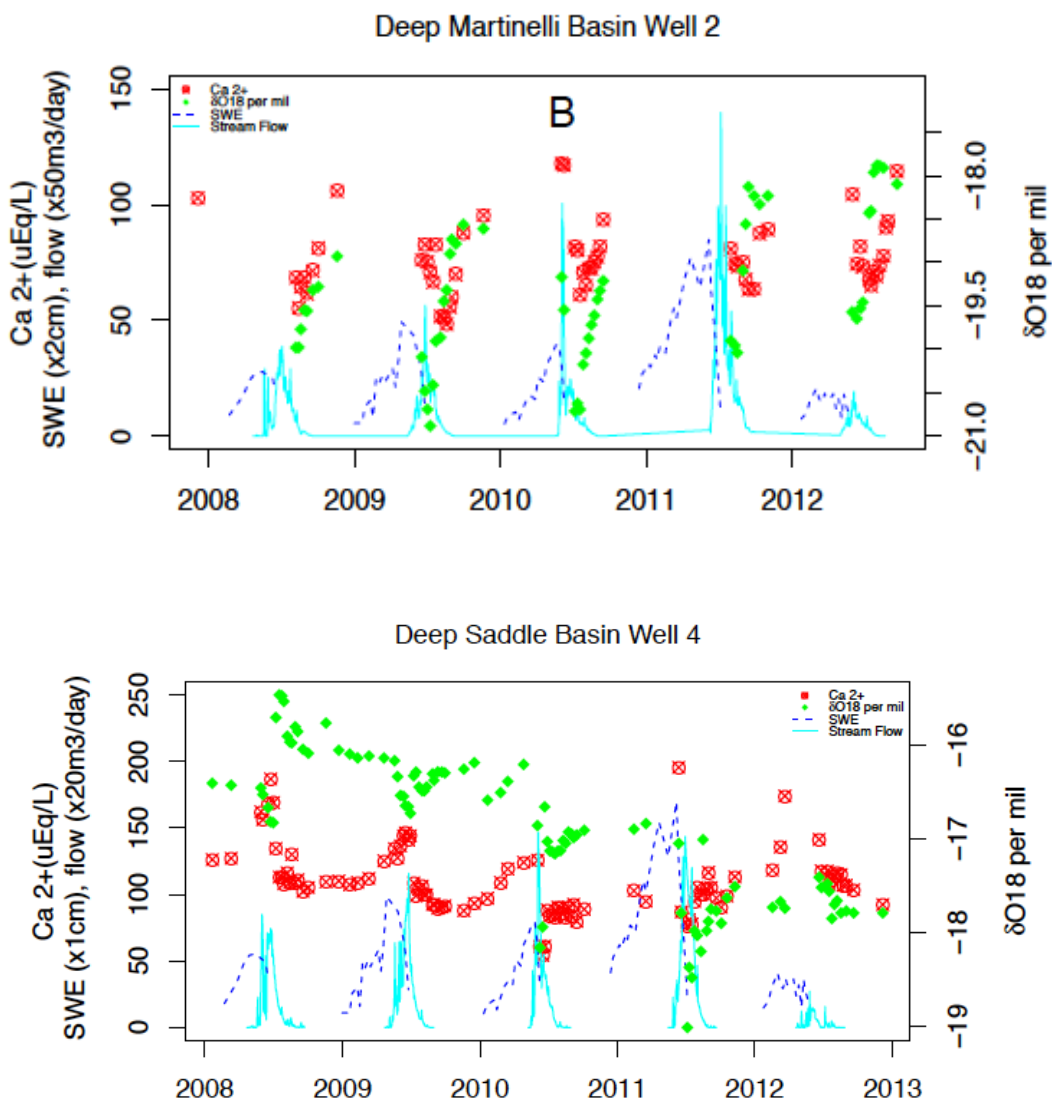


Figure 2.6: Annual meltwater influence is observed in the pulse of ion dilution and isotope depletion of groundwaters across a spectrum of water years. 2011 experienced a record high snowpack, while 2012's snowpack was a record low. Here, deep groundwater from Martinelli well 2 (MD2, top) Saddle well 4 (SD4, bottom) groundwater  $\text{Ca}^{2+}$  (red markers) and  $\delta^{18}\text{O}$  (green



diamonds) values are shown with the basin hydrograph (cyan) and the recorded SWE at the Saddle site (blue dashed line).

The western Saddle groundwater system (SD4 shown in Figure 2.6 bottom panel) displays a memory of previous hydrologic conditions over progressively larger snow years from 2008-2011. Larger influxes of new melt water influence inter-annual trends in lower ion concentrations and more depleted waters. Notably no isotope depletion signal is observed in 2012 in SD4 although  $\text{Ca}^{2+}$  concentrations increase. This indicates that SD4 groundwater in 2012 is likely relic from autumn 2011 and is more reacted due to additional holding time. The lack of dilution mechanism in 2012 suggests that new water inputs may not have exceeded aquifer capacity, resulting in little-to-no groundwater flushing in 2012 and giving a general estimate of aquifer storage volume.

Looking more closely at the seasonal variation during an average water year in 2010 all Martinelli groundwater have depleted  $\delta^{18}\text{O}$  waters ranging from -18.5‰ and -20‰ indicating the direct importance of snowmelt on this groundwater system (Figure 2.7, right). Martinelli isotopic signatures reveal the highest depletion levels in mid-to-late summer on June 9 (MD3, -19.8‰), July 19 (MD2, -20.7‰), and August 8 (MD1, -20.0‰). Martinelli streamflow mimics Martinelli's groundwater isotopic values and response, with a plunge in response to snowmelt and 2‰ recovery throughout the summer. The close pairing of isotopes between groundwater and streamflow indicate strong correspondence between groundwater and surface waters in Martinelli.

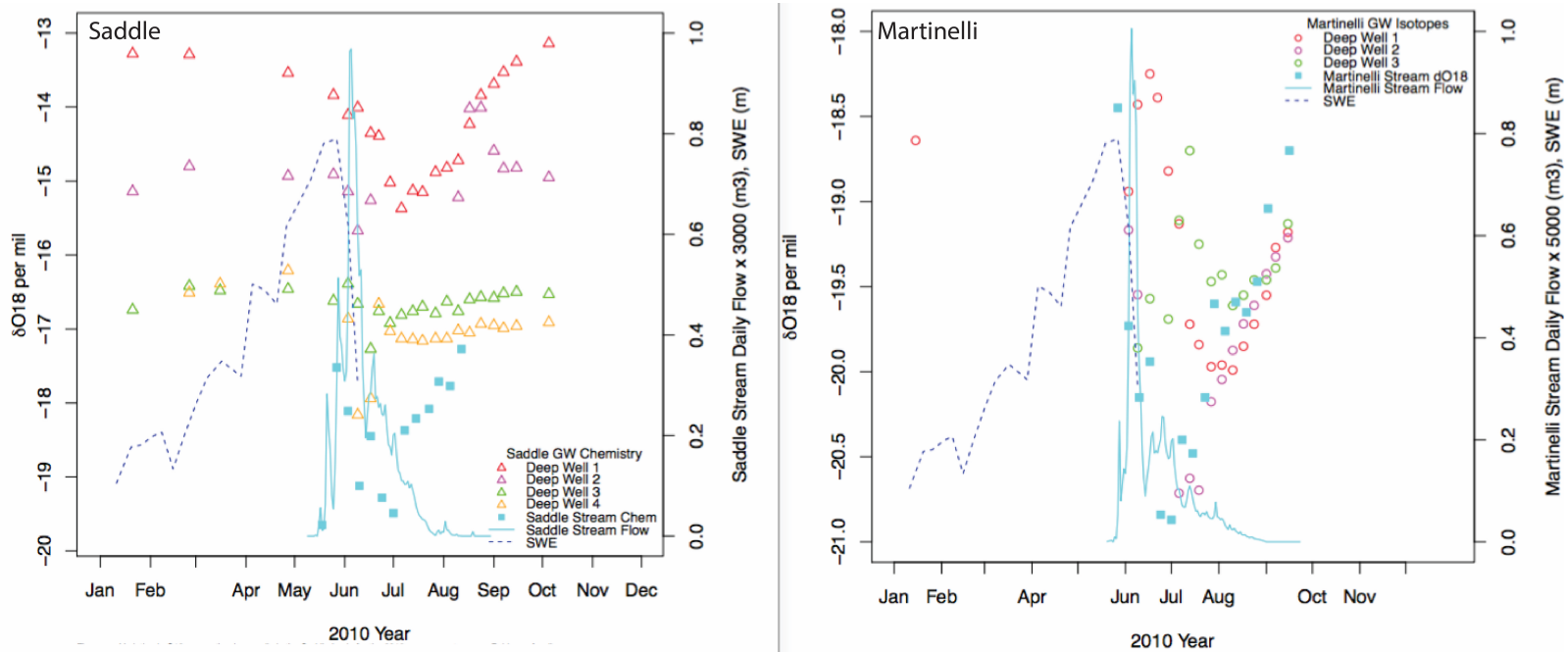


Figure 2.7: Isotope variations ( $\delta^{18}\text{O}$  presented here) in groundwater over an average year in 2010 in the Saddle (left) and Martinelli (right) wells. Martinelli and Saddle isotopic response shows the depletion signal in response to snowmelt onset. Depleted snowmelt sources dominate in Martinelli while a mixture of more enriched rain and snow sources are indicated for Saddle groundwater.

Isotopic signatures in groundwater across the Saddle basin in 2010 are significantly different than Martinelli ( $p < 0.01$ ) and show a rain and snow source water mix that varies largely even at small scales (Figure 2.7, right). The enriched source water signal decreases from east to west, with SD1 having the most enriched year round isotope signatures (ie, the most rain), and SD4 having the most depleted (ie, the most snow). New water mixing in SD1 is considerably lagged from snowmelt onset with maximum depletion of  $-15.37\text{‰}$  on July 13. SD3 and SD4 isotopic signatures pair closely and are affected nearly immediately by melt onset (May 27) with maximum depletion of  $-17.27\text{‰}$  (June 17) and  $-18.16\text{‰}$  (June 4), respectively. After varying timeframes to allow for mixing, the Saddle wells appear to have a relatively enriched “base” isotopic composition for the fall, winter and early spring (e.g.,  $-13\text{‰}$  for SD1,  $-15\text{‰}$  for SD2 and between  $-16$  and  $-17\text{‰}$  for SD 3 and 4) when there are few new water inputs. Saddle streamflow is more depleted than all Saddle groundwaters throughout the entire 2010 streamflow season, with a higher magnitude depletion in response to snowmelt than any sampled groundwater in the basin. The discrepancy between streamflow and groundwater isotopes suggests direct input from depleted source waters (melt) to the stream.

Trends in ion concentrations in the Saddle basin show two distinct regimes (Figure 2.8).  $\text{Ca}^{2+}$  concentrations were highest in the deep Saddle piezometers on the eastern side of the catchment in SD1 and SD2. The mean concentrations of  $\text{Ca}^{2+}$  in SD1 of  $5,116 \mu\text{eq/L}$  and SD2 of  $1,026 \mu\text{eq/L}$ , were one or two orders of magnitude higher than any other expected source of water or groundwater from either the Saddle or Martinelli catchments (Figure 2.8, left). While the water table in SD1 and SD2 rises in response to snowmelt, indicating meltwater is routed to SD1 and SD2, these extremely concentrated chemical tracer results suggest that SD1 and SD2 are essentially isolated from the groundwater-surface interactions in the study domain.

Meltwater entering into the SD1 and SD2 flowpaths does not appear to re-emerge in the alpine stream flow, at least not to the extent that it has been captured at the Saddle Stream sampling point (Figure 2.1). Saddle basin snowmelt may instead service regional groundwater systems via deeper and/or longer flowpaths, possibly fracture flow through bedrock from SD1 and SD2, with outlets further afield. With little possibility of influence from the SD1 and SD2 groundwater to Saddle Stream water, these wells will not be discussed further.

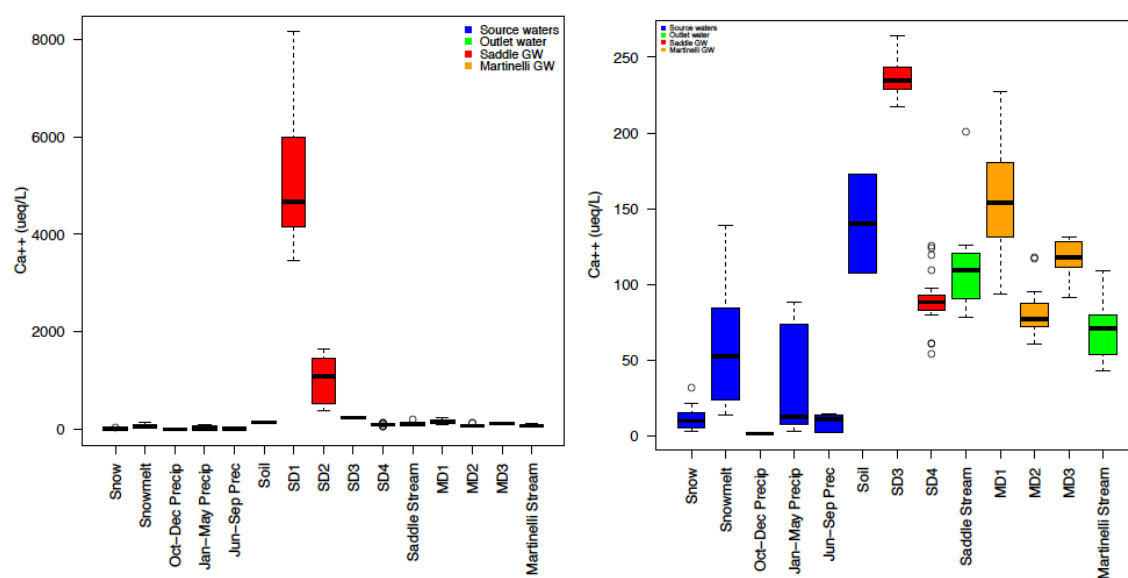


Figure 2.8: The range of chemical tracer concentrations in WY2010 indicates two distinct regimes: highly concentrated groundwaters in the eastern Saddle basin (left) and moderate concentrations throughout all other source waters, groundwaters and surface waters (right, excludes SD1 and SD2). Boxes relate to interquartile range, with whiskers identifying data falling within 1.5 times the interquartile range.

Groundwater ion concentrations (Figure 2.9, Ca<sup>2+</sup> shown as representative solute) across all wells in 2010 dip after snowmelt onset, with groundwaters exhibiting the expected dilution signal to old water due to new unreacted snowmelt inputs. The annual dilution pattern is similar for both basins. SD3 and SD4 (western Saddle wells) remain consistently low (<500 µeq/L),

plotting closely to ion concentrations in Saddle stream. The western Saddle wells appear to be a well mixed system as evidenced by the small range in concentrations throughout the year.

Martinelli groundwater ion concentrations have similar variation to SD3 and SD4 and have an overall small range. Maximum ion concentrations for MD1, MD2 and MD3 are 227, 118 and 131  $\mu\text{eq/L}$  respectively. The maximum change in ion concentration in 2010 in Martinelli wells was 134  $\mu\text{eq/L}$  in MD1. Maximum ion dilution from snow melt onset experienced in MD3, MD2 and MD1 increases from west to east on June 29, July 19 and August 24, respectively, implying sooner and faster infiltration of new melt at MD3 than MD1.

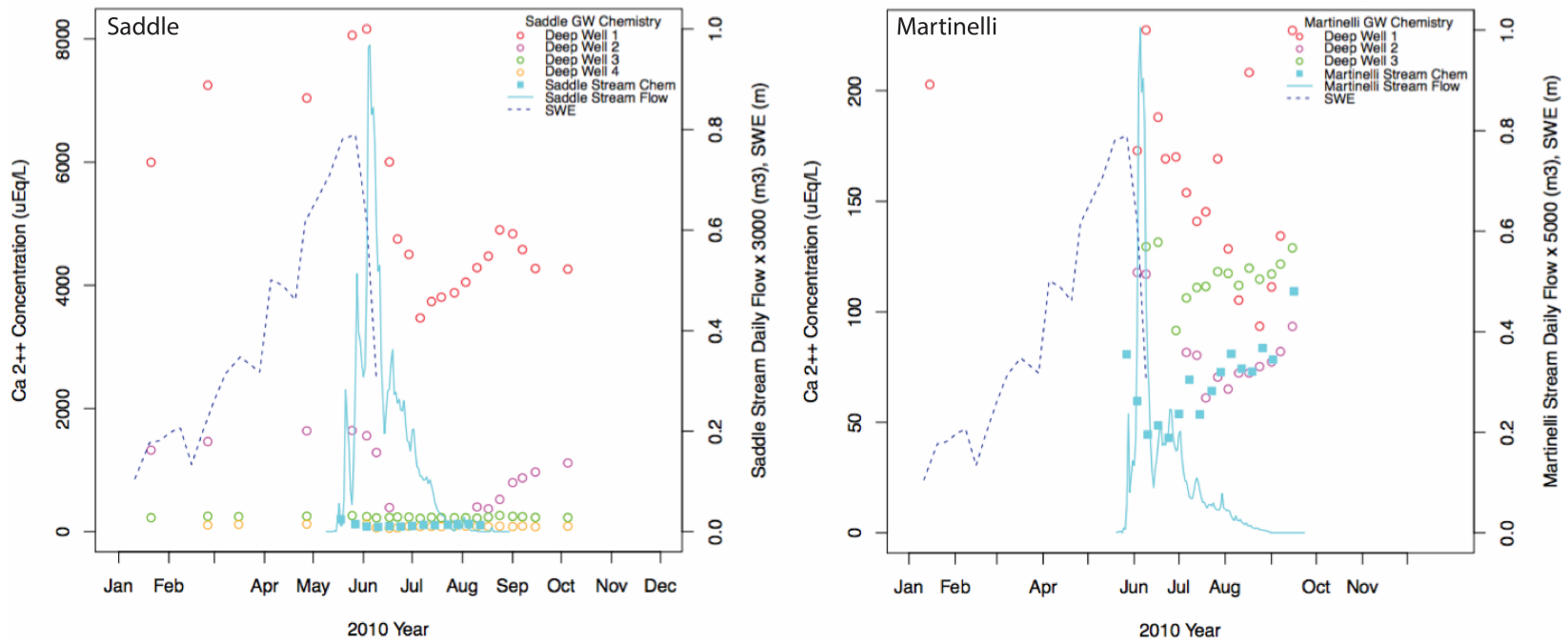


Figure 2.9: Time series of ion concentrations across all wells. Ca<sup>2+</sup> shown here as representative ion. Contrasting ion concentrations in Saddle (left) and Martinelli (right) identify major differences between the basins and highlights spatial heterogeneity in Saddle groundwater behavior even at small scales.

## 2.4.4 End Member Mixing Analysis (EMMA)

### 2.4.4.1 Model preparation, diagnostics and tracer selection

In the Saddle basin residuals for all tracers showed random scatter in 2D space ( $R^2 < 0.5$ ) (Figure 2.10). Silica had the largest RRMSE (Si = 3.5% RRMSE).  $Ca^{2+}$  has the highest change in RRMSE between 1 and 2 D space (Ca = -5% RRMSE).  $Ca^{2+}$  is well known to be a generally conservative tracer and was retained. In Martinelli,  $Cl^-$  residuals ( $R^2 = 0.48$ ) did not meet the  $R^2$  threshold, and it was removed from the tracer suite.  $Ca^{2+}$  showed the largest RRMSE (1.2%) which was still small overall in the context of other studies. Si had the largest difference in RRMSE when projected in 1D and 2D space of -2.5%. In both Saddle and Martinelli basins despite these results  $Ca^{2+}$  and Si were kept in the tracer suite for further testing. Final tracer combinations are the result of running the above diagnostics and trouble shooting model performance with concentration reconstructions, thereby allowing poorly modeled tracers to be removed to eliminate their influence over the EMMA projection.

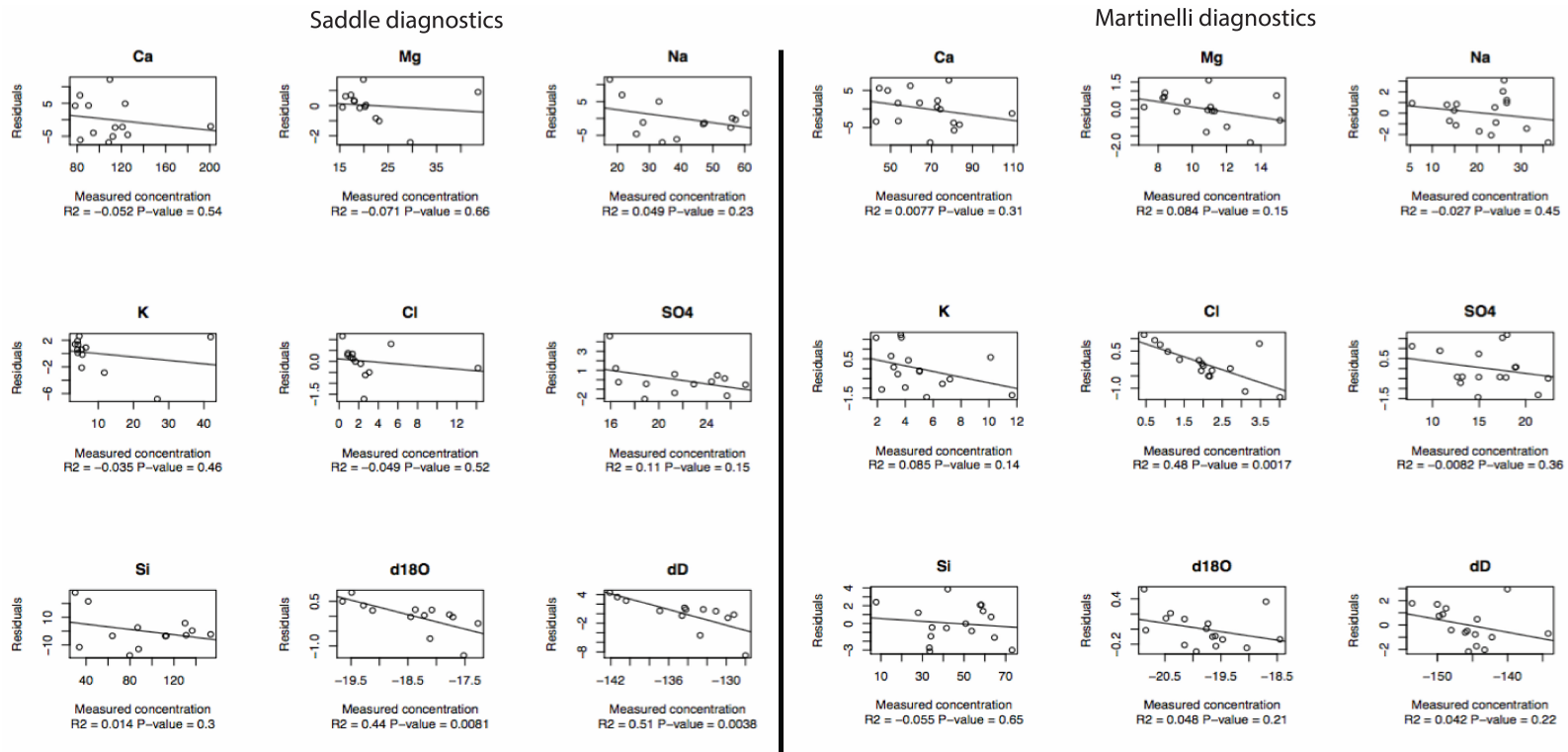


Figure 2.10: EMMA diagnostics for Saddle (left) and Martinelli (right) show random residuals indicating conservative tracer behavior.



In general, EMMA requires a parsimonious but balanced consideration for tracer selection that achieves appropriate model complexity, explanation of variance in the data, and desired model performance. These factors are inherently interrelated but the threshold chosen for complexity and performance will dictate final model architecture.

The Final selected tracer combinations are for the Saddle basin are:  $\text{Ca}^{2+}$ ,  $\text{Mg}^{2+}$ ,  $\text{Na}^+$ ,  $\text{Cl}^-$ ,  $\text{Si}$ ,  $\delta^{18}\text{O}$ , with 87.2% of variance explained. The final tracer combinations for the Martinelli basin were:  $\text{Ca}^{2+}$ ,  $\text{Na}^+$ ,  $\text{SO}_4^{-2}$ ,  $\text{Si}$ ,  $\delta^{18}\text{O}$ ,  $\delta$  with 96.3% of variance explained.

Variation in the data explained by 2 principal components (2 dimensions, 3 end members) are nicely visualized in principal component biplots (Figure 2.11). Stream observations that lie close together have a similar chemical and isotope fingerprint because these variables drive the PCA axes. Tracer vectors clustered in the same space indicate similar explanation in the PCA (e.g., in Martinelli, Figure 2.11 right panel, a change in  $\delta^{18}\text{O}$  corresponds to change in  $\delta\text{D}$ ). Tracers lying on the unit circle are well explained by the two principal components, as is the case for most of the selected tracers. Lesser distance from the center pivot suggests a 3<sup>rd</sup> dimension is required to more fully explain the variation presented by the tracer concentrations. That  $\delta^{18}\text{O}$  lies in the inner circle in the Saddle basin (Figure 2.10, left) may

explain why the  $\delta^{18}\text{O}$  reconstruction is not entirely satisfying.

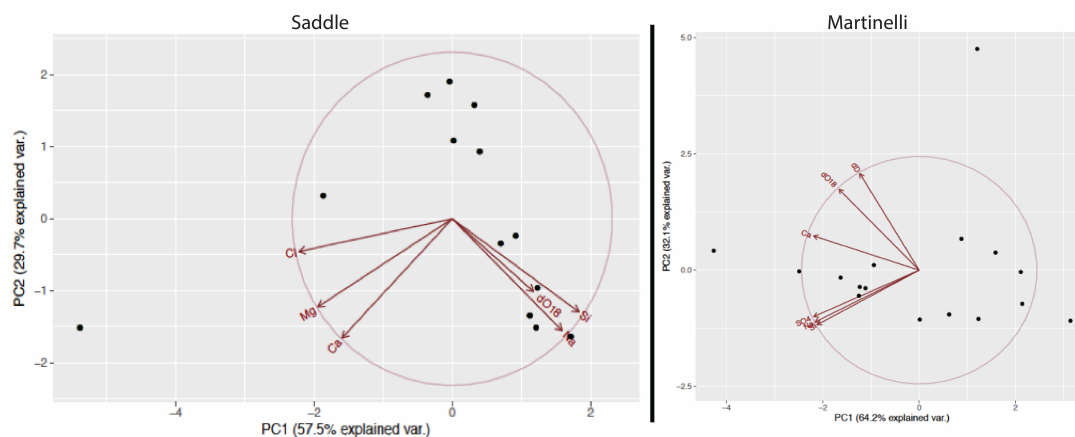


Figure 2.11: Bi-plots demonstrate the influence of tracers in determining the principal components. Stream samples (observations) are black dots and vectors are the tracers (variables) in the PCA.

#### 2.4.4.2 End member selection

PCA was calculated utilizing the selected tracers, and all stream and end members were projected into a U-space plot (Figure 2.12). Euclidean “S” distances calculated for each tracer are provided in Tables 2.2 and 2.3. A composite S distance metric provides a single, combined value across tracers for S distance comparison between end members, and it is calculated as the root of the sum of squares across all analytes for each end member. End members with small composite metrics and appropriate geometries in the U-space plot were selected for calculation of relative contributions to each stream sample. Considerations and metrics for end member selection are summarized in Table 2.4.

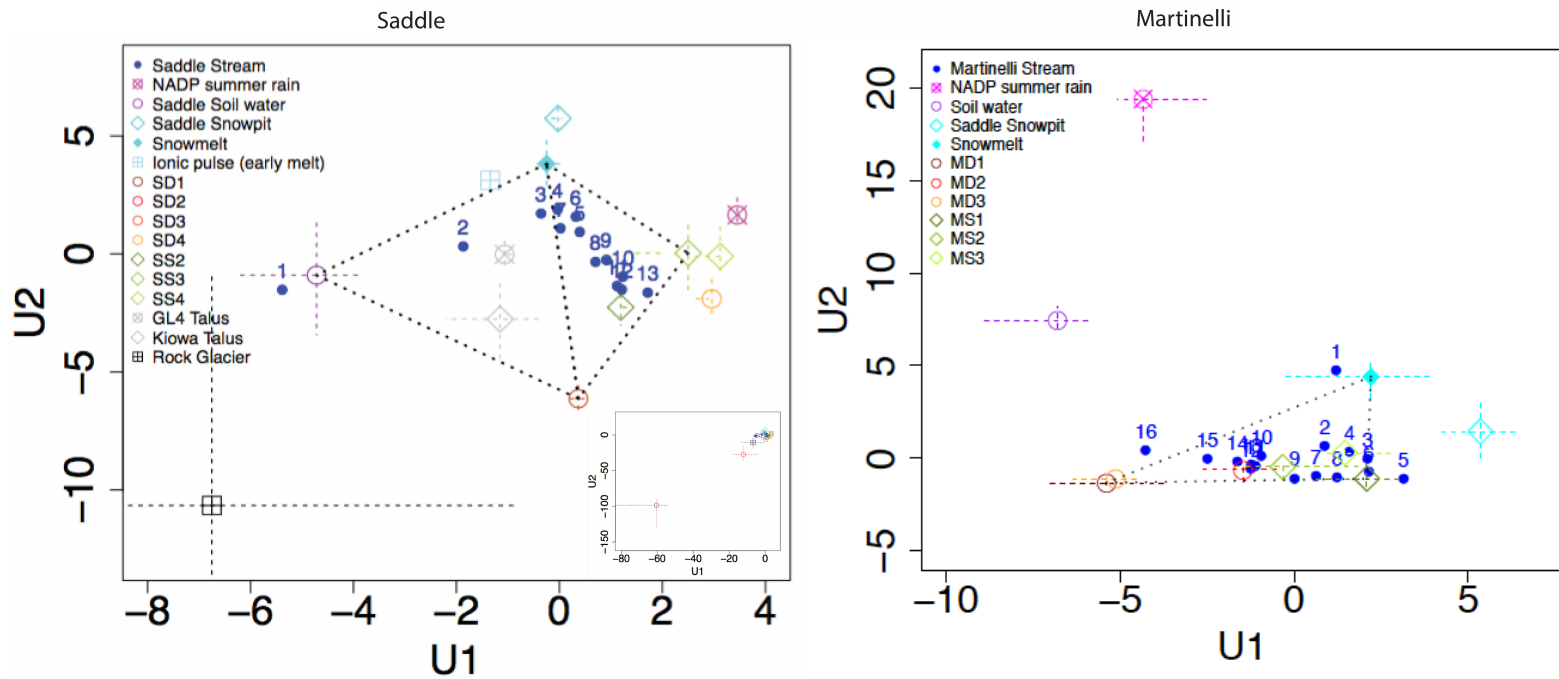


Figure 2.12: U-space diagrams for Saddle (left) and Martinelli (right) show transformed stream sample and end member observations into a space characterized by PCA's eigen values. Selected end members ideally enclose most (if not all) stream samples within the U-space geometry. Stream samples are numbered chronologically, starting with the first sample of the season in late May. Inset in Saddle diagram (left) shows larger scale U-space plot incorporating end members not in main plot (SD1, SD2).

Table 2.2: Euclidean distances for all possible end members in the Saddle basin derived from PCA using conservative tracers  $Ca^{2+}$ ,  $Mg^{2+}$ ,  $Na^+$ ,  $Cl^-$ , Si,  $\delta^{18}O$ . Selected end members are in bold.

End member	$Ca^{2+}$	$Mg^{2+}$	$Na^+$	$Cl^-$	Si	$\delta^{18}O$	Composite metric
Rain (NADP CO2)	24%	678%	518%	437%	270%	-4%	9.96
<b>Soil (Subnivian)</b>	<b>30%</b>	<b>61%</b>	<b>28%</b>	<b>56%</b>	<b>53%</b>	<b>-3%</b>	<b>1.06</b>
Snow pit (Saddle)	53%	102%	112%	102%	483%	0%	5.19
<b>Snowmelt</b>	<b>13%</b>	<b>47%</b>	<b>26%</b>	<b>54%</b>	<b>160%</b>	<b>0%</b>	<b>1.77</b>
SD1	45%	103%	88%	714%	326%	-10%	7.98
SD2	31%	25%	17%	390%	76%	-4%	3.99
<b>SD3</b>	<b>11%</b>	<b>16%</b>	<b>8%</b>	<b>6%</b>	<b>3%</b>	<b>0%</b>	<b>0.22</b>
SD4	25%	38%	0%	135%	13%	-1%	1.43
SS2	27%	36%	8%	87%	18%	-2%	1.00
<b>SS3</b>	<b>32%</b>	<b>74%</b>	<b>12%</b>	<b>147%</b>	<b>6%</b>	<b>-2%</b>	<b>1.68</b>
SS4	62%	72%	2%	165%	17%	-2%	1.91
Talus (GL4)	18%	16%	18%	52%	5470%	0%	54.70
Talus (Kiowa)	13%	25%	26%	20%	5559%	-1%	55.59
Rock Glacier	12%	10%	69%	150%	3%	-4%	1.66

Table 2.3: Euclidean distances for all possible end members in the Martinelli basin derived from PCA basin projected into U-space using conservative tracers  $Ca^{2+}$ ,  $Na^+$ ,  $SO_4^{2-}$ , Si,  $\delta^{18}O$ ,  $\delta D$ . Selected end members are in bold.

	$Ca^{2+}$	$Na^+$	$SO_4^{2-}$	Si	$\delta^{18}O$	$\delta D$	Composite metric
PrecipCO2	177.7%	1610.4%	143.7%	4239.3%	-4.9%	-11.2%	45.41
Soil water (ZT from subniv)	4.5%	19.2%	11.5%	2.8%	-1.5%	-2.2%	0.23
Snow (Saddle)	33.1%	221.4%	36.6%	90.6%	-1.4%	-0.7%	2.44
<b>Snowmelt</b>	<b>5.7%</b>	<b>69.5%</b>	<b>16.9%</b>	<b>100.3%</b>	<b>-1.0%</b>	<b>-0.4%</b>	<b>1.23</b>
<b>MD1</b>	<b>1.0%</b>	<b>4.4%</b>	<b>1.4%</b>	<b>1.3%</b>	<b>-1.1%</b>	<b>-1.1%</b>	<b>0.05</b>
MD2	4.1%	12.5%	8.1%	1.9%	-0.3%	-0.2%	0.16
MD3	2.6%	4.5%	8.1%	6.5%	-1.8%	-1.0%	0.12
<b>MS1</b>	<b>5.8%</b>	<b>18.3%</b>	<b>5.4%</b>	<b>11.3%</b>	<b>-0.2%</b>	<b>-0.1%</b>	<b>0.23</b>
MS2	7.7%	17.0%	19.4%	7.1%	-0.4%	-0.4%	0.28
MS3	20.5%	34.1%	29.7%	2.6%	-1.4%	-0.2%	0.50

Table 2.4: Summary of end member selection criteria, decision making and evaluation metrics.

Basin	Tracers used	End Member	Euclidean distance (%)	End member selection justification
Saddle basin	Ca <sup>2+</sup> , Mg <sup>2+</sup> , Na <sup>+</sup> , Cl <sup>-</sup> , Si, δ <sup>18</sup> O	Meltwater	1.77	Obvious source water in the Saddle basin. Geometrically well placed to enclose stream samples, with much lower Euclidean distance than alternative end member (snowpack).
		SD3	0.22	Geometrically well placed to enclose stream samples, with much lower Euclidean distance than alternative end member (SS2).
		SS3	1.68	Geometrically well placed, slightly better location and with lower Euclidean distance than alternative end member (SS2).
		soil water	1.06	Explains the anomalous chemistry in early stream samples; aids in geometrically capturing early stream samples when considering 25/75th percentile range of soil end member.
Martinelli basin	Ca <sup>2+</sup> , Na <sup>+</sup> , SO <sub>4</sub> <sup>-2</sup> , Si, δ <sup>18</sup> O, δD	Meltwater	1.23	Important for characterizing early season stream samples; acceptable Euclidean distance.
		MD1	0.05	Well positioned in U-space plot; lower Euclidean distance than MD3.
		MS1	0.23	Needed to constrain majority of stream samples in U-space plot; acceptable Euclidean distance.

The Saddle basin experiences two stream generation stages, necessitating 4 end members (Figure 2.12, left). An early season stage utilizes SD3 (deep groundwater), meltwater (lysimeters) and soil water. From mid summer onwards, the Saddle basin end members are SD3 (deep groundwater), meltwater (lysimeters) and SS3 (shallow groundwater). This two-stage approach allows for better capturing the anomalous chemistry of the initial stream samples owing to the high Cl<sup>-</sup> content characteristic of soil water's chemical signature. For the Martinelli basin (Figure 2.12, right), selected end members are MD1 (deep groundwater), MS1 (shallow

groundwater) and meltwater (lysimeters). Using selected end members, the PCA matrix is solved for relative proportions from each member to streamflow (Table 2.5).

Table 2.5: Relative end member contributions to streamflow for each stream sample.

DOY	Date	<i>Saddle basin</i>				<i>Martinelli basin</i>		
		melt	SD3	Soil water	SS3	melt	MD1	MS1
138	18-May	0.00%	0.00%	100%	0.00%	no sample		
147	27-May	44.60%	16.90%	38.5%	0.00%	88.8%	11.2%	0.0%
154	3-Jun	76.20%	18.80%	5.00%	0.00%	33.1%	16.7%	50.2%
161	10-Jun	78.40%	17.90%	0.00%	3.80%	19.4%	0.0%	80.6%
168	17-Jun	59.50%	22.00%	0.00%	18.50%	27.3%	7.1%	65.6%
175	24-Jun	66.90%	16.00%	0.00%	17.10%	0.0%	0.0%	100%
182	1-Jul	70.10%	25.90%	0.00%	4.00%	6.8%	0.0%	93.2%
189	8-Jul	41.20%	31.30%	0.00%	27.50%	3.6%	19.6%	76.7%
196	15-Jul	36.70%	27.10%	0.00%	36.20%	1.6%	11.5%	87.0%
204	23-Jul	22.80%	30.00%	0.00%	47.10%	2.0%	27.8%	70.2%
210	29-Jul	22.20%	36.10%	0.00%	41.70%	23.6%	40.9%	35.5%
217	5-Aug	18.60%	36.40%	0.00%	45.00%	14.7%	43.1%	42.2%
224	12-Aug	5.10%	30.30%	0.00%	64.60%	11.9%	44.9%	43.2%
231	19-Aug	no sample				15.3%	44.7%	40.0%
238	26-Aug					19.1%	50.1%	30.8%
245	2-Sep					22.1%	61.6%	16.3%

It is important to consider that EMMA recognizes chemical fingerprints as the differentiating feature between samples. An ‘end member’ is not a physical component (ie, a specific point in space or sample itself) but rather a representation of water with a specific isotopic and chemical signature. The end members selected here represent any water that has undergone a similar path and experience, and therefore looks chemically similar to the sampled end member. For example, SD3 does not just denote groundwater from the deep Saddle well 3, but rather any water coming from other locations that has a similar chemistry profile.

#### ***2.4.4.3 Model performance***

To confirm end member selection and evaluate model performance, concentrations of the observed stream flow samples were reconstructed using the modeled relative proportions of end member contributions to streamflow (Table 2.5). A perfect model fit would show model versus observed regression to have a slope,  $m$ , of 1 and  $R^2 = 1$ . Comparing the model to the observed streamflow concentrations (Figure 2.13), most tracers across both basins demonstrate a reasonable data fit to the regression ( $R^2 > 0.75$ ), but with both high and low bias of modeled concentrations.

A notable exception to concentration reconstruction performance is in the Saddle basin with  $\delta^{18}\text{O}$  ( $R^2 = 0.37$ ,  $m = 0.53$ ) (Figure 2.13, bottom). This poor performance is due to two anomalous, non-predictable values that exert a large influence on the modeled vs. observed regression. The first stream flow sample of the year on May 18 has an extremely depleted  $\delta^{18}\text{O}$  value (-19.65 ‰) and the second sample has the second most enriched of the season at  $\delta^{18}\text{O} = -17.52\text{‰}$ . Removing these two early samples from the analysis somewhat increases modeled isotope performance ( $R^2 = 0.6$ ). While this result calls into question the use of  $\delta^{18}\text{O}$  or  $\delta\text{D}$  as a tracer, isotope tracers are a key differentiator between rain and snow making it imperative for mixing modeling work. To eliminate both  $\delta^{18}\text{O}$  and  $\delta\text{D}$  would restrict the model's ability to differentiate these source waters, and this is an important separation in the context of this study. For this reason,  $\delta^{18}\text{O}$  has been retained for the Saddle model despite its mediocre reconstruction result.

Saddle

Martinelli

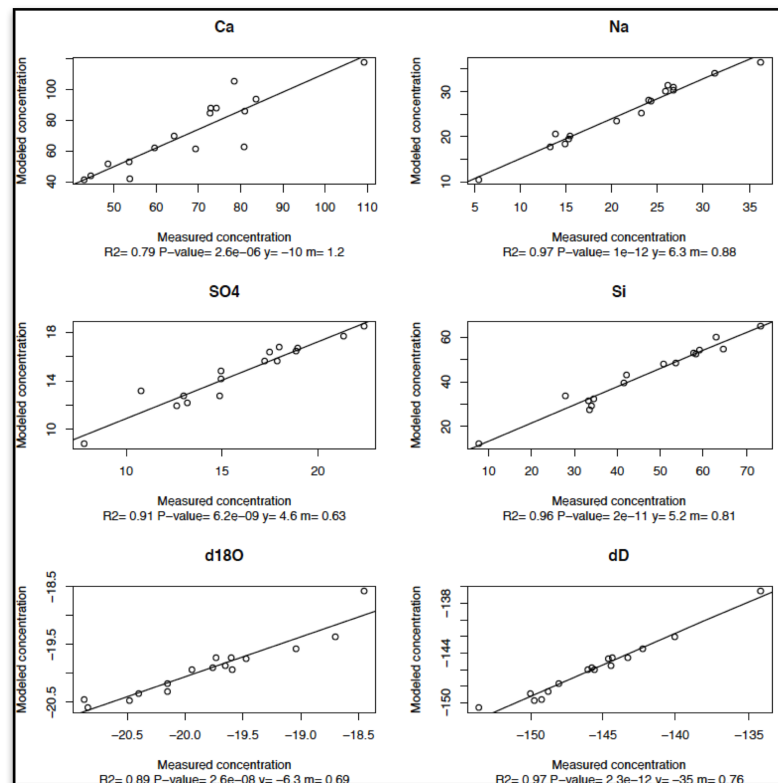
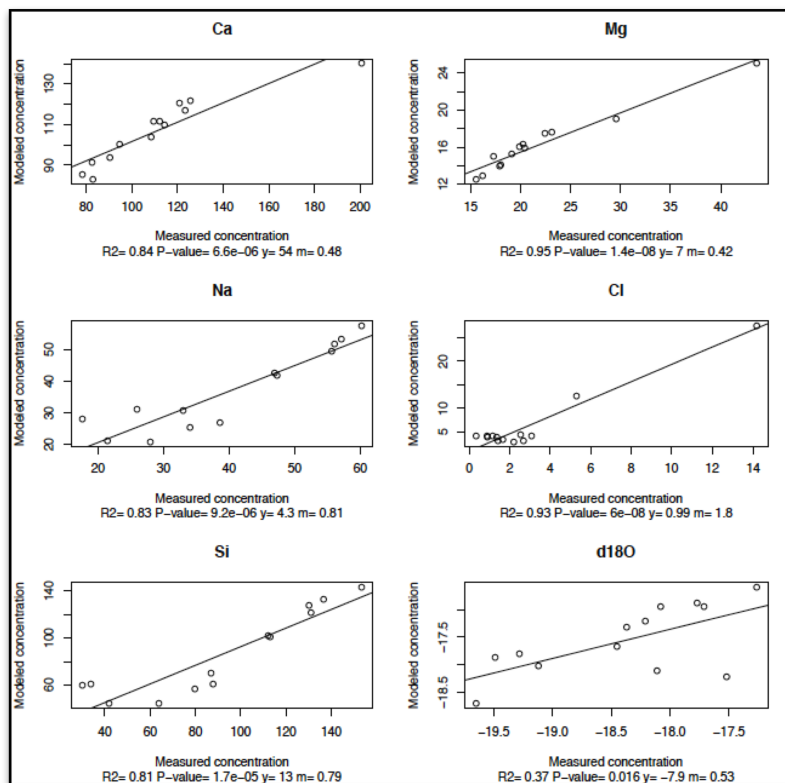


Figure 2.13: Concentration reconstructions for the conservative tracers driving EMMA models in the Saddle (left) and Martinelli (right).



#### ***2.4.4.4 Exploration of temporal changes to groundwater stream flow contributions***

Saddle groundwater appears to be a well mixed combination of meltwater and rain as demonstrated by the small range of isotope values through out the season and the isotope value itself lying between summer and winter precipitation (Fig. 2.5). Given the poor concentration reconstruction we hypothesized that groundwater contributions to streamflow varied temporally throughout the season, preventing end member selection from accurately modeling the isotope values found in streamflow.

To further investigate this hypothesis and the unsatisfying concentration reconstruction of the Saddle EMMA model, Euclidean “S” distances were calculated treating each individual groundwater sample in the Saddle basin in 2010 as a possible end member. Euclidean distances closer to zero indicate a better representation of the data in 2-D space, and therefore they make better selections for end members. Using S distances as a diagnostic for temporal changes to groundwater inputs to the stream, we find that SD3 is the best end member choice throughout the season using only S distance as a selection criteria (Fig. 2.14). There are no significant trends in the S distance data, and much data scatter especially for the shallow groundwater wells. These results do not support the hypothesis that groundwater influence depends on time, but it does provide a helpful diagnostic for trouble shooting, or in our case ruling out, possible drivers of poor model performance.

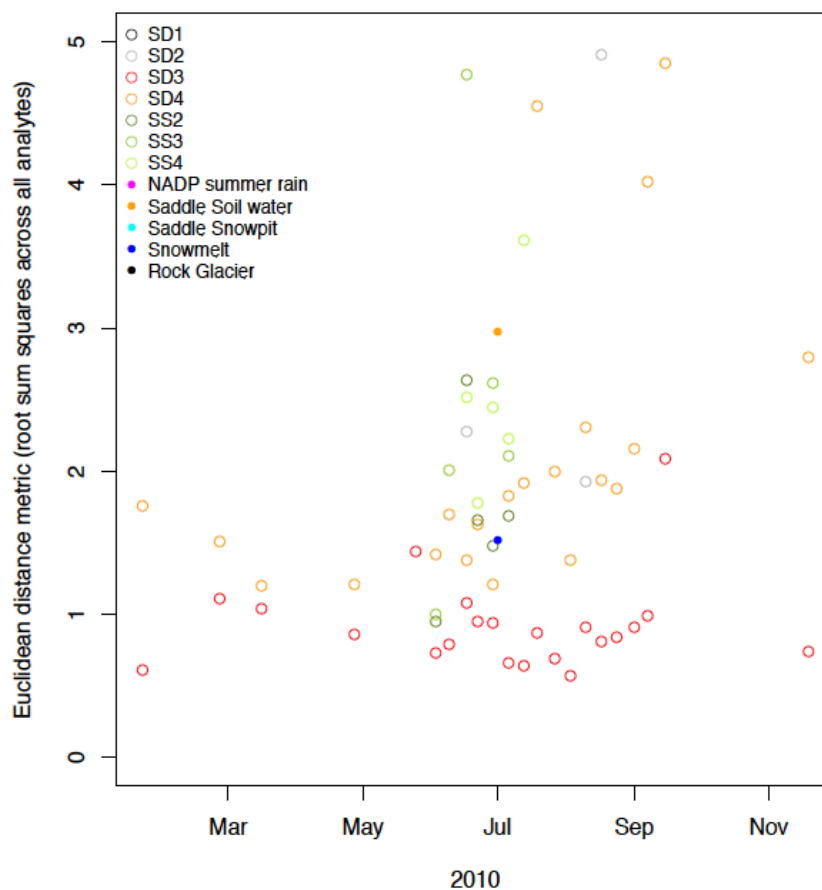


Figure 2.14: Euclidean “S” distances calculated for all groundwater samples in the Saddle basin in 2010. Non-groundwater end members (seasonal medians) with small S distances also shown.

#### 2.4.4.5 Hydrograph separation

Snowmelt is the dominant water input to Niwot Ridge, although there are small water inputs from summer rain. The key differentiation that we aimed to make in the hydrograph separations is not whether streamflow is from melt, but rather if meltwater flows overland direct to channel or if it is routed subsurface, and if the latter how much time does it spend underground? To quantify this distinction the relative contributions to streamflow from end members (Table 2.5) were utilized to separate the daily hydrograph. Streamflow samples were collected approximately weekly. Daily changes in end member proportions were linearly interpolated between samples.

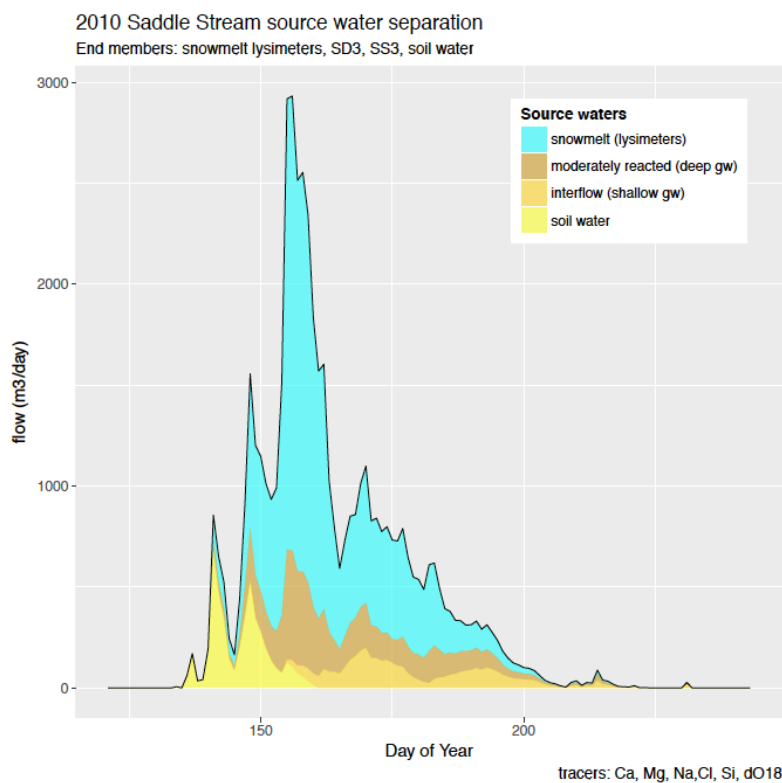
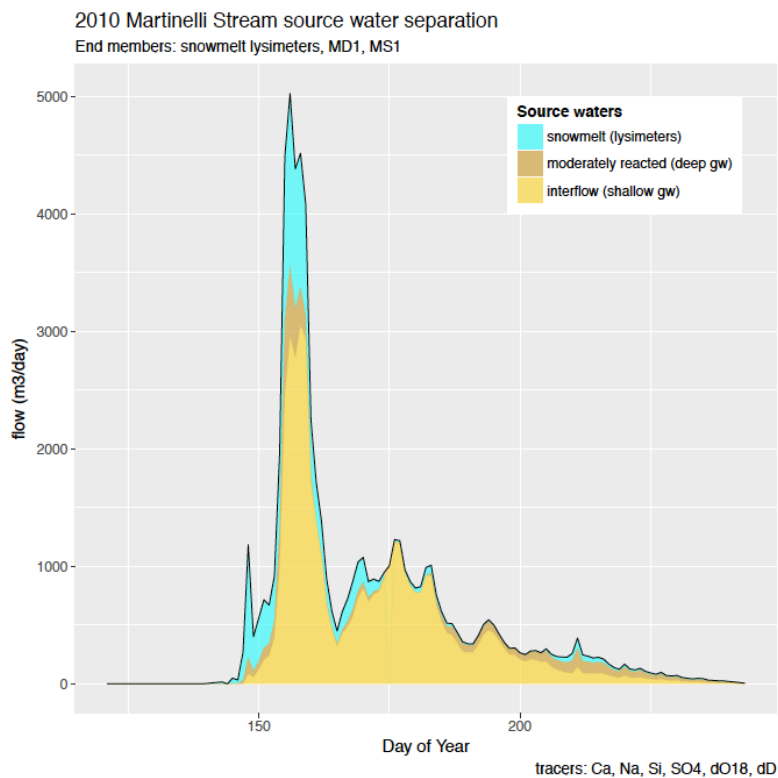
The dominant streamflow sources on an annual scale are direct melt inputs to the stream (overland flow) and shallow groundwater flow (interflow). Comparing the two basins (Table 2.6), these sources are present in roughly inverse proportions, with Saddle being dominated by direct melt runoff and interflow playing a large role in Martinelli. Deeper, more reacted groundwater is a subsidiary source to stream flow in both basins.

Table 2.6: Summary of overall proportions of sources to annual river flow in both basins.

		Melt (overland)	Reacted groundwater	Interflow	Soil water
Saddle	Volume (m <sup>3</sup> )	33,152	10,094	4,173	4,817
	% of seasonal flow	63%	19%	8%	9%
Martinelli	Volume (m <sup>3</sup> )	14,171	7,008	45,824	n/a
	% of seasonal flow	21%	10%	68%	

Temporal variations in streamflow sources provide insight into the streamflow generation mechanisms throughout the summer flow season. In the Martinelli catchment (Fig 2.15, top), snowmelt overland flow generates the initial streamflow pulse before interflow, rapidly moving shallow groundwater, supersedes as the dominant discharge source on the rising limb of the seasonal discharge peak in early June. Interflow serves as the principal flow generation mechanism through much of the summer until late July when low flow conditions are more equally a combination of deep and shallow groundwater, as well as melt.

Saddle's streamflow is generated via two regimes (Fig 2.15, bottom). At snowmelt onset through the early season flow pulse soil water is responsible for the majority of discharge. On the rising limb of the hydrograph peak, snowmelt overland flow dominates as the central streamflow source water until late July. A mixture of melt, deep groundwater and interflow contributes late season low flows.



**Figure 2.15:** Hydrograph separations for the Martinelli (top) and Saddle (bottom) basins over the average 2010 season differentiate between melt that travels overland (cyan) versus subsurface (yellows).

## 2.5 Discussion

### 2.5.1 Geology's impact on how and when the water stored in seasonal snowpacks is routed downstream from the point of melt on Niwot Ridge

Snowmelt's path to local alpine streamflow in both geologies appears to be primarily a function of the depth of porous material over bedrock. In both geologic environments snowmelt infiltrates into the subsurface and accounts for the vast majority of groundwater recharge. The depth of the material overlying bedrock in large part dictates the capacity of the colluvial aquifers in each system and thus the amount of meltwater that the system can receive before saturation. Once colluvium is saturated, new melt is likely forced downslope overland and directly into surface water channels.

While the Saddle basin is characterized as having bedrock subsurface, more correctly this should be described as having a shallow overlying colluvial aquifer underlain by bedrock. The bedrock of the Saddle basin has been classified as being heavily fractured, but fractures have not been mapped and the accessibility of overlying water to a fracture flowpath in bedrock is uncertain in the study site. Depending on the size and alignment of fractures, bedrock aquifers with high secondary porosity have the potential to convey water efficiently and could provide an outlet for infiltrating waters into the overlying colluvium. The hydrograph separation results suggest that fractures are not accessible in the western Saddle catchment as indicated by the generation of saturated overland flow in early summer, suggesting the Saddle's thin overlying colluvial aquifer has reached capacity without an outlet (drain) at the bedrock-colluvium interface. Without an accessible fracture in the underlying bedrock, the Saddle basin functions as a colluvial aquifer like Martinelli, only smaller. Conversely, the deeper (and larger) colluvial aquifer in Martinelli can accommodate a larger volume of melt, routing most meltwater through

the subsurface prior to stream discharge and experiencing minimal overland flow.

Many studies have shown that assumptions pertaining to groundwater recharge in unconsolidated sediments that act as porous media such as the colluvial components of both Saddle and Martinelli basins do not pertain to the underlying bedrock aquifers [e.g., *Praamsma et al.*, 2009]. Snowmelt recharges bedrock aquifers in our study as observed in the water table changes in the deep Saddle wells. Fracture flow paths do not likely play a role in alpine stream flow generation or the local transport of snowmelt in this study, but the eastern Saddle wells may have more direct communication to fractures that transport Niwot Ridge meltwaters further afield. Uncertainty regarding important fracture characteristics such as size and alignment limits our ability to define specific flow paths for these areas. Spatial heterogeneity in horizontal hydraulic conductivity in bedrock can yield large changes in the size of recharge and discharge zones (Harte, 1996; Oxtobee & Novakowski, 2002) resulting in a regional swath of potential discharge locations for fracture flow originating on Niwot Ridge.

Snowmelt waters have short residence in colluvial aquifers on Niwot Ridge. The annual flushing and cycle (the aquifer pulse, Figure 2.6) of both ions and isotopes implies that aquifer waters are exchanged yearly with new incoming meltwaters. Inherent in these findings are 1) the alpine groundwater capacity appears to be less than or similar to the size of the snowpack itself, 2) in average or wet years snowmelt residence time is less than one year, and 3) the water supplies afforded by alpine groundwater provides little insurance in the way of buffering water supplies from forecasted changes to the amount of snow accumulation of winter snowpacks.

To the latter two points, the record low snowpack in 2012 demonstrates the vulnerability of groundwater to snow accumulation amount. In the Saddle basin meltwater from 2011 appears

be held over through 2012 due to lack of new inputs as seen by its constant meltwater isotopic signature but higher ion concentration that suggests longer-than-normal residence time. In 2012, the low snowpack had little impact on Martinelli flow due to the semi-permanent snowpatch that maintained new melt inputs despite the anomalous winter precipitation. Groundwater that is reliant on seasonal snowmelt for recharge, as opposed to a permanent snow or rain, is most susceptible to depletion in a changing climate. Climate shifts bring the potential for variability in snowpack size and shifts in precipitation falling as rain rather than snow.

### **2.5.2 Impact of geology on alpine streamflow generation mechanisms**

Snowmelt transport paths and streamflow generation mechanisms differ substantially between the catchments. As described above, most of the streamflow generation differences are tied to the capacity of the colluvial materials in the system.

Martinelli's early season pulse (prior to DOY 155) is sourced by overland meltwater flow, possibly a consequence of a winter ice lens observed at the ground-snow interface that provides an impermeable lateral surface and prevents early season infiltration. As observed in similar geologies (Clow et al., 2003; Liu et al., 2008), Martinelli's colluvial sediments generally provide interflow (small amounts of water-rock interaction time) yielding low solute concentrations. Rapid groundwater flow is in response to changes in hydraulic head gradients imposed by infiltrating melt waters and Martinelli's steep topography. Meltwater infiltrates into the colluvial subsurface limited either by the infiltration capacity of the soil or by soil saturation. Initial infiltrating melt displaces water stored in the pores of the soil matrix (soil water) at the time of snow melt as supported by the similarity of  $\delta^{18}\text{O}$  in soil water with Martinelli groundwater (MD1 ( $p=0.21$ ), MD2 ( $p=0.14$ ) or MD3 ( $p=0.29$ )). As melt progresses, the increased head resulting from continual melt inputs from Martinelli's semi-permanent snow field

force the majority of meltwater to move rapidly downslope as shallow subsurface interflow. As melt rates and inputs recede in later summer, groundwater levels decrease yielding a low-flow late summer flow regime. While behavior across Martinelli's wells is relatively uniform, variations in aquifer geometry and the sediment porosity likely affect each well's capture zone that may explain the difference in the timing of peak dilution marking meltwater's arrival.

In the Saddle basin early season stream flow is generated by soil water that has been bound in the soil matrix from the previous year's late season summer rain. Saddle's soil water is characterized by high  $\text{Cl}^-$  concentrations relative to other waters in the catchment. At the end of May (DOY 149), the porous colluvial material is saturated, forcing meltwater overland when it becomes the primary stream flow source. Overland meltwater flow remains a prominent end member for the majority of the streamflow season. The combination of meltwater overland flow, moderately reacted groundwater (deep piezometers representing 'old' groundwater from a previous year) and interflow persists throughout the summer, showing that meltwaters both infiltrate (mobilizing interflow) and produce surface runoff.

### **2.5.3 Confounding factors**

While this paired catchment study affords similarity in site location and climate in many ways, several confounding factors require consideration amidst the findings presented here. Differences in wind protection between the two sites yields a contrast in wind redistribution processes. A wind scoured eastern Saddle catchment contrasts with Martinelli's wind deposition zone and its resulting semi-permanent snow field. Thin snowpacks and sometimes bare ground over winter in the eastern Saddle make the topsoil susceptible to freezing over winter (Appendix 2.7.1). Melt infiltration varies inversely to the amount of ice in the soil at the time of snowmelt



(Maule et al., 1994), so frozen soil may create an impermeable boundary to snowmelt waters during the spring freshet thereby having a hydrologic impact to the melt-groundwater-surface water behavior. Frozen soil may also be related to the anomalously high solute concentrations in the eastern Saddle wells insofar as thawing frozen soil or permafrost in the areas that lack insulation from winter snow cover are known to exhibit similarly concentrated chemistry (Toohey et al., 2016).

Recent thermal infrared drone imagery (Figure 2.16, courtesy Oliver Wigmore, image acquisition on June 21, 2017) provides qualitative input regarding surface flow paths, outlets and ponding extent in the Saddle basin occurring mid-melt season. The imagery identifies springs that daylight downslope from the Saddle wells and feed a marshy area below. The higher and somewhat steep topography to the west funnel melt from persistent snow patches to this area and so we surmise that the ponding noted by the red oval in Figure 2.16 may extend west to areas underneath the snowfield downslope of wells SD3 and SD4. The springs suggest that interflow (rapid shallow groundwater flow) is prominent in this part of the catchment prior to their outlet at the surface, with saturated overland flow resulting en route to the marshy areas.

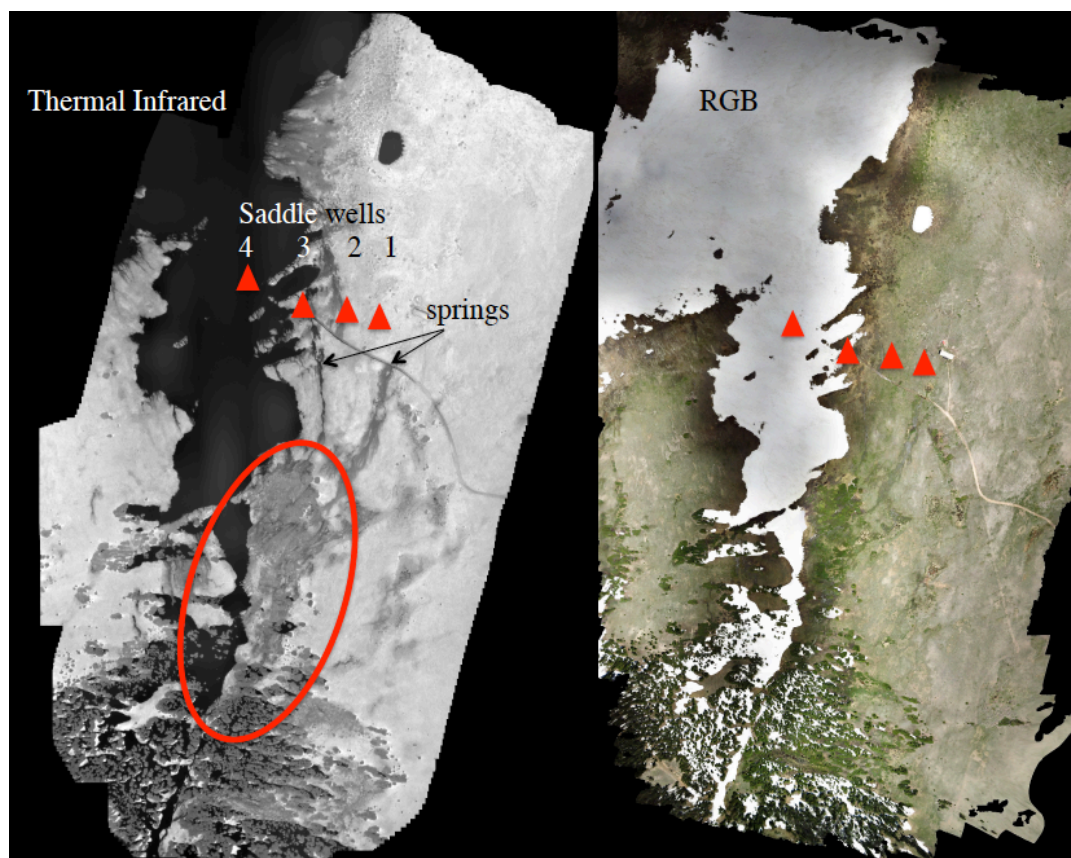


Figure 2.16: Thermal-infrared drone imagery (left) as compared to RGB (right) captures the Saddle basin mid-melt on June 21, 2017. Black indicates snow. Gray surface expressions indicate high water content. Marshy areas identified by red oval, piezometers by red triangles. Image credit: Oliver Wigmore.

Image acquisition in Figure 2.16 in 2017 is different than the water years studied in this chapter (2008-2012, with a focus on 2010). However, annual patterns remain largely consistent for average water years like 2010 and 2017 with general patterns of water flow shown in Figure 2.16 likely pertinent to 2010. While this singular image was the only available at the time of writing, a time series of TIR drone imagery is a promising new data source to clarify hydrologic processes in mountain environments, especially for small study basins where other lower-resolution satellite products providing TIR bands can not capture the level of detail necessary to parse out processes in small basins.

## 2.6 Conclusions

Reliance on the snowpacks of the Colorado Rocky mountains and ranges around the globe will continue to increase as demands rise for municipal, industrial and agricultural water resources. These demands necessitate clarification of how meltwater moves downstream because this understanding will help us forecast, plan and adapt to changes in water availability in a changing climate. Groundwater moderates the stream flow response to snowmelt, and the moderation itself depends on the underlying geology. At the local alpine scale, streamflow source waters and hydrograph shape is centrally a function of the depth and capacity of the porous aquifer overlying bedrock. Most melt is routed subsurface if the colluvial aquifer and topography can efficiently infiltrate and move water downslope as in the Martinelli basin. Basins with thin colluvial material like the Saddle saturate more quickly, and meltwater will be transferred overland directly to open channel flow. On a regional scale, the fracture networks known to exist in mountain block units like the one underlying the study sites can transfer meltwater farther and possibly faster but details of these processes are largely unknown.

This work assists in continually evolving conceptual models of alpine hydrologic systems. Although the discipline-wide challenge of managing the high heterogeneity of mountain environments persist, here we show that the presence of colluvial porous material present on most mountain slopes is a controlling aspect to the nature and timing of melt water transport at a local scale. Inversely, the hydrologic response of headwater streams may inform hypotheses regarding geologic stratigraphy since sequence and layer depth are notoriously challenging data to acquire in environments like Niwot Ridge.

## 2.7 Appendices

### 2.7.1 Appendix 1: Frozen soil dynamics

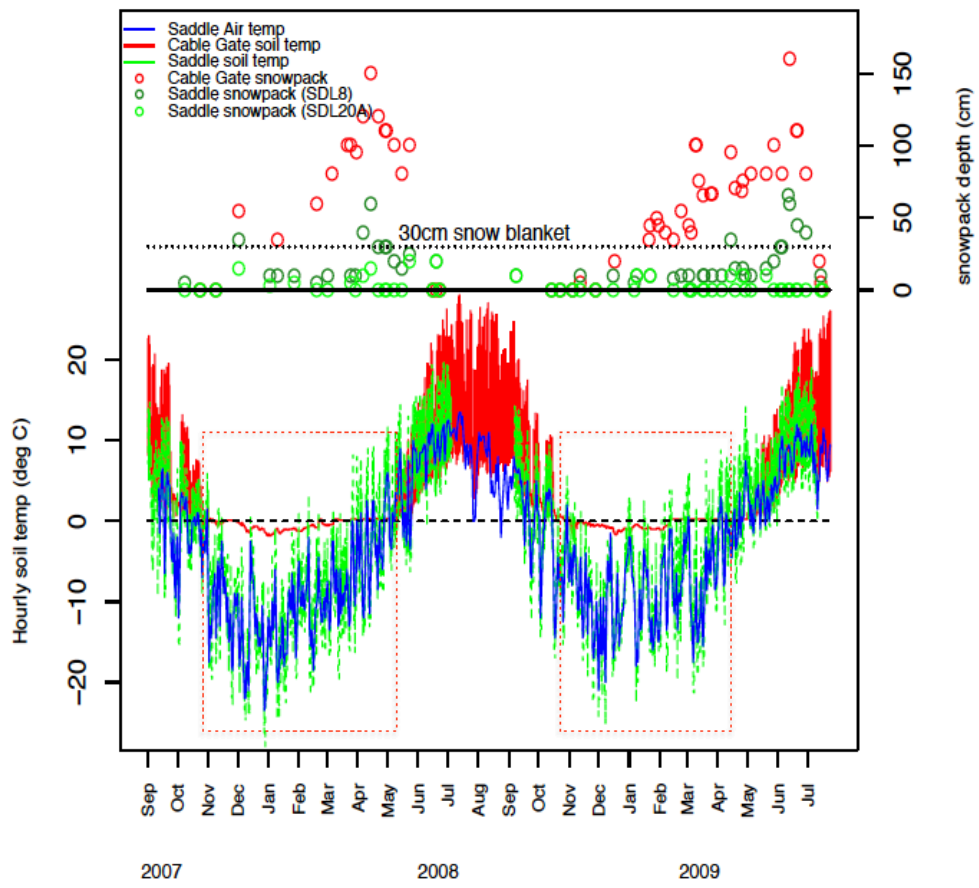


Figure 2.17: Soil and air temperature data on Niwot Ridge show a distinct de-coupling at snow scoured sites (red dashed boxes) in areas not afforded snow blanket insulation from the sub-zero winter temperatures.

## CHAPTER 3

### **3: HYDROLOGIC CONTROLS AND WATER VULNERABILITIES IN THE NARYN RIVER BASIN, KYRGYZSTAN: A SOCIO-HYDRO CASE STUDY OF WATER STRESSORS IN CENTRAL ASIA**

#### **Abstract**

Water vulnerabilities in Central Asia are affected by a complex combination of climate sensitive water sources, trans-boundary political tensions, infrastructure deficiencies and a lack of water management organization from community to federal levels. This study aims to clarify the drivers of water stress across the 440km Naryn River basin, headwater stem to the Syr Darya and the disappearing North Aral Sea. We use a combination of human and physical geography approaches to understand the meltwater-controlled hydrology of the system (using hydrochemical mixing models) as well as the human-water experience (via community surveys). Surveys indicate that current water stress is primarily a function of water management and access issues resulting from the clunky transition from Soviet era large-scale agriculture to post-Soviet small plot farming. Snow and ice meltwaters play a dominant role in the surface and ground water supplies to downstream communities across the study's 4220m elevation gradient, so future increases to water stress due to changes in volume and timing of water supply is likely given frozen waters' high sensitivity to warming temperatures. The combined influence of social, political and climate induced pressures on water supplies in the Naryn basin suggest the need for proactive planning and adaptation strategies, and warrant concern for similar melt-sourced Central Asian watersheds.

This body of work is a modified version of an article published March 2017 in *Water*. I would like to acknowledge my co-authors Cholpon Kozubekovna Minbaeva, Alana M. Wilson and Rysbek Satylkanov. Published material not presented in this chapter is the social research and methods that I neither designed nor analyzed, and which is principally the work of Cholpon Minbaeva.

### **3.1. Introduction**

Meltwater from snow and glaciers feeds downstream rivers and is a critical part of water supplies around the world (Barnett et al., 2005). Peak meltwater flows in the spring and summer coincide with increased demand from human users for irrigation and hydropower. Rising temperatures associated with climate change will influence the timing and magnitude of this annual cycle (Wilson et al., 2017). The uncertainties associated with climate change translate to uncertainties about the timing and volume of meltwater contributions to river discharge (Immerzeel et al., 2010).

In eastern Kyrgyzstan, the glaciers and snowpack of the Tien Shan Mountains form the headwaters of the Naryn River Basin. The Naryn flows westward across Kyrgyzstan before crossing the border into Uzbekistan where it joins the Kara Darya (River) to create the Syr Darya, central source to the disappearing North Aral Sea. The trans-boundary nature of the Syr Darya river basin and its tributaries, such as the Naryn, mean that there is an overtly political dimension to their flows. In a semi-arid region already facing water stress, the development of new infrastructure such as dams or diversions have the potential to create tension with downstream neighbors (Wilson et al., 2017). This will play out in yet to be determined ways in the Naryn River Basin, as Russian financing for the Upper Naryn cascade and Kambarata-1

hydropower projects is in limbo (EurasiaNet, 2016). Similar examples of competing water demands as a conflict spark can be found across the trans-boundary mountain sourced rivers of Central Asia (Gleick & Heberger, 2014; The Economist, 2014).

With the myriad of demands on melt sourced rivers in Central Asia, clarification of the stressors on these system – in terms of both water quantity as well as infrastructure issues — can provide a basis for water management planning and adaptation across sectors. With this study we present water chemistry data from the Naryn River Basin as a method for identifying changing source water contributions to river discharge from the mountain headwaters downstream to agricultural areas serving larger populations. In addition to collecting water samples, our field work included community surveys along the river in order to understand how water availability and access has changed over time, and to understand what challenges the people of the Naryn basin face in obtaining adequate water supplies. Our unique combination of data sets allows us to address the following objectives: 1) Utilize geochemical and isotopic hydrochemistry data to clarify the role that melt water plays in summer water supplies from mountain headwaters to downstream agricultural areas, and 2) present a narrative of community water issues observed along a 440 km stretch of the Naryn River. Methods and results pertaining to the second objective are not presented in this dissertation, but are part of the published article.

The summer timing of our data collection is particularly valuable as a contribution to understanding the partition of river water between meltwater and other sources (e.g. groundwater and rain) during the irrigation season. Water issues for communities in the basin range from irrigation infrastructure and water availability that became problematic after the fall of the Soviet Union to the long-lasting impacts of relocation due to construction of the Toktogul Dam when many communities were moved to new sites in the 1960s.

The human relationship with water in the Naryn River basin is multi-faceted and is influenced by water quality, water volume, access to water and varying degrees of reliance on water for livelihoods. In the headwaters the Kumtor Gold Mine, which has been in operation since 1997, has accounted for up to 12% of Kyrgyzstan's GDP and half of its exports in a given year (The Economist, 2013), adding a unique but complex facet touching many factors that define the human-water relationship. All of these factors are in turn impacted by local, regional, and national government management approaches.

Analysis of our coupled hydrologic and socio-hydro datasets responds to recent calls for interdisciplinary consideration of “the glacier run off problem” (Carey et al., 2017)– how glacier recession affects downstream populations acknowledging the sometimes disproportionate impacts that socio-political factors may have on melt water access. We incorporate both the physical context for water resource management and the socio-political dimensions of water availability and use at the community level. Thus our work is able to more realistically evaluate and uniquely inform the need for adaptive planning and resiliency strategies for the Naryn River basin and basins with similar characteristics across Central Asia.

## **3.2 Materials and Methods**

### **3.2.1 Quantifying the hydrologic setting**

Hydrologic inputs to the system include rain, seasonal snow and glacial melt. Remotely sensed products were utilized to quantify these inputs due to the dearth of *in situ* data available for the basin. The MODIS Snow Covered Area and Grain Size (MODSCAG) algorithm (Painter et al., 2009) was utilized to develop a snow probability map using snow cover fraction.

Compared to traditional MODIS maps, this approach results in increased accuracy particularly



amidst complex land cover types (Rittger et al., 2013). Snow cover probability for a pixel represents the chance on any given day that the pixel was snow covered, and it is calculated based on clear sky acquisitions by MODIS satellites from 2001-2014. Snow probabilities less than 30% are ignored and re-set to 0 given the difficulties of differentiating clouds from snow cover. Glacier surfaces are mapped using the Randolph Glacier Inventory (RGI) (Pfeffer et al., 2014), a product of the Global Land Ice Measurements from Space (GLIMS) glacier monitoring project (Raup et al., 2007). Precipitation across the basin was calculated using downscaled 2001-2014 MERRA reanalysis data.

River discharge records are available at three locations within the study domain. While historical records are more extensive for some gauges, records overlap at all gauges for the four year period between 2012-2015.

### **3.2.2 Synoptic sample design**

A central challenge of conducting field work at regional scales in austere mountain environments is finding the balance between achievable sample numbers given challenging terrain and access, and sufficient variety to characterize change throughout the basin. The study domain includes an upstream glaciated alpine region that transitions through to plains over 440 river kilometers.

Our study area captures a diverse spectrum of characteristics and is defined as the Naryn River basin upstream of Uch Terek, at the head of Toktugul Reservoir. This catchment covers an area of 48,085 km<sup>2</sup> and spans an elevation range between 898 m and 5116 m. Ecosystems transition from a semi-desert classification at the lowest elevations, up through steppe, sub-alpine meadow, alpine meadow, and culminating in a glacial environment. Vegetation is

predominantly grass, shrubs, with a sparse presence of small trees. The Naryn River basin has a severe continental climate, with temperatures below  $-50^{\circ}\text{C}$  in winter and exceeding  $40^{\circ}\text{C}$  in the summer. The geologic setting is primarily metamorphic, with the Naryn-Sonkul fault zone of the Northern Tien Shan stretching approximately 200 km in a general east-west trend along the river basin.

Our sampling design aimed to target water chemistry information to capture key hydrologic transitions over this diverse domain resulting in low sample numbers but highly explanatory data. This is in contrast to a sample design based on sampling at a pre-determined distance interval or site selection triggered by any tributary input.

Surface water sampling sites in this study initially focused on tributaries that either drained a significant sub-basin, thereby providing an integrated chemistry snapshot of a substantial drainage area, or tributaries with unusual landscape features that were hypothesized to have an impact on water chemistry. In total 23 surface water samples were collected including 13 mainstem and 10 tributary samples (Figure 3.1) with a synoptic Lagrangian approach, a sampling scheme that aims to follow roughly the same plug of water as it moves downstream.

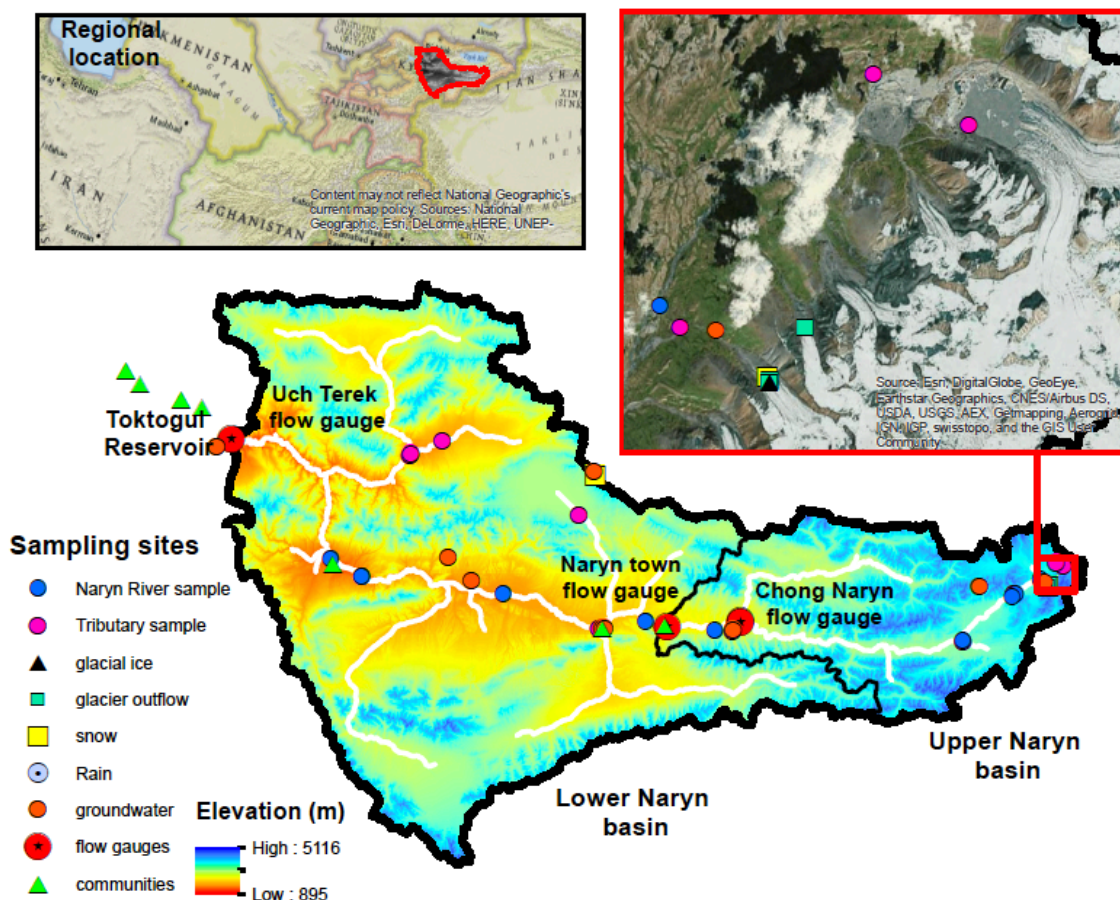


Figure 3.1: Water sampling, surveyed communities and stream gauge locations across the glacier-to-plains study domain. The Upper Naryn basin is defined upstream of the Naryn town gauge, and the Naryn River and major tributary alignments are shown (white line). Top right inset: Glacial headwater source water sampling locations. Top left inset: Naryn basin study domain location within the Central Asian region.

We utilize End Member Mixing Analysis (EMMA) to distill multi-variate water chemistry data from samples to quantify the contributions of river source waters to flow (Christophersen & Hooper, 1992). To do this effectively, it is important to have a chemical fingerprint of possible end members contributing to river flow. In the case of the Naryn River, much of the water inputs to the system occur at higher elevations in the form of snow. Accordingly, end member samples collected for this study include glacial ice (n=2, duplicate), snow (n=2, one snow on glacier, one snow on land), and glacial outflow (n=3). Glacial outflow

is a conglomerate of individual water sources originating on or adjacent to glaciers. These waters access and are routed through glacial plumbing, eventually discharging at the glacier snout. Glacial outflow components include ice melt, snow melt, groundwater and rain, but are dominated in the Naryn basin during the study period by the cryospheric contributions. We experienced no rain while conducting field work in the Naryn but rain water was acquired in the adjacent Kyzyl Suu basin (n=1).

Due to the importance for acquiring spatial representation of groundwater throughout the domain, groundwater sites were sought across the elevation gradient from a high elevation spring adjacent to Bordu glacier (3707m) and at a high headwater pass (4005m) to a low lying spring adjacent to Toktogul Reservoir (1036m). Samples were collected at both naturally exiting groundwater springs and hand-pumped wells established for community water supplies. Depending on the site (well versus spring) and the level of ion concentrations in the waters, groundwaters are classified into three categories: reacted deep (wells), reacted shallow (high elevation springs), and unreacted shallow (interpreted as lateral 'quickflow') groundwater. Higher ion concentrations in groundwater suggests longer flow paths, longer residence times, or tortuous paths across reactable substrate (i.e., talus fields, rock glaciers), whereas low concentrations imply rapid movement at shallow depths (Liu et al., 2004).

### **3.2.3 Water sample collection and analysis**

Samples for geochemical and isotopic analysis were collected and analyzed following the protocols and methods described in Wilson et al. (2016), with analysis performed at the Arikaree Water Chemistry Laboratory (ions) and the Ecohydrology Laboratory (isotopes) at the

University of Colorado-Boulder. Stable water isotopes are reported as a ratio of the sample to the Vienna Standard Mean Ocean Water (VSMOW):

$$\delta^{18}O, \delta D = \left[ \left( \frac{R_{sample}}{R_{VSMOW}} \right) - 1 \right] * 10^3 \quad (1)$$

where R is the ratio of  $^{18}O/^{16}O$  or  $^2H/^1H$ . Results are reported as  $\delta$  (per mil, or ‰).

### 3.2.4 Mixing models and source water separations

EMMA is traditionally employed with a time series of data to calculate the hysteresis of source waters over a relatively small spatial domain (e.g., Christophersen et al., 1990; Cowie et al., 2017; Liu et al., 2004). These studies generally anticipate a set pool of end members that are consistent throughout the time series. In this study, we utilize a synoptic survey in July and August 2016 to evaluate changes in water sources to river flow over space, not time. End member options for river water sources continually change throughout the catchment due to the availability of new inputs and as the nature of groundwater evolves.

To apply EMMA to this unique study, we divide the basin into two sub-regions that we hypothesize are controlled by separate but related source waters and processes: the headwaters (Upper Naryn) and the plains (Lower Naryn) (Figure 3.1). This allows for the outflow river composition at the lower headwater boundary to feed the inflow river composition at the upstream extremity of the plains, and recognizes that there are discrete differences to possible inputs (i.e., melt inputs) between the headwaters and plains that warrants the systems to be considered separately.

The headwaters (Upper Naryn) starts as the Kumtor River and is fed initially by the Petrova glacier's terminal lake, Petrov Lake. The Kumtor River and the Kichi Naryn River come together 32 km upstream of Naryn town and collectively make up the headwater sources to

the larger Naryn River. The Lower Naryn sub-region spans from Naryn town to Toktogul reservoir over 255 km.

End-member mixing analysis was employed separately for the Upper Naryn and Lower Naryn. Following Hooper (2003a), the dimensionality of the mixing space and identification of conservative tracers was determined. Conservative tracers were utilized to distill the multivariate chemistry dataset into two principal components for a 3-member mixing space. The two principal components serve as the basis for axes in a “U-space” plot (a mixing diagram) where all end members and surface water samples are projected (Christophersen & Hooper, 1992).

End member selection is derived using several diagnostics (Hooper, 2003a). Triangles formed by three end members will ideally encapsulate all river samples in the mixing diagram. To further evaluate end member fit the distance between the projected point and the actual point, the so-called Euclidean distance, is calculated as a percent of the original tracer concentration. Ideally the Euclidean distance is minimized for selected end members (Liu et al., 2008). Percent contributions of each selected end member are then quantified for each surface water sample. To evaluate the model performance and confirm end member selection, tracer concentrations were re-constructed using end member concentrations and the percent contribution results from EMMA. Poor concentration reconstructions for any tracer may prompt further consideration such as testing use of different conservative tracers or different end members in the mixing model.

### 3.3. Results

#### 3.3.1. Hydrologic setting

Peak flow in the Upper Naryn occurs in late July or early August, while the Lower Naryn experiences an earlier peak in late May or early June. The Naryn River hydrograph shape across elevations demonstrates the transition from ice-to-snow melt sourced waters as the river progresses downstream. The upper gauge (Chong Naryn) exhibits a typical sustained late summer flow shape of a glacier sourced system, while the lower elevation gauge at Uch Terek shows more water mass and higher flows earlier in the year coincident with the spring snow melt season (Fig. 3.2). The ‘flashy’ character of the annual hydrograph’s rising limb suggests a river system that is fairly responsive to the highly variable precipitation inputs over the course of the year (Fig. 3.2a).

Rain during the drier months almost always comes in multi-day storms, and in the rainy months the intensity can vary by an order of magnitude from day to day. Based on the 14 years of MERRA precipitation data across nine 500m elevation bands (500m to 4500m), 70% of the months record both rain and snow event within the same elevation band. This suggests rain-on-snow events may exacerbate the high magnitude response of stream flow to new precipitation inputs across elevations. Since glaciers play a role reducing both intra- and inter-annual flow variability by providing a consistent ice melt supplied baseflow through the melt (summer) season that is independent from storm spikes, depletion of ice mass in glacier systems will lessen the water they supply to river systems over the long term and may impose a hydrograph that is even more responsive to changes in weather.

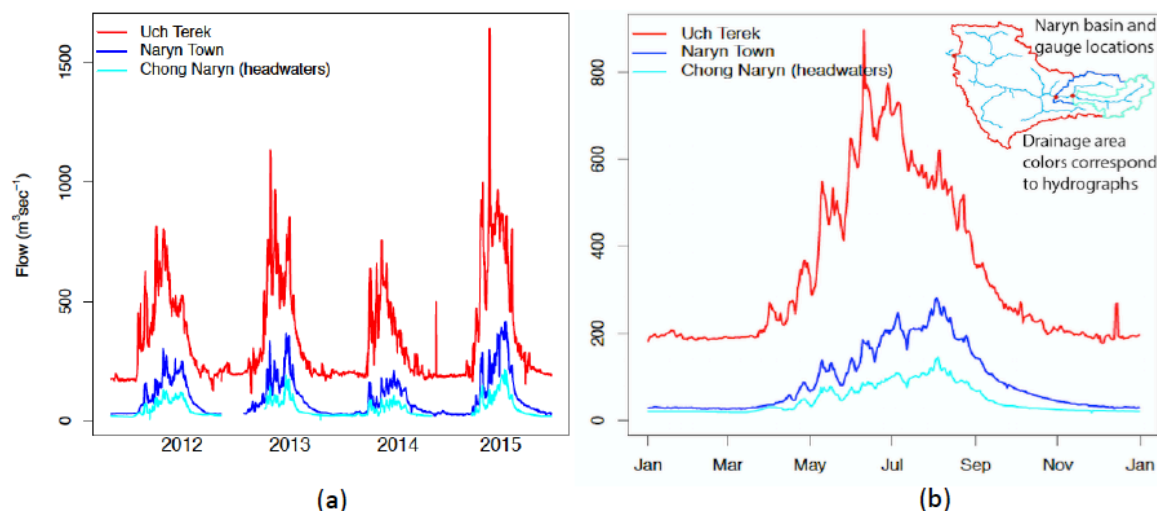


Figure 3.2: Melt-dominated hydrographs at the three gauge locations in the study domain. (a) Time series of flow record demonstrating inter-annual variability and (b) the daily average of the four-year flow record over 2012-2015. Top right inset: drainage area outlines correspond to the color of each hydrograph.

A substantial baseflow of approximately  $200 \text{ m}^3\text{s}^{-1}$  is observed outside of the melt season at the regional basin scale shown at the Uch Terek gauge, while consistent but smaller baseflows are present in the Upper Naryn. A small run-of-river reservoir is located immediately upstream of Uch Terek flow gauge and may account for the highly consistent winter flow recorded at this point.

Precipitation across the basin averages 27.13 cm per year, with 63% falling as rain and 27% falling as snow, however above 3000 m the total precipitation inputs are approximately half rain and half snow. In relation to the way the basin is split in this paper for analysis, approximately 40% of precipitation in the Upper Naryn falls as snow. Within the Lower Naryn Basin, annual precipitation inputs are comprised on average of 89% rain.

In the Upper Naryn basin, 84% of the area (8632  $\text{km}^2$ ) has snow probability  $>30\%$  while this figure applies to 54% (20,424  $\text{km}^2$ ) of the Lower Naryn basin area (Fig. 3.3). Glaciers are present at the headwaters and provide melt inputs to both headwater stems as well as to the Ak-



Tal, a major tributary joining the Naryn River at Dostuk. Glacier ice covers 994 km<sup>2</sup>, or 2% of the entire study domain.

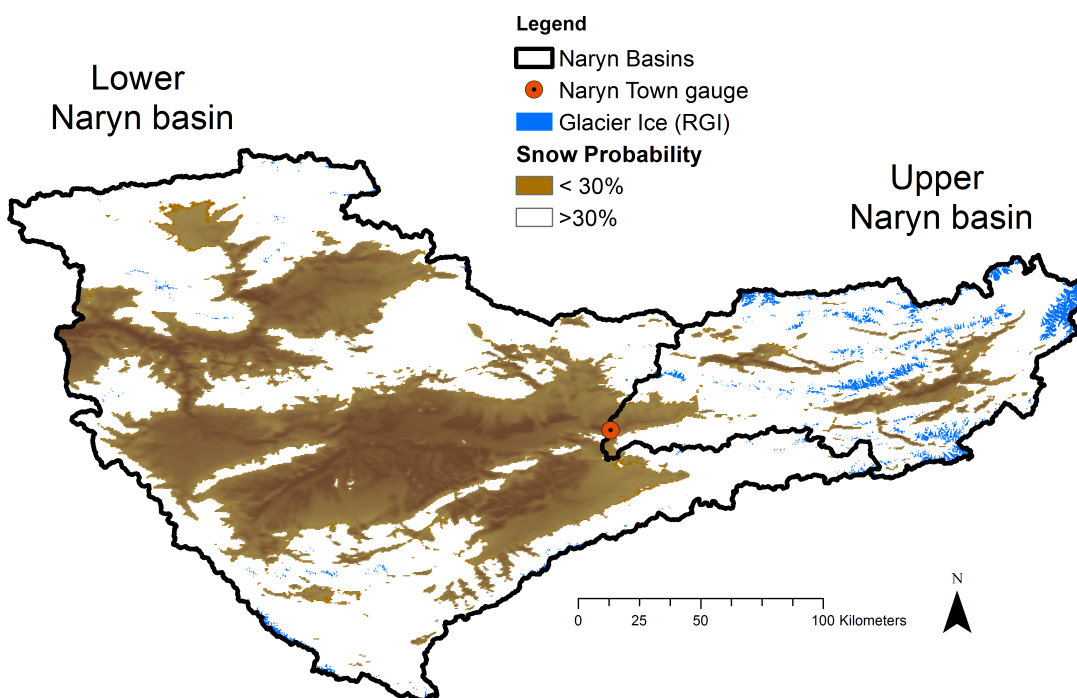


Figure 3.3: The Upper Naryn basin receives substantial snow cover and houses the vast majority of glaciated systems in the study domain, while the lower elevation Lower Naryn basin receives less. Snow probability is defined as the likelihood that the pixel will be snow covered on any given day, and is based on all clear sky MODIS acquisitions from 2001-2014. MOD10A1 snow cover data provided by Karl Rittger.

### 3.3.2. Hydro chemistry elevation gradient

Isotope variation of Naryn River waters across the elevation gradient show a strikingly consistent isotope value throughout the basin (Fig 3.4a).  $\delta^{18}\text{O}$  values for mainstem waters hover around -12‰ from the highest elevation sample all the way through to Toktogul Reservoir. Tributary sample  $\delta^{18}\text{O}$  values vary more than the mainstem ranging from -13‰ to -9‰. Notably, cryospheric end member samples – snow, ice, glacial outflow and high elevation groundwater – bracket the isotope values found in the Naryn River. In contrast, the rain sample

acquired in the adjacent Kyzyl Suu basin has a  $\delta^{18}\text{O}$  value of 0‰, suggesting that surface waters in the Naryn basin are dominated by melt water sources. With the exception of the groundwater spring at Kazarman Pass (2299m, -16‰), groundwater isotopes throughout the basin (-13‰ to -11‰) also hover near the isotopic values of the high elevation melt water group and are discretely different than rain.

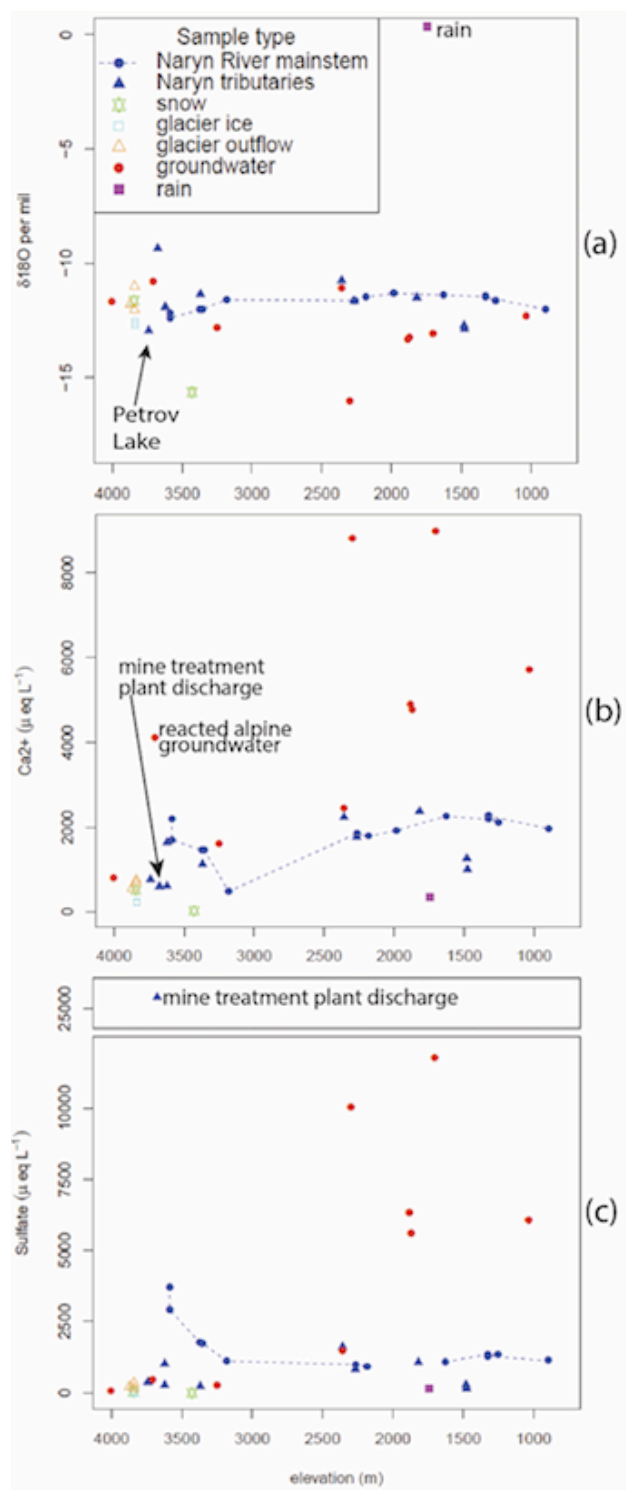


Figure 3.4: Hydro-chemical trends over the study domain elevation gradient. (a) Naryn River  $\delta^{18}\text{O}$  values show a remarkably consistent melt source water signal, and all waters are notably different than rain. (b)  $\text{Ca}^{2+}$  and (c)  $\text{SO}_4^{2-}$  concentrations in groundwater increase with decreased elevation indicating longer flow paths and/or residence times. Mine discharge is elevated in some ions (c) but not in others (b).

The ion concentration progression demonstrates the combined influence of groundwater contributions and mine discharge on the chemical signature of mainstem waters (Figs. 3.4b, 3.4c). The mine discharge sample provides exceptionally high levels of  $\text{SO}_4^{2-}$  ( $25387 \mu\text{eq L}^{-1}$ ) and  $\text{Na}^+$  ( $24596 \mu\text{eq L}^{-1}$ ) to the mainstem waters. However, it is  $\text{Ca}^{2+}$  poor ( $599 \mu\text{eq L}^{-1}$ ) and does not account for the high  $\text{Ca}^{2+}$  values observed in both mainstem waters and tributaries that are hydrologically disconnected from the mine discharge waters (e.g., Bordu Stream and Arabel River). Extremely elevated levels of  $\text{Ca}^{2+}$  ( $4116 \mu\text{eq/L}$ , twice the level of  $\text{Ca}^{2+}$  in the mainstem) were found in the Bordu alpine groundwater sample that logically also contributes to high elevation river flow. These groundwaters are  $\text{SO}_4^{2-}$  and  $\text{Na}^+$  poor ( $453 \mu\text{eq L}^{-1}$  and  $238 \mu\text{eq L}^{-1}$ , respectively), and so there is intuitively a joint contribution from mine discharge waters and groundwater that accounts for the elevated ion profile of the Kumtor (Upper Naryn) River.

Dilution of ions with decreasing elevation likely result from added ion-poor snowmelt contributions as the catchment expands to include major additional sub-basins adding significant alpine areas and snow cover to the basin. This dilution trend is observed until 3182m in the  $\text{Ca}^{2+}$  profile (Fig. 3.4b), then reverses towards an increasing concentration pattern likely a result of groundwater contributing increasing proportions to the river flow.

### **3.3.3 EMMA diagnostics and mixing model results**

#### ***3.3.3.1. Upper Naryn***

Diagnostic tests for conservative tracers examining the randomness of residuals between actual and projected tracers suggest that the following tracers are conservative for the Upper Naryn:  $\text{Ca}^{2+}$ ,  $\text{Na}^+$ ,  $\text{Mg}^{2+}$ ,  $\text{K}^+$ ,  $\text{Cl}^-$ ,  $\text{SO}_4^{2-}$ ,  $\delta^{18}\text{O}$  (Liu et al., 2008). Solute concentration

reconstructions using all of the tracers and two principal components rendered poor concentration reconstructions for  $\text{Mg}^{2+}$  and  $\text{Cl}^-$  so these tracers were dropped from the model and re-run with only  $\text{Ca}^{2+}$ ,  $\text{Na}^+$ ,  $\text{K}^+$ ,  $\text{SO}_4^{2-}$ ,  $\delta^{18}\text{O}$ . With this combination of tracers, 1 dimensional space (two end members explains only 64% of the variance in the data. Two principal components (three end members) explain 94% of the chemistry variation indicating three dimensions is a more appropriate model space (Fig. 3.5).

In the Upper Naryn, three end members were used to describe stream flow compositions for all samples, however a change in end member selection from mine discharge waters to snow is due to dilution of river water with downstream distance from the mine. Note that for the three samples influenced by the mine discharge, snow is not considered an end member. Conversely, for all other surface water samples in the Upper Naryn, mine discharge is not considered an end member

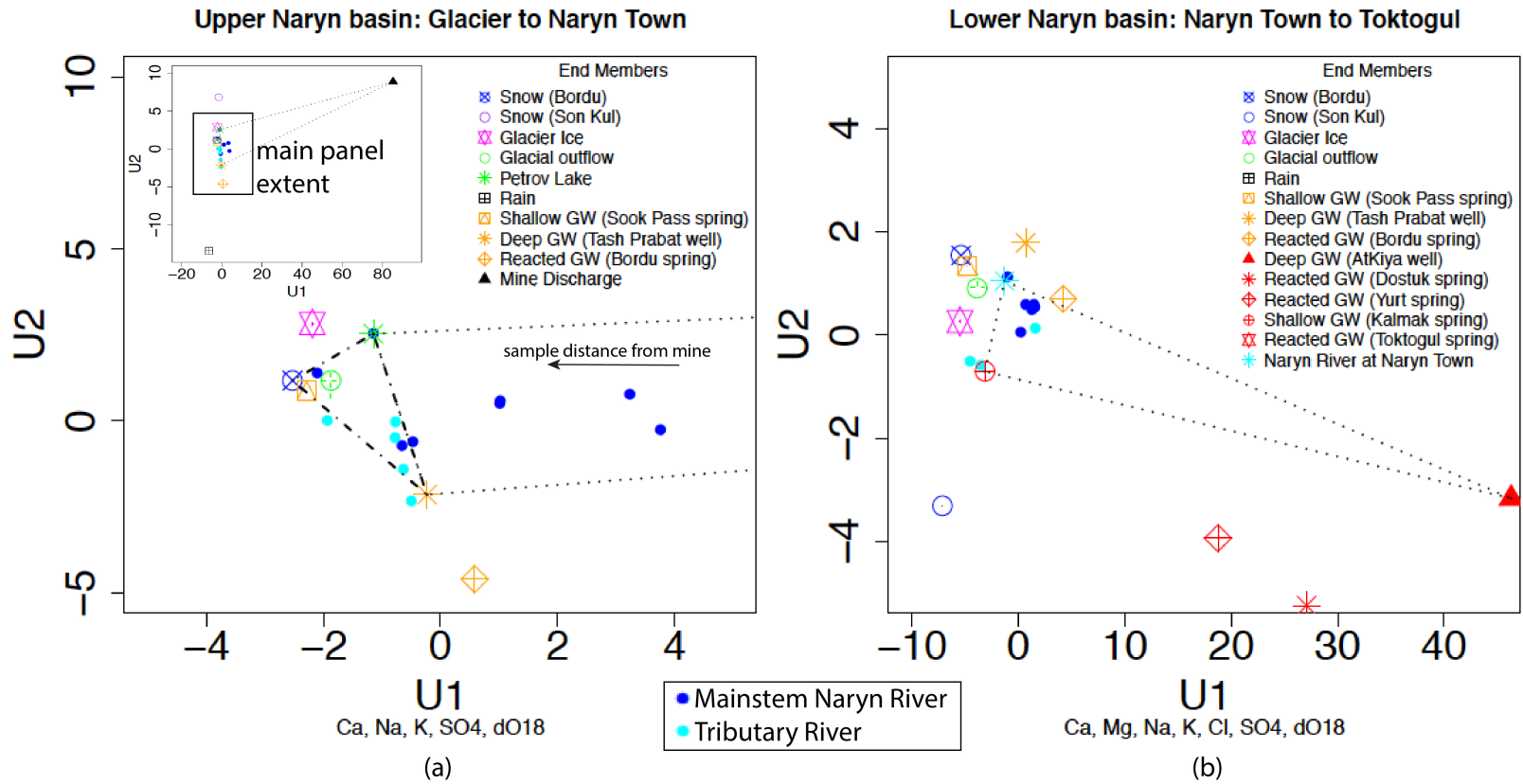


Figure 3.5: EMMA diagrams including mainstem Naryn River and tributary samples as well as all possible end members. (a) Upper Naryn basin EMMA diagram shows the gradual dilution of mine discharge waters with increasing distance from the mine. (b) While deep groundwater does not appear to be a good geometric fit in the Lower Naryn basin EMMA diagram, it is selected due to other diagnostics (Table 3.1).

End members were selected based on the quantitative tests described in ‘Methods’ above. Decision making rationale for end member selection is shown in Table 3.1. Percent contributions of end members to river flow across the elevation gradient are shown in Figure 3.6. The headwater reach is fed by Petrov Lake and deep upstream groundwater, with an influence from the mine discharge. Petrov Lake is in essence a modified version of glacial outflow because some combination of snow and ice melt, groundwater and rain – the same combination expected to produce glacial outflow – combine to run-off and fill Petrov Lake. While in Petrov Lake, ponded water has the potential to fractionate via evaporation, somewhat modifying the isotopic character of Petrov Lake as compared to glacial outflow samples that do not experience prolonged exposure to surface fluxes in an arid climate. Petrov Lake is considered a proxy to glacial outflow in the realm of source waters while acknowledging some difference between the two end members’ isotopic signatures.

Mine discharge and Upper Naryn groundwater sources are high in some ions but not in others. While these end members have relatively higher ion concentrations, meltwaters that do not travel through the subsurface have relatively lower ion concentrations. The source waters of the most upstream site (3587m) are dominated by reacted upstream ground water and glacial outflow, with mine discharge contributions to river flow calculated to be 5% or less at all headwater sites (Fig. 3.6).

Table 3.1: Methodology and rationale for end member selection for Upper Naryn and Lower Naryn EMMA models.

REACH	Tracers used	End members	Sample used to characterize end member	End member selection rationale
UPSTREAM: From glacier snout to Naryn town	$\text{Ca}^{2+}$ , $\text{Na}^+$ , $\text{K}^+$ , $\text{SO}_4^{2-}$ , $\delta^{18}\text{O}$	Mine discharge	Mine discharge tributary	Clear explanatory power regarding chemical progression of upstream samples
		Seasonal snow	Bordu snow	Well positioned to constrain samples in EMMA diagram, acceptable Euclidean distances but important for concentration reconstructions
		Glacial outflow	Petrov Lake	Well positioned to constrain samples in EMMA diagram, Low Euclidean distances
		Reacted upstream groundwater	Tash Prabat groundwater well	Well positioned to constrain samples in EMMA diagram, Low Euclidean distances
DOWNSTREAM: From Naryn town to Toktogul Reservoir	$\text{Ca}^{2+}$ , $\text{Mg}^{2+}$ , $\text{Na}^+$ , $\text{K}^+$ , $\text{Cl}^-$ , $\text{SO}_4^{2-}$ , $\delta^{18}\text{O}$	Upper Naryn River	Naryn River above Naryn town	Well positioned to constrain samples in EMMA diagram, Low Euclidean distances, an obvious source water to downstream flow
		Reacted downstream groundwater	At Kiya well	Low Euclidean distances, EMMA diagram location encapsulates samples despite not being a 'tight' fit.
		Unreacted (lateral flow) groundwater	Kalmak spring	Well positioned to constrain samples in EMMA diagram, Low Euclidean distances



The gradual ion dilution effect observed across the elevation gradient is echoed by the gradual movement of the more downstream river samples in the EMMA diagram away from the mine discharge position (Fig. 3.5). After the confluence of the Chong Naryn and Kichi Naryn, river samples are sourced by snow, reacted upstream groundwater and Petrov Lake/glacial outflow. The rise of snow as an end member supports the idea of low-ion concentration dilution waters as the basin expands to include more snow covered area through to the confluence of the Chong Naryn and Kichi Naryn at the Chong Naryn gauge site (Figs. 3.1 & 3.3). The inflow of the more reacted Kichi Naryn tributary waters mixes with the Chong Naryn and increases some ion concentrations once again. With decreasing elevation, river sources transition from being majorly sourced by glacial outflow with groundwater as a subsidiary contributor, to the inverse just above Naryn town (Fig. 3.6). Logically, the importance of glacial waters wanes with distance from the glacier.

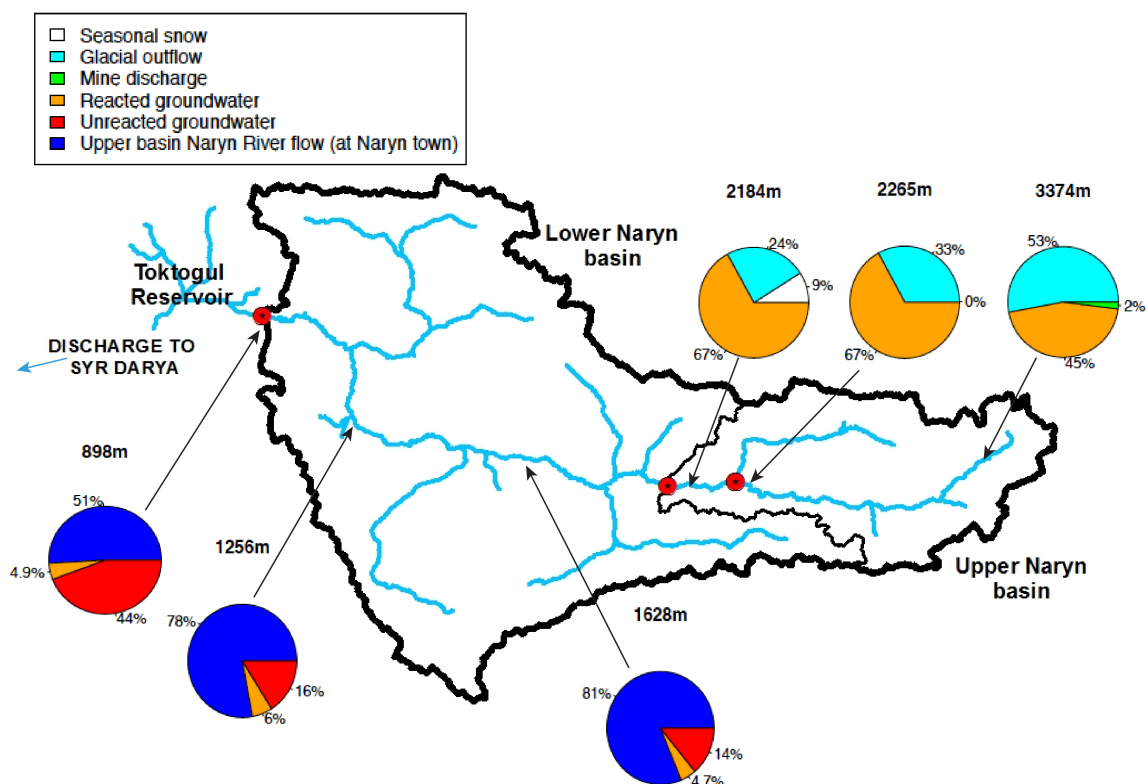


Figure 3.6: Source water separation results across the 440km study site show the importance of both meltwater and melt-sourced groundwater to river flow. Direct contributions from glacier melt wane with distance from snout.

Of note, the shallow ‘quickflow’ groundwater appears to be a similarly good fit as an end member as snow in both Euclidean distances and EMMA diagrams (Fig. 3.5a). Utilizing shallow groundwater instead of snow as an end member yields a much poorer reconstruction, including an inverse relationship between modeled versus observed isotopes. Snow as an end member appears indispensable for the mainstem above Naryn town. Tracer concentration reconstructions show significant linear fits ( $p < 0.01$  for all tracers,  $R^2 > 0.9$  except for  $\text{Cl}^-$  and isotopes) (Table 3.2), but there are some biases in the model with both under and over prediction of concentrations across tracers.

Table 3.2: Summary of  $R^2$  for modeled vs. observed concentrations based on concentration reconstructions for model validation. All reconstructions yield significant relationships ( $p < 0.01$ ). Reconstruction plots provided in supplementary information.

Analyte	Ca <sup>2+</sup>	Mg <sup>2+</sup>	Na <sup>+</sup>	K <sup>+</sup>	Cl <sup>-</sup>	NO <sub>3</sub> <sup>-</sup>	SO <sub>4</sub> <sup>2-</sup>	δ18O	δD
Downstream Naryn basin	0.92	0.43	0.95	0.95	0.68	0.95	0.9	0.78	0.77
Upstream Naryn basin	0.84	0.84	0.96	0.83	0.94	0.79	0.9	0.92	0.85

### 3.3.3.2 Lower Naryn

As with the upper basin, Ca<sup>2+</sup>, Na<sup>+</sup>, Mg<sup>2+</sup>, K<sup>+</sup>, Cl<sup>-</sup>, SO<sub>4</sub><sup>2-</sup>, δ<sup>18</sup>O were deemed to be conservative as per the diagnostic tests from Hooper (2003a). Also as with the Upper Naryn, two principal components were selected for analysis as they explain 94% of the data as compared to 78% variance explanation with 2 end members (1 dimension) (Fig. 3.5b).

Naturally, the Naryn River inflow from the Upper basin feeds the downstream reach and is an obvious end member selection for the Lower Naryn. While we treat the Naryn River inflow as an end member in and of itself, it is important to recall the composition of these waters derived from the Upper Naryn mixing model: 67% reacted groundwater, 24% glacial outflow and 9% snow. Meltwater plays an inherent role in this end member. Along with Naryn River inflow, deep reacted downstream groundwater and shallow lateral flow groundwater are the other end members. While we acknowledge that the deep groundwater point does not appear to be a geometrically tight fit to the EMMA diagram, the Euclidean distances for other end members ruled them out as compared to the selected point (Table 3.1).

The Naryn River immediately below Naryn town is naturally dominated by the Upper Naryn inflow end member at Naryn town. The system progresses to a river flow roughly equally partitioned into water coming from the Upper Naryn (51%) and downstream groundwater sources (49%) just above Toktogul Reservoir (Fig. 3.6).

Concentration reconstructions perform soundly for the Lower Naryn samples ( $p < 0.01$  for all tracers,  $R^2 > 0.84$  except for  $\text{NO}_3$ ) (Table 3.2) however under prediction and some minor over prediction of solutes/isotopes is observed.

#### ***3.3.3.3 Mixing model validation***

Primarily mixing model validation was performed via concentration reconstructions to assess adequate performance by comparing the modeled concentrations to the observed values (Table 3.2, Figure 3.7).

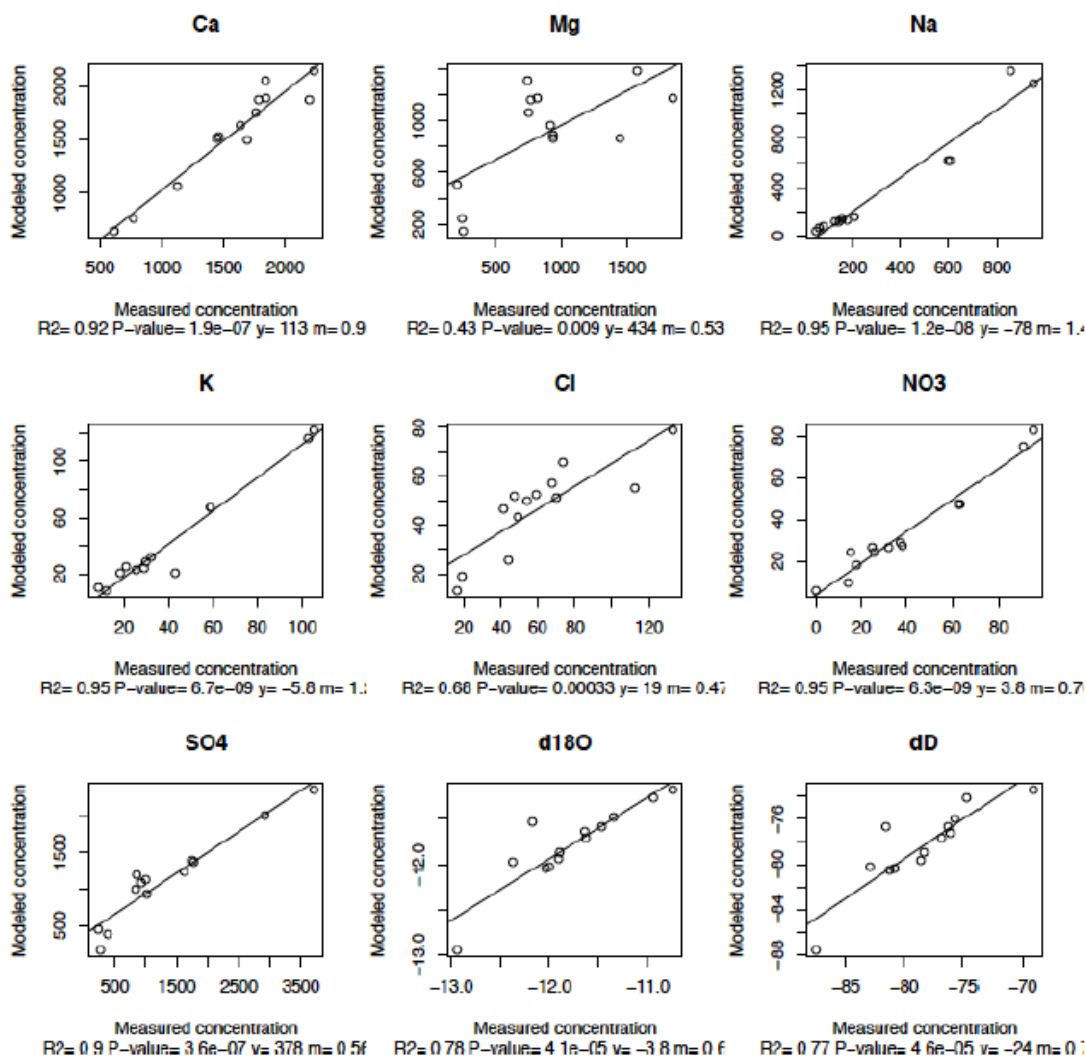


Figure 3.7: Concentration reconstructions of modeled results (y axis) for all tracers, plotted against observed values (x axis).

Model validation was also afforded on a conceptual basis by contrasting model results between diurnal samples collected at 1) the Bordu River tributary site adjacent to Bordu glacier and 2) on the mainstem Naryn above Kazarman. On the Bordu River samples were collected at 6pm and 6am at a site 3622m in elevation. While isotope values are similar during both times, lower ion concentrations in the evening support the notion of the afternoon being a time when higher melt rates contribute more snow and ice melt transferred directly to the river composition

relative to other times. The 6am sample has higher ion concentrations by a factor of 3-4 as compared to the 6pm sample. This agrees with our general understanding of diurnal fluctuations in glacial systems where melt-sourced groundwater makes up a larger portion of river flow in the early morning, after cold nights mitigate overland flow melt inputs to the channel.

Similarly, at 1328m in the Lower Naryn basin, samples were collected at 6pm and 10am on the Naryn River upstream of Kazarman town. In contrast to the diurnal hydrologic behavior of Bordu glacial stream, the Naryn River near Kazarman shows no significant variation in chemistry between early evening and mid-morning. This is an expected result given the groundwater dominated source waters of the mainstem Naryn River at this location. The agreement between these results and what we know about glacial melt patterns and larger river systems contributes to validation of Upper and Lower Naryn mixing models.

Further validation of our two-regime hypothesis is provided by poor model performance when using all samples to derive a single source water separation for the entire glacier-to-plains study domain.

### **3.4. Discussion**

#### **3.4.1 Use of EMMA over regional scales**

Use of EMMA over a regional domain, especially in data-poor mountain environments, appears to be a useful first and best shot at hydrologic characterization in areas that we currently know little (or nothing) about. Due to the large spatial domain, there are likely many small contributions from sources that are not captured in mixing models with 3 -- or even 4 or 5 -- end members. The imperfect reconstruction of concentrations from model results implies this is the case, with under and over estimates of recreated concentrations. A perfect fit is unreasonable

given that only major end members are represented in the model calculations (Liu et al., 2017). For these types of austere environments and large scale study domains, we can improve our understanding of major water sources to the river system by using sound methods with the little data we have. Unlike the melt dominated Naryn basin, systems with more complex hydrologic inputs may not be well suited to this approach.

### **3.4.2 Hydrologic controls on river flow**

The physical hydrologic results suggest that the hydrology of the Naryn basin is a headwater controlled system where both snow and glacial melt waters are an important element of sustaining river flows through direct (overland flow) and indirect (groundwater recharge) channels. As compared to the more heavily studied Eastern Himalaya where monsoon rains can supply upwards of 50% of the precipitation inputs to a basin (Kundzewicz et al., 2009) the Naryn watershed and the larger Syr Darya appear especially vulnerable to climate induced changes to snow and ice.

In the Upper Naryn, melt inputs directly contribute to surface water flows by way of both glacial outflow and snowmelt. The isotopic values for groundwater suggest that it, too, is dependent on meltwater sources for recharge, compounding meltwater's dominance in the Upper Naryn basin. In the Lower Naryn basin, meltwater likely plays a similarly prominent role albeit indirectly. While river flow at Naryn town is an end member for the Lower Naryn mixing model, embedded in this end member is an inherent combination of melt-sourced snow, glacial outflow and groundwater. At lower elevations we observe increasing ion concentrations but similarly depleted isotopic values in groundwater, suggesting that melt-sourced groundwater

may be recharged at higher elevations requiring longer, more tortuous flow paths to reach lower lying elevations.

These melt-controlled results bring to bear important questions about compounding water vulnerabilities to downstream supplies. As observed in survey responses, local awareness of shifting melt timing suggests changes the amount and timing of melt sources to river flow will affect the livelihood of agricultural workers in the Naryn basin. Forecasts for continued shifts towards earlier melt, more precipitation falling as rain than snow, and higher glacial melt rates suggest that historical patterns in melt dominated river basins are unreliable. Indications from this study that groundwater recharge also relies on meltwaters may exacerbate water vulnerability.

Groundwater has often been viewed as a buffer to water stress in times of drought, but what happens if this buffer wanes because it, too, is sourced by melting snow and glaciers? A time lag between changes to melt patterns and volumes and groundwater supplies will depend on residence times but may afford additional time to adapt to altered hydrologic norms. Awareness of these difficult-to-observe subsurface groundwater changes during the time lag could lead to detrimental groundwater drawdowns before effects are realized, and a precautionary approach to groundwater management is recommended. Ultimately, in a melt-dominated catchment such as the Naryn, climate change will inevitably induce changes in the timing and volume of river discharge and groundwater supplies.

### **3.5 Conclusion**

Current water stress for communities in the study domain is closely linked to water management practices and distribution infrastructure as discovered by the socio-hydro research



coupled with this work, but not presented here. The clumsy transition from large-scale agricultural practices during the Soviet era to individualized small plot farming now in place has led to unreliable water access in the region despite current sufficient supply. The importance of melt water supplies to both surface and groundwater suggests increased future water stress across the region. Over reliance on groundwater given the uncertain buffer provided by groundwater reserves brings about additional water vulnerability and risk, especially given the area's reliance on agriculture for human livelihood. Adaptation strategies will likely require a two-pronged approach addressing both infrastructure and management as well as increasing community resilience by diversifying income sources and farming practices in light of long term forecasts for changes to melt inputs in the context of a changing climate.

## CHAPTER 4

### **4: CLARIFYING REGIONAL HYDROLOGIC CONTROLS OF THE MARAÑÓN RIVER, PERU THROUGH RAPID ASSESSMENT TO INFORM SYSTEM-WIDE BASIN PLANNING APPROACHES**

#### Abstract

Remote, data-scarce river systems are under increased hydropower development pressure to meet rising energy demands. The upstream-downstream river continuum, which serves as a conduit for resource exchange across ecosystems, is at risk, potentially endangering the people, environments, and economies that rely on river resources. The Marañón River, one of the final free-flowing headwater connections between the Andes and the Amazon, is subject to myriad large-scale hydropower proposals. Due to challenging access, environmental data are scarce in the upper Marañón, limiting our ability to do system-wide river basin planning. Here we use remote sensing to enhance the interpretation of the first baseline dataset of hydrologic, isotopic and hydrochemical variables spanning 620km of the upper Marañón River, from the steep alpine canyons to the lower lying jungle. We capture key processes and transitions in the context of hydropower development. Two hydrologic regimes control the Marañón dry-season flow: in the higher-elevation upper reaches, a substantial baseflow is fed by groundwater recharged from wet season rains, in contrast to the lower reaches, the mainstem discharge is controlled by rain-fed tributaries that receive rain from lowland Amazon moisture systems. Sustainability of the upper corridor's dry season baseflow appears to be more highly connected to the massive natural

storage capacity of extensive wetlands in the puna (alpine grasslands) than from cryospheric water inputs. The extent and conservation of puna ecosystems and glacier reservoirs may be interdependent, bringing to bear important conservation questions in the context of changing climate and land use in the region. More generally, this case study demonstrates an efficient combined remote sensing and field observation approach to address data scarcity across regional scales in mountain basins facing imminent rapid change.

This chapter is under review for publication in *Elementa: Science of the Anthropocene* (submitted September 2017). I would like to acknowledge my co-authors Robert Stallard and Karl Rittger.

#### **4.1 Introduction**

In response to rising energy and water demands of an increasing population, agriculture, and consumptive industries, rivers are being dammed and diverted in ever more remote and pristine parts of the world. Rivers provide an upstream-downstream continuum that is critical for maintaining healthy environmental, social, and economic conditions along the corridor, and for connecting distinct and diverse ecosystems that are geographically disparate, but that share a common river passage (Vannote et al., 1980). Connectivity across ecosystems is central for a natural system's ability to respond to change (Groves et al., 2012). Hydropower potentially introduces a twofold disruption on a river system's resilience by simultaneously imposing major disturbance and physically disconnecting the river continuum.

Conserving the functioning of the river continuum is intrinsic to protecting highly valued environmental and social aspects of the river. Recent calls for a system-wide, holistic approach

to river development are gaining momentum to more accurately balance perceived economic benefits of hydropower with impacts to biodiversity, ecosystem services, and local communities (Winemiller et al., 2016). These calls, and the creative responses from federal and local governments, non-governmental organizations, and environmental groups (Bremer et al., 2016; Hartmann et al., 2013), reiterate the need to address interdisciplinary issues in conjunction with river development-proposals. Dams compromise historic biotic and abiotic regimes locally and regionally (Bruno & Siviglia, 2012; Konrad et al., 2012), so why not plan for them over the same scale?

Advocates of basin-scale water-management planning acknowledge that hydropower plays a role in the energy mix of Latin America. As compared to a narrowly focused project-by-project environmental evaluation that has been the norm for hydropower proposals (Brismar, 2004), planning on a basin scale can allow for optimizing infrastructure and site selection while mitigating impacts to social and environmental resources (Castello & Macedo, 2016; Hartmann et al., 2013; Schmitt et al., 2016). It is important that this planning process takes place before considerable financial resources have been spent on a project, because later, after financial investment has been made, the ability to alter hydropower development proposals (Fearnside, 2002) or reject them altogether (Sadler, 2000) diminishes drastically.

Basin-scale planning, however, requires up-to-date, spatially explicit, accessible data for inventorying environmental and social landscapes (Hartmann et al., 2013). Limited data is a common challenge for scientists and planners studying remote river systems subject to current development pressures. Generally more easily accessible hydropower sites have been prioritized for development, with remote mountain rivers that pose technical construction and energy transmission challenges now being targeted to meet increasing energy demands. Because of

difficult access and steep terrain, field data and hydrologic monitoring records are deficient in many remote montane watersheds. Compounding field-data scarcity is a lack of financial support for research and science in project host countries that further limits the ability of local researchers to engage in such studies. Filling gaps in our knowledge of core data sets for key biophysical variables, such as flow, sediment transport, and biodiversity, is required to understand the upstream-downstream linkages across regional basins (Groves et al., 2012). More recently, remote sensing imagery holds promise to additional data but cloud cover in mountain regions often provides only intermittent clear-sky acquisitions for optical sensors while passive microwave sensors can see through clouds but perform poorly in forests (Chang et al., 1996; Foster et al., 1997), and saturate for deep snowpack (Chang et al., 1987).

The Marañón River, which drains the eastern flanks of the Peruvian Cordillera Blanca, is one such poorly studied, yet highly important, river corridor under strong development pressure. Since the 1700s the Marañón River, when compared to the longer, but lower discharge, Ucayali River, is a major headwater source of the Amazon River (Lee et al., 2014), and it is one of the last major free-flowing connections from the glaciated crest of the Peruvian Andes to the Amazon jungle. As many as 81 dams have been proposed for the Marañón River and its tributaries (Finer & Jenkins, 2012), with plans for construction of 20 large dams on the mainstem itself as part of the Peruvian government's Supreme Decree for the Marañón River, passed in 2011 (Hill, 2015).

After many years of aggressively pursuing pre-development site studies, in 2017 dam developers shelved plans of some of the originally proposed large projects on the Upper Marañón River including Chadin2, Rio Grande 1 and 2 and Lorena (the latter formally called Rentema). This postponing is the result of multiple factors including corruption scandals and

financial instability of the dam developer, Odebrecht, low energy prices due to a current surplus of supply, and local community opposition (Casey & Zarate, 2017; Cholan, 2015; Lo Lau, 2016). In contrast to these stalled projects, the Veracruz dam proposal on the upper Marañón, which is not owned by Odebrecht, is poised to commence when economic conditions are ready. The current Peruvian government is not publicly supporting dams in the lower-lying Amazonia but has also not passed binding legislation prohibiting dam development over the long term (Belling, 2016). A change in the economic or political environment in Peru's mining sector, broader energy markets, and federal government may reactivate some dam proposals.

The need to increase our holistic understanding of the important Marañón corridor remains throughout the changing development climate. Recent work shows the profound sediment trapping effect the proposed Pongo de Manseriche Dam (downstream of our study region) will have on the sediment and nutrient fluxes on the Marañón and in Amazonia (Forsberg et al., 2017), but we still lack core biophysical data sets on the upper Marañón to enable an informed development process. This includes records of biodiversity, hydrologic variables, and sediment transport above Pongo de Manseriche to begin to address basin-wide questions and fill the data gaps.

Hydrology is particularly important to system-scale planning because it provides the context for ecosystem geography, sediment dispersal, water quality, and human-development patterns along the river. This paper focuses on a dry-season transect to help fill a hydrologic data gap for the upper Marañón River by identifying key hydrologic processes and transitions in the context of hydropower development. We address these goals:

1. Map intra-basin geographical variations in precipitation inputs and cryospheric resources to better understand the role that new water plays in the basin's water resources.

2. Utilize hydrochemical and isotopic data from samples to describe dominant hydrologic input processes over a 1,745m elevation gradient and spanning key ecologic transitions from the arid alpine (2,100m ASL) to the humid jungle (355m ASL).
3. Clarify the relative source water contributions to the Marañón's discharge and consider potential changes to the river's long-term discharge due to climatically sensitive ice and snow resources found throughout the corridor.

More broadly, to respond to data gaps on similar rivers in remote regions, we present this case study as an example of a combined approach using field observations and remote-sensing image-processing techniques to efficiently characterize mountain-basin hydrologic controls at regional scales.

## **4.2 Study site**

The Marañón River originates at the glacierized crest of the Cordillera Blanca, an Andean sub-range with the highest concentration of tropical glaciers in the world (Kaser & Osmaston, 2002). The river flows south to north from its mountainous headwaters before it turns eastward to join the Ucayali River to form the upper Amazon River near Iquitos (Fig. 4.1A).

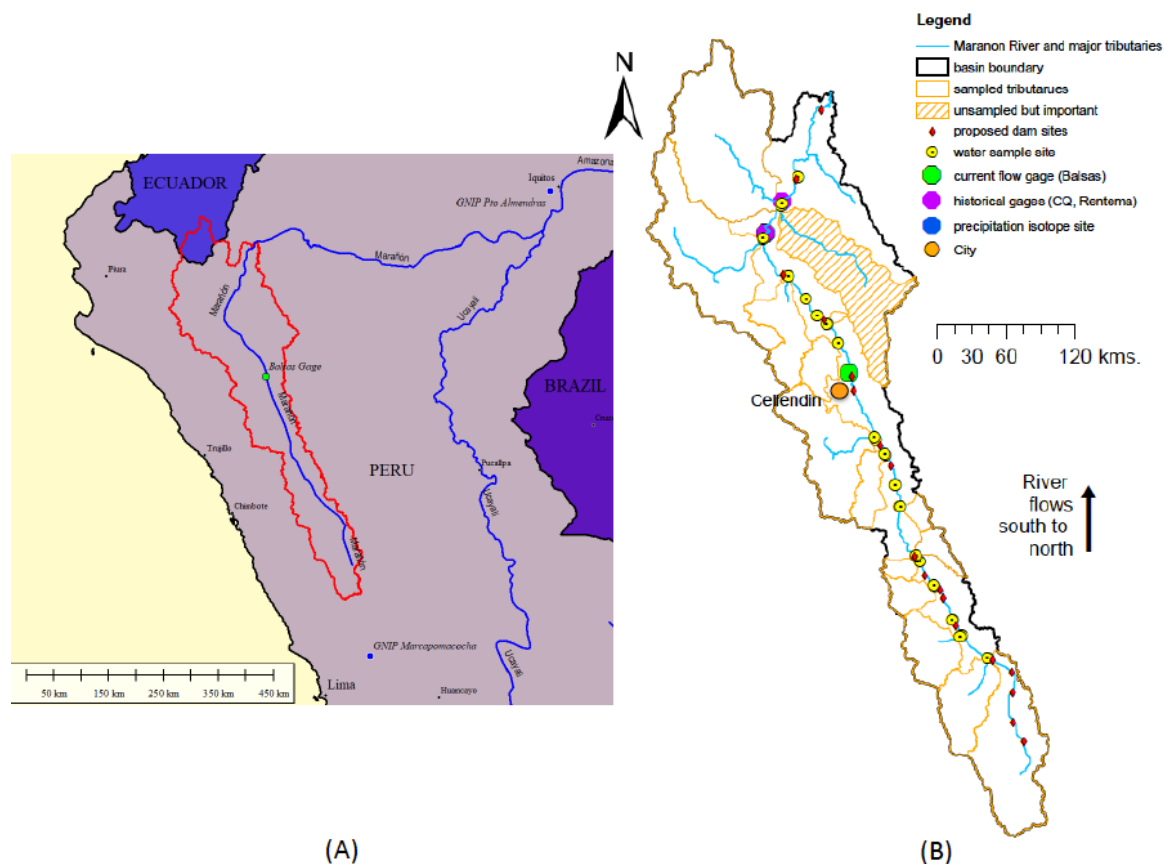


Figure 4.1: The study site spans 620km of Peru's Marañón River. (A) Regional location of study domain (red outline). (B) The Marañón River study domain including all sampling sites and proposed dam locations to date. Sampled sub-basins (orange outlines) represent tributaries sampled for hydrochemistry, whereas the hatched Utcubamba basin is a major unsampled tributary, see Figure 2 for tributary names. Discharge gages are shown as green (operational) and purple (historical). Cellendin, the largest municipality, is also indicated (orange circle). The nearest Global Network of Isotopes in Precipitation (GNIP) precipitation isotope sampling sites are the Marcapomacocha site inland from Lima and the Puerta Almendres site below the Marañón-Ucayali confluence at Iquitos (blue dots on (A)).

Our study entailed sampling at key transitions across the alpine headwaters to the humid, lush, lower-lying jungle (Fig. 4.2). For the purposes of defining and understanding these transitions, we have categorized the study domain into three reaches: alpine, transitional, and jungle zones (Fig. 4.2C). The alpine reach flows through a series of narrow, cascading and highly eroded canyons with an average gradient of 4.1m/km, whereas the transitional reach has a shallower fall (average gradient 2.2 m/km) through a combination of broader canyons and wide,



agricultural valleys. The jungle zone is characterized by lush vegetation, with the river passing through constrictions (pongos) in rugged moderate-elevation mountains, where high discharge and shallow gradient creates massive whirlpools and roller-coaster-like rapids (average gradient 0.94 m/km).

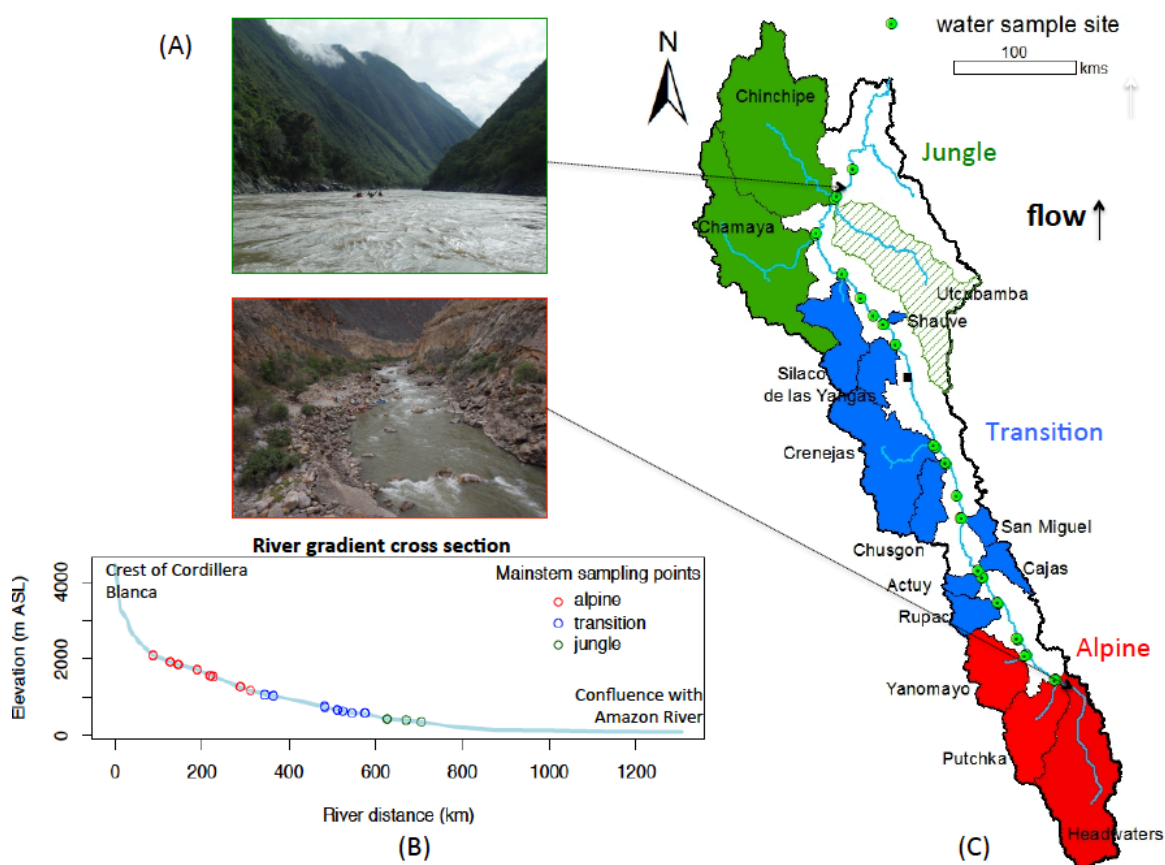


Figure 4.2: Study domain zonal designation and river sampling elevation transect. (A) Images from the edges of the study domain. The river progresses from a steep, low-volume alpine stream (bottom plate outlined in red, reference rafts on river edge for scale) to a high-volume jungle river system (top plate outlined in green, reference kayakers in river for scale). Note the difference in discharge and vegetation. (B) River transect along elevation gradient of the sampling domain. The sampling points were selected to represent the entire headwaters-to-jungle transition. (C) The study site was divided into three zones anticipated to represent different but related hydrologic regimes: alpine, transition and jungle. Sampled sub-basins are named.

The Marañón River corridor runs between two geologically distinct Andean sub-ranges (Appendix 4.1). Eastern tributaries drain the Marañón complex, comprising crystalline plutonic

and strongly metamorphosed rock. Western tributaries have geology that is dominated by a mix of younger marine sedimentary rocks (limestone, sandstone and fluvial conglomerates), younger volcanics, and some ore deposits.

Vegetation along the study site varies dramatically. The higher elevation arid zones (2,100 m) are dominated by shrublands (locally called *matorrales*) with some open montane forests. In contrast, the lush forest below 400 m is dense tropical forest as seen by the deep greens in satellite images and in Figure 4.2A (top plate). The puna ecosystem, a tropical Andean high-elevation land cover in the headwaters of the Marañón and its tributaries, is generally a combination of wetland and tussock grasslands including graminoids and forbs that is traditionally sandwiched between snowline and treeline (Young et al., 2017). Wetlands, peatlands, fens and bogs are common in alpine regions of the Cordillera Blanca, with ponded water in the wet season and still-saturated slowly draining soils during the dry season (Polk, 2016). Puna (local term for the more general ‘páramo’) is prized for its water regulation and its role as an efficient water reservoir (Hall et al., 2015; Poulenard et al., 2001) thereby providing important ecosystem services. Alpine ecosystems have been modified over time by both people and climate, with changes of vegetation character and extent in the Cordillera Blanca being driven by agriculture, temperature fluctuations, and reductions of glacial and snow melt water inputs (Polk, 2016).

Glacier surface coverage in the Marañón basin is restricted to areas that are sufficiently cold year round to allow for persistent perennial snow fields. Tropical glacier systems are highly susceptible to even small perturbations in temperature and humidity (Kaser, 1999; Wagnon et al., 1999) as well as larger climate systems (Schauwecker et al., 2014). With increasing ambient temperatures recorded from the 1970s to the present, the glacial extent in the Cordillera Blanca

has decreased rapidly over the last few decades with glacier termini moving to higher elevations especially on eastern aspects (Marañón side) of the range (Racoviteanu et al., 2008). Previous Andean studies (Baraer et al., 2012; Bury et al., 2013) show that many basins adjacent to the Marañón headwaters have undergone, or are about to undergo “peak water” (Jansson et al., 2003), a term used to describe the short term increase in glacial melt-water generation during the final loss of the frozen-water reserves as ice masses wane in a warming climate.

Glacier meltwater is reported to be responsible for the majority of stream flow in some Cordillera Blanca headwater catchments (Mark et al., 2005) and has been shown to be especially critical for dry-season discharge (Baraer et al., 2012). The percent glaciated area of headwater catchments is significantly related to the specific discharge of that basin (Mark & McKenzie, 2007), with ice melt’s role diminishing for larger basins where rainfall and snowmelt dominate. This is also demonstrated over somewhat larger scales in the Himalaya (Racoviteanu et al., 2013; Wilson et al., 2016).

Small communities with populations of generally 1,000 or less, and single-family subsistence farms occupy the banks of the Upper Marañón. Larger population centers developed adjacent to rivers on nearby road corridors many of which have existed for centuries. Celendin (pop. 14,600, Figure 4.1B), the major population center along the study transect, lies atop the deep Marañón canyon and is accessed by the only major bridge crossing the upstream reaches of the Marañón at Balsas. Celendin was the center for operations of, and opposition to, the controversial Conga mine project, one of the largest foreign-investment and energy projects proposed in the history of Peru. In April 2016, the Conga Project was put on hold due to local opposition to the project (Jamasmie, 2016). The proposed mine’s huge energy demands had in part motivated the demand for hydropower energy production on the Marañón (Hill, 2016).

### **4.3 Methods**

We used boats to collect a Lagrangian hydrochemistry data set, by following water downstream as it mixes and evolves (Moody, 1993). We sampled for 30 days, during which there were no major storms in our location that had a noticeable impact on discharge, covering 620 kilometers of the upper Marañón River in July and August 2015. This data-collection design is ideal for evaluating the environmental response to landscape and discharge as it changes with distance downriver (Konrad et al., 2012). Together with the use of remotely sensed imagery and mapping techniques, we used hydrochemistry and isotopic tracers from water samples to address study goals and to estimate tributary contributions using two-end-member mixing models. Other research activities during this study, but not presented here, included sampling for presence and abundance of freshwater invertebrates, beach pebble counts and aerial filming to use for structure-from-motion sediment quantification. This work represents the first baseline biophysical data set on the upper Marañón River.

#### **4.3.1 Sample design**

The extensive study domain necessitated prioritization of sampling locations in order to capture the diversity of sub-basins within the system in a reasonable time frame. Sampling at larger tributaries was prioritized because these represent an aggregated hydrochemical signature of significant landscapes of the upper Marañón basin. The final sampling plan aimed to achieve a balance between tributaries meeting a basin-area threshold, practicality of sampling, sample count, spatial representation over the 620-km reach, and representativeness of landscape features anticipated, based on published maps and remote sensing, to have a hydrochemical impact (e.g.,

unique geologic deposits, odd uplands, faults, geothermal source waters, etc.). Attributes of sampled sub-basins are summarized in Appendix 4.3.

### 4.3.2 Field sampling

River-water samples (n=16 mainstem, n=16 tributaries) were mostly collected in pairs to allow for rigorous mixing calculations of river discharge (Fig. 4.3, Appendix 4.2). Samples were collected upstream of the targeted confluences at locations that ensured little to no influence of hyporheic flow. Three additional samples were collected based on observed anomalies in the field: one downstream of the Vijus mine wastewater pipe (km 225), one in a low volume tufa limestone deposit on Rio Magdalena (km 437), and one at Rio Conjun (km 458) to increase representation of right bank sub-basins in the dataset.

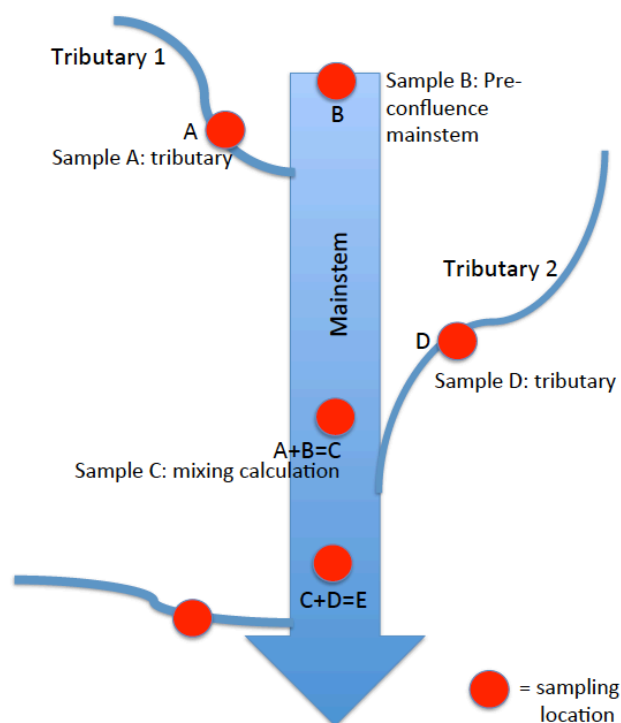


Figure 4.3: Water sampling configuration utilized to capture tributary and mainstem samples for mixing analysis. Sample design allowed for quantifying major inputs through mixing models while minimizing sample numbers.

Care was taken to access well-mixed channels for all sampling. Bottled samples were collected using 60-mL polypropylene Nalgene<sup>1</sup> bottles that were triple rinsed with deionized water, air dried on a sterile paper towel, and capped until used for sampling. A 350-mL sampling container was used for sample collection. Sample bottles and the sampling container were rinsed three times with sample water by vigorously shaking and then emptying a capped partially filled bottle. The sampling container was then filled mid-channel by plunging the opening upstream at arm's depth from the boat or from a wading individual, whichever was feasible given the river depth at that point. Ultraviolet treatment (Steripen<sup>1</sup>, 1-L sterilization) was used to disinfect the water from live biota. Sample water was filtered using a pressure syringe filtering system and 47-mm Gelman<sup>1</sup> A/E glass fiber filters with an approximate 1- $\mu$ m pore size. Three times the sample volume (3 $\times$ 60-mL) from the sampling container (350-mL) was pushed through the filter prior to filling the sterile 60-mL sample bottles. A positive meniscus was attained prior to capping to eliminate any air headspace in the sample. The sterilized, filtered samples were stored in a dark cooler for long-term transport on boats for the remainder of the expedition.

### **4.3.3 Laboratory analysis**

All water samples were transported to the University of Colorado for analysis. Instruments, methods, precisions, and detection limits for all analytes are provided in the supplementary material (Appendix 4.5). The Geological Sciences Department's Laboratory for Environmental and Geological Sciences analyzed samples for dissolved silica, copper, iron and

---

<sup>1</sup> Any use of trade, firm, or product names is for descriptive purposes only and does not imply endorsement by the U.S. Government or the State of Colorado.

cations (Calcium –  $\text{Ca}^{2+}$ , Magnesium –  $\text{Mg}^{2+}$ , Sodium –  $\text{Na}^+$ , Potassium –  $\text{K}^+$ ) by means of Inductively Coupled Plasma Mass Spectrometer (ICP-MS). The Kiowa wet chemistry lab at the Institute for Arctic and Alpine Research analyzed samples for pH, anions (Chloride –  $\text{Cl}^-$ , Nitrate –  $\text{NO}_3^-$ , Sulfate –  $\text{SO}_4^{2-}$ ) and isotopes of oxygen ( $\delta^{18}\text{O}$ ) and hydrogen ( $\delta\text{D}$ ). Stable water isotopes are reported as a  $\delta$  (per mil, or ‰) ratio of the sample to Vienna Standard Mean Ocean Water (VSMOW), calculated as:

$$\delta^{18}\text{O}, \delta\text{D} = \left[ \left( \frac{R_{\text{sample}}}{R_{\text{VSMOW}}} \right) - 1 \right] * 10^3 \quad (1)$$

where R is the ratio of stable isotopes of oxygen or hydrogen,  $^{18}\text{O}/^{16}\text{O}$  or  $^2\text{H}/^1\text{H}$  respectively.

#### 4.3.4 Two-end-member mixing models

Two-end-member mixing models were used to estimate the size of each sampled tributary discharge relative to the Marañón mainstem. This work extends a historical legacy of mixing models since one of the oldest two-end-member mixing models ever implemented was used by Antonio Raimondi in 1879 (Raimondi, 1879) to estimate the relative discharges of the Marañón and Ucayali Rivers. In the present study, the two ‘end members’ are considered to be tributary discharge and the Marañón River discharge upstream of the tributary confluence with the mainstem (Appendix 4.4). Using conservative tracer concentrations, discharge contributions from tributaries relative to the mainstem were calculated using equation 2.

$$C_a \times \text{percent flow}_a + C_b (1 - \text{percent flow}_a) = C_c \quad (2)$$

Subscripts in equation 2 relate to the sampling configuration in Figure 3, where  $a$  refers to the tributary sample,  $b$  refers to the mainstem sample upstream of the confluence, and  $c$  refers to the mainstem sample downstream of the confluence. The tracer concentration in the sample is referred to as  $C$ .

Discharge contributions were calculated for the suite of conservative tracers (ions and isotopes) analyzed in water samples yielding a range of discharge contribution fractions for each tributary. An error-weighted mean (EWM) was determined for each tributary to be used as the modeled discharge contribution for that tributary. Tributary and mainstem discharges were calculated at each sub-basin using the discharge record at the Balsas gage on August 3, 2015 ( $196 \text{ m}^3 \text{ s}^{-1}$ ), the day we passed the gage. Discharges calculations were propagated upstream and downstream from the Balsas location using the EWM percent contribution solution for each sub-basin.

Error-weighted mean is preferred over other metrics because it considers uncertainty,  $w$ , in the mixing model results due to propagated analytical error as calculated by equation 3.

$$w_{f_{trib}} = w_{f_{upstream}} = \sqrt{\frac{(w_{C_{trib}} f_{trib})^2 + (w_{C_{upstream}} f_{upstream})^2 + w_{C_{downstream}}^2}{(C_{upstream} - C_{trib})^2}} \quad (3)$$

where  $w_{C_{sample}} = w_c \times C_{sample}$  or the method detection limit (supplementary table 3), whichever is greater.

In equation 3,  $f$  refers to the fraction of discharge contribution calculated from mixing model,  $C$  is the constituent concentration,  $w_c$  is the analytical uncertainty in laboratory analysis



specific to the constituent analysis, and  $w_f$  is the analytical uncertainty propagated through to the mixing model fraction. This study did not replicate samples or perform duplicate laboratory analysis on samples due to limited sample volumes, therefore  $w_C$  is based on the annual laboratory analytical precision (percent relative standard deviation) over all runs in a year (between 4,000-6,000 samples) for a given analyte. Accordingly,  $w_C$  is the same across end members for each constituent and these values are provided in table ST3 in supplementary material.

As is evident from equation 3, mixing model calculations with two end members of similar concentrations have larger associated uncertainties than models with end members that have disparate concentrations. Error-weighted means (EWM, equation 4) allow for the lower-uncertainty mixing models to dominate the tributary discharge calculation while still considering all model results across analytes.

$$\text{error weighted mean}_{\text{tributary}} = \frac{\sum \frac{f_{\text{tributary}}}{(w_{f_{\text{tributary}}})^2}}{\sum \frac{1}{(w_{f_{\text{tributary}}})^2}} \quad (4)$$

To understand the most influential constituents in the EWM calculation, we calculated an “influence metric” using equation 5 for each constituent. This provides additional guidance for hydro-chemical interpretation for results.

$$\text{influence}_{\text{constituent}} = \frac{\frac{1}{(w_{f_{\text{tributary}}})^2}}{\sum \frac{1}{(w_{f_{\text{tributary}}})^2}} \quad (5)$$

Total error to the final EWM mixing fraction integrates error across constituents and was calculated as follows (equation 6):

$$w_{f, Total} = \sqrt{\sum_{all\ constituents} (w_{f_{tributary}})^2 \times influence} \quad (6)$$

To evaluate mixing model performance for all mixed mainstem samples concentration reconstructions were computed using the EWM solution. Normalized error for each sample was calculated to compare reconstructed concentration with observed concentrations (equation 7) and to examine model bias, if any.

$$normalized\ error = \frac{modeled\ C - observed\ C}{observed\ C} \quad (7)$$

#### 4.3.5 Discharge data

Discharge gages at three locations on the upper Marañón River recorded data over varying historical periods (Figs. 4.1B): 1) Balsas (855m ASL) from 2015-present, 2) downstream of the Chamaya River confluence at Corral Quemado (CQ, 410m ASL) from 1977-1981, and 3) downstream of the Chinchipe and Utcumbamba confluences at Rentema (355m ASL) from 1977-1981.

The Balsas gage recorded discharge during the 2015 study period however there are no on-going discharge records downstream of Balsas. To understand the relationship between Balsas discharge and discharge records at CQ and Rentema, we examine multi-year average historical discharges for 1977-1981 at CQ and Rentema as compared to a smoothed historical-

average discharge at Balsas. The smoothed Balsas hydrograph is reconstructed from graphs presented in the 2014-2015 Peru Ministry of the Environment National Meteorological and Hydrologic Service (SENAMHI) hydrologic monitoring report (Servicio Nacional de Meteorología e Hidrología del Perú (SENAMHI), 2015).

#### **4.3.6 Precipitation**

The 620 km, south-north, linear Marañón River flows through varying hydro-climatology regimes related to elevation gradients and river distance from headwaters. Climate monitoring stations in the Peruvian Andes are sparse, and those stations with precipitation data cover time periods that often do not overlap. To better characterize precipitation distribution over the Marañón basin we used the WorldClim data set (version 1.4) (Hijmans et al., 2005). WorldClim utilizes an interpolated spline algorithm to produce global maps of terrestrial climate from weather station data that adequately represent spatial climate variations, even over remote data-scarce regions. Monthly average precipitation inputs over the length of the dataset (1960-1990) were calculated at 30-arcsecond resolution (~0.93 km at the equator). These gridded monthly means were averaged at the sub-basin scale to assess the range of precipitation inputs to major tributaries across the Upper Marañón basin.

Rain samples were not collected during the study; however, a monitoring site of the Global Network of Isotopes in Precipitation (GNIP) (IAEA/WMO, 2016) is located at 4477m ASL at Marcapomacocha near the Marañón headwaters and was used to provide representative rain isotopic values for precipitation inputs to the upper elevations of the Marañón basin (Figure 4.1A). Similarly, no GNIP record exists for the lower elevations within the study domain, however the Puerto Almendras at Iquitos GNIP precipitation record near the eastern extreme of

the Marañón basin (98m ASL) provides representative isotope values for lower elevation, Amazonian precipitation systems likely to affect the lower sub-basins of the Marañón.

#### **4.3.7 Meltwaters**

Standard snow maps that exploit band difference ratios of snow surfaces (Dozier, 1989) classify a pixel as either snow covered or snow free. Their performance is degraded in alpine environments such as the Peruvian Andes where mixed land cover pixels are common at NASA's Moderate Resolution Imaging Spectroradiometer (MODIS) satellite (Justice et al., 1998) resolution (500m pixel size). Spectral un-mixing algorithms that calculate the snow cover fraction of each pixel (Nolin et al., 1993; Rosenthal & Dozier, 1996) yield snow maps that are more accurate and exhibit less sensitivity to different land cover types (Rittger et al., 2013). Snow cover maps were created using the MODIS Snow Covered Area and Grain Size (MODSCAG) algorithm (Painter et al., 2009) to estimate fractional snow cover. We quantify the probability of snow cover in a given pixel by calculating the number of positive observations divided by the total number of clear-sky observations over the 2001-2014 period. Snow probabilities are then averaged over all pixels in each sub-basin to understand the overall influence that snow may have on a water sample taken just above the sub-basin's confluence with the mainstem Marañón.

Given the difficulty in separating snow from clouds with MODIS data (Rittger et al., 2013), we ignore snow probabilities less than 30% and re-set all pixels with probabilities under this threshold to 0. Doing so potentially biases lower elevation sub-basin snow cover statistics where pixels hovering just below 30% snow cover probability are brought to 0. This bias is not anticipated to impact results in this study because precipitation amount, not elevation, dictates

snow cover. The inverse snow cover probability-elevation relationship is observed whereby lower-elevation sub-basins, which receive abundant precipitation, have the highest mean snow cover probability across the study domain.

The Randolph Glacier Inventory (RGI) (Pfeffer et al., 2014) was used to map and quantify glacier surface areas in the Marañón Basin using glacier area data for the Cordillera Blanca (submitter analysts Cogley et al., 2015; Racoviteanu, 2007) and geographic information system (GIS) software. RGI is a processed subset of the Global Land Ice Measurements from Space (GLIMS) (Raup et al., 2007) glacier monitoring project.

## **4.4 Results**

### **4.4.1 Hydro-climatology**

The Marañón basin undergoes pronounced seasonal swings in precipitation, melt patterns and river discharge. During the dry season (June-September) World Clim monthly mean precipitation decreases in all areas, but lower elevation sub-basins are noticeably wetter (47-122 mm rain/month) than upper sub-basins (10-28 mm rain/month) (Fig. 4.4). During the wet season (October-March) the difference in magnitude of precipitation between lower and higher elevation basins is not as large as the dry season. Peak mean monthly precipitation occurs in March (118-178 mm/month) for all sub-basins (Fig 4.4A).

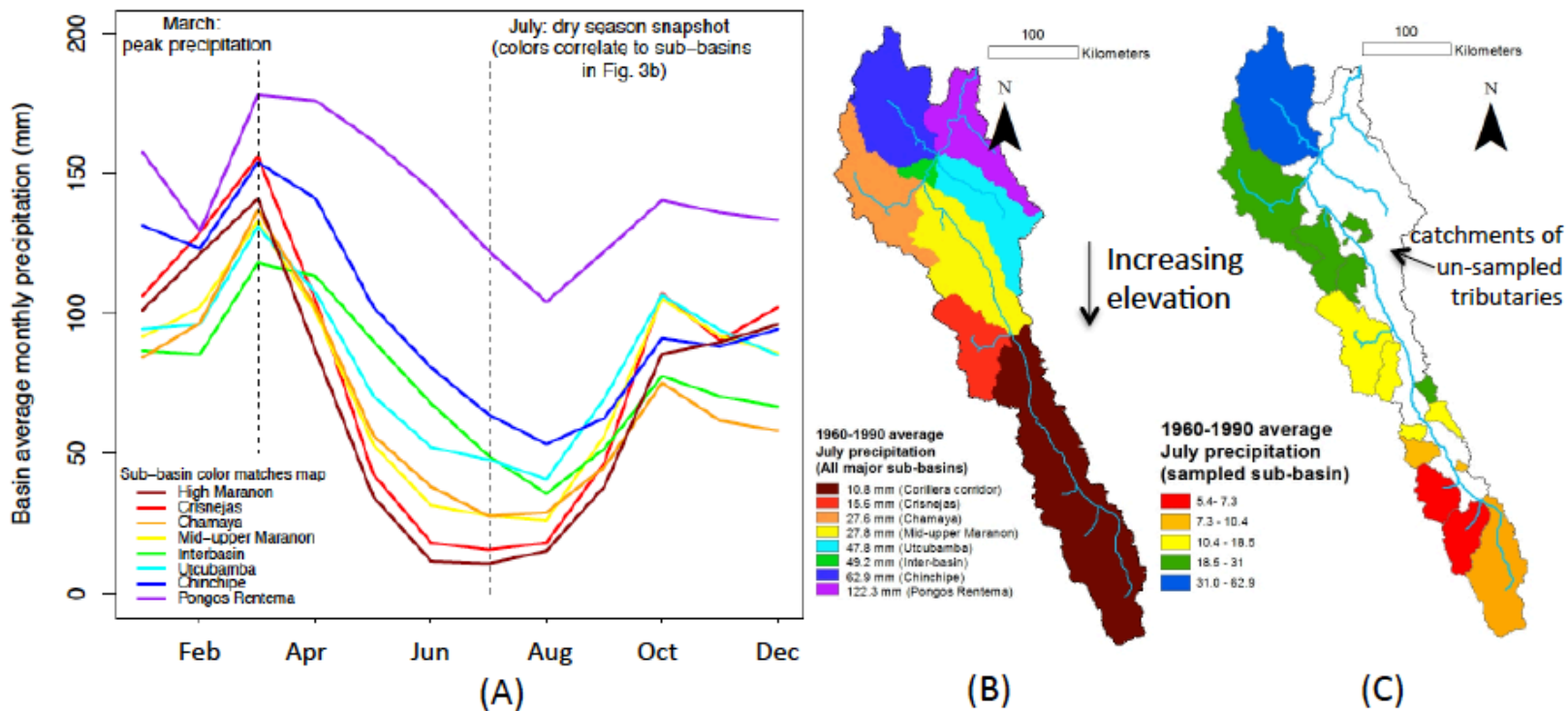


Figure 4.4: Precipitation patterns across the Marañón basin. (A) Mean precipitation calculated for major sub-basins across the upper Marañón basin show a drier trend at higher elevations (southeastern region of the basin) year round as compared to lower lying watersheds. This geographic behavior is accentuated during the dry season as demonstrated by average precipitation values calculated across watersheds for July (right dashed vertical line) in (B) major sub-basins and (C) sampled sub-basins. Line colors in (A) match basin colors in (B). In (C) white areas represent tributary watersheds of the upper Marañón basin that were not sampled.

Discharge recorded at gages (Fig. 4.5A) observes a ‘flashy’ or rapid response to individual storms in hydrographs across the catchment (Fig. 4.5B). Rentema discharge peaks appear to be strongly affected by localized storms in the low-elevation, high-discharge tributaries, Chinchipe and Utcubamba rivers (blue and cyan in Fig 4.4B, respectively). The Chamaya basin (orange in Fig. 4.4B) measured at Corral Quemado (CQ), exhibits a subdued flashy behavior compared to Rentema that is consistent with the lower rainfall there. The three large lower basins, Chamaya, Chinchipe and Utcubamba, are hereafter referred to as the lower-lying basins (LLB). Dry season in the LLB is in August and September, with rain events and resultant discharge peaks that are smaller than at other times of the year.

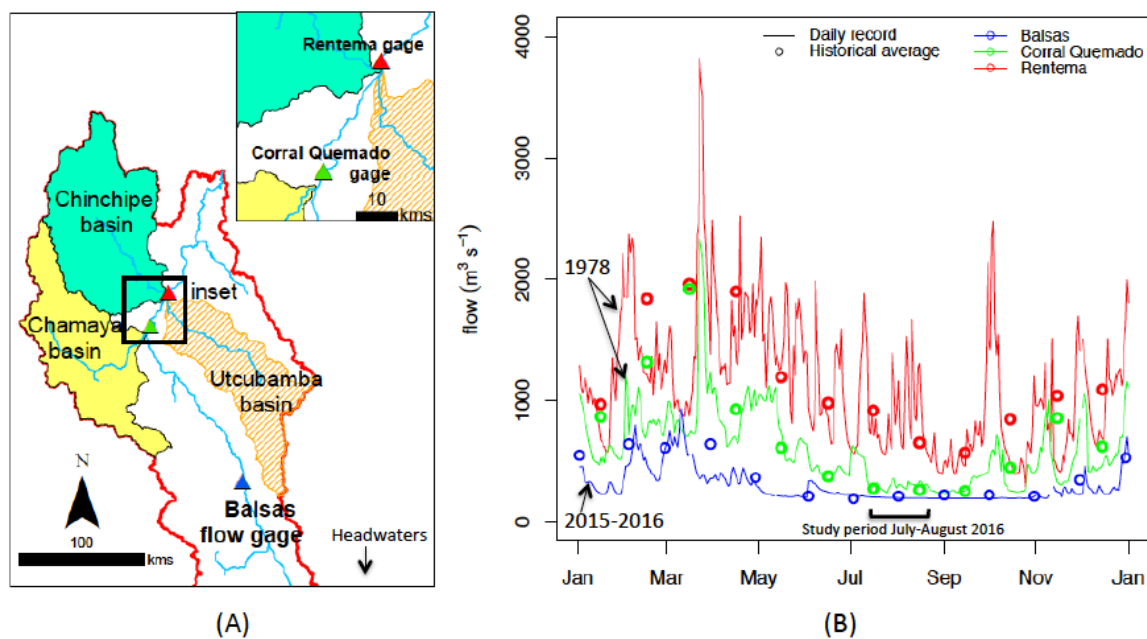


Figure 4.5: Marañón River gage locations and discharge records. (A) The only operational discharge gage in the study domain is located at Balsas (blue triangle). Records were previously kept in the late 1970s and early 1980s at Corral Quemada (green triangle) and Rentema (red triangle), which is downstream of several high-discharge tributaries. (B) Representative daily discharge records are shown for 1978 (CQ and Rentema) and 1 June 2015 – 31 May 2016 for Balsas. Four-year monthly averages (dots) for CQ and Rentema gages are shown for the period

of record, 1977-1981. Balsas historical average was recreated from the 2014-2015 Peru Ministry of the Environment National Meteorological and Hydrologic Service (SENAMHI) hydrologic monitoring report. Discharge records indicate a highly responsive catchment, with events at lower elevation causing high variability year round while higher elevations demonstrate little-to-no new inputs during the dry season such as during the study period (bracketed).

In contrast, high-elevation catchments demonstrate few dry-season discharge peaks due to a general lack of storms over this period (Fig. 4.5B). Despite little precipitation during the June through September dry season, the higher-elevation reaches of the Marañón have an impressive  $200 \text{ m}^3\text{s}^{-1}$  baseflow suggesting substantial groundwater or meltwater contributions throughout the dry season. The water storage of approximately  $1.5 \text{ km}^3$  is required to sustain this baseflow for the three-month dry season and equates to nearly 3.5 times the volume of California's Hetch Hetchy reservoir at maximum capacity.

The smoothed monthly average historical discharge record at Balsas indicates the discharge during the study period was within its normal range and that discharge observed at this location is considerably less than the discharges of CQ and Rentema (Figs. 4.5, 4.11).

The fractional contribution of meltwaters from snow and ice varies considerably across the basin. Snow presence at the sub-basin scale in the Marañón corridor is surprisingly not controlled by elevation ( $p=0.12$ ,  $R^2=0.10$ ) but is instead shows a stronger influence by dry season precipitation (July and August,  $p=0.03$   $R^2=0.24$ ). For example, Chinchipe, the sub-basin with the highest mean snow probability (19.65%) has the lowest mean elevation (1692m ASL) and the highest average July precipitation (62.9mm) (Fig. 4.6). In contrast, the two sub-basins with the highest mean elevations, Putchka (3993m ASL) and Headwaters (4031m ASL), have modest mean snow probabilities of 5.24% and 5.22%, but average July precipitation of less than 10mm.



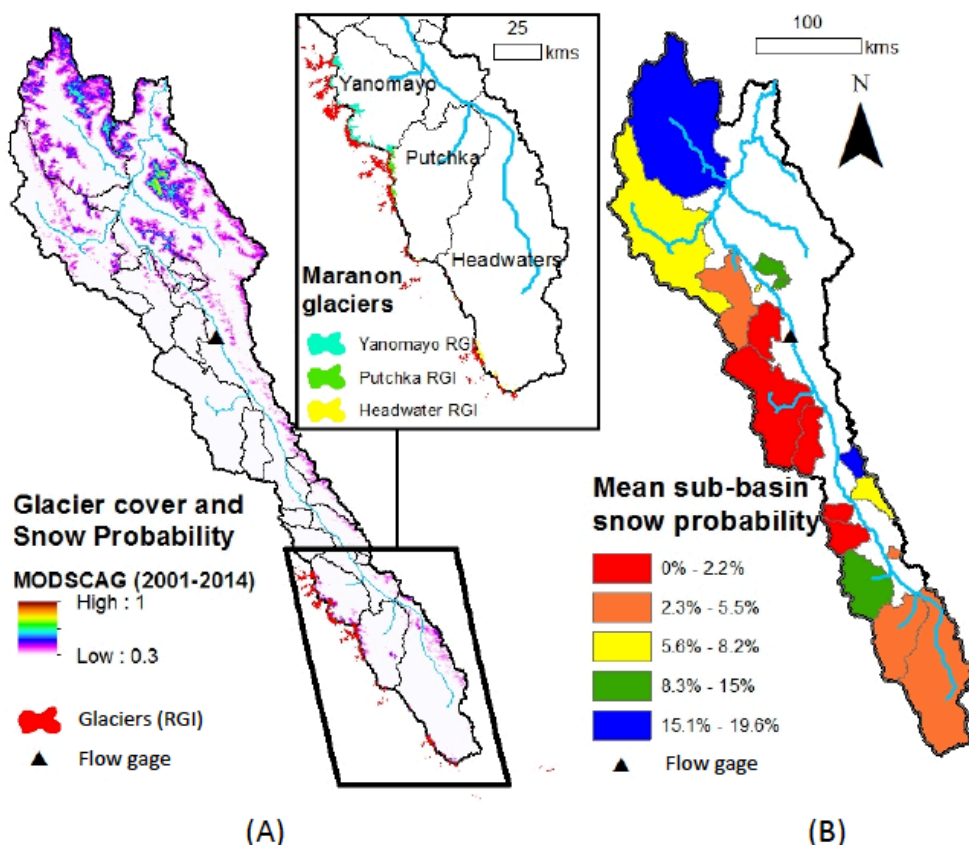


Figure 4.6: Cryospheric inputs to the Marañón basin. (A) Snow and ice cover throughout the study domain. Inset: Glaciers are present in three high elevation basins: Yanomayo, Putchka and the uppermost Marañón basins. (B) Mean snow probabilities for each of the sampled basins indicate generally that lower, wetter basins have a greater chance for snow cover than higher (colder) and drier basins suggesting precipitation amount – not temperature – control snow cover.

Only the three highest elevation sub-basins have glacial sources: Yanomayo, Putchka, and Marañón headwaters. The percent (area) of these sub-basins that is glacier covered ranges from 0.43% (27.6 km<sup>2</sup>) in the Marañón headwaters to 4.66% (105.8 km<sup>2</sup>) in the Yanomayo basin (Fig. 4.6A). Total glacier-covered area in the study domain is 168.5 km<sup>2</sup>. Glacier mass balance budgets are dominated by exchanges on the glacier surface (snowfall and melt) (Cuffey & Paterson, 2010) suggesting low seasonal snow occurrence in the high elevation glacierized sub-basins is unlikely to reverse glacial ablation trends in the basin.

#### 4.4.2 Isotopes

The Marcapomacocha GNIP station data demonstrates the temporal variability of precipitation isotopic composition throughout the year and is also used to determine the local meteoric water line (LMWL) for the Marañón headwaters (Fig. 4.8). This station is located at 4,477m ASL in an arid alpine environment similar to the headwaters of the Marañón. At the Marcapomacocha site, the wet season (October-May,  $\delta\text{O}18$  ranging -18.9‰ to -15.2‰) is more isotopically depleted than the dry (June-September,  $\delta\text{O}18$  ranging -10.7‰ to -7.1‰) (Fig. 4.7A, left bars). Precipitation isotopes in the jungle are more enriched than in the alpine as demonstrated by the Puerto Almendras-Iquitos GNIP record at 98m ASL (Fig. 4.7A, right colored bars).

Marañón basin surface-water isotopic values fall within the range of alpine GNIP precipitation (Fig. 4.7A), with high-elevation mainstem and tributary isotope values more closely related to wet-season alpine precipitation than dry-season precipitation, indicating the marginal role of dry-season rain in the high elevation water balance and the likelihood that wet season precipitation is stored in natural reservoirs for dry-season release. Prevailing air masses during the June-September dry season come from south easterly trade winds that move  $\delta\text{O}^{18}$ -enriched recycled moisture from the Amazon Basin into the Andes (Windhorst et al., 2013). The dry-season isotopic values in the jungle LLBs are consistent with receiving moisture from the Amazon lowlands to the east.

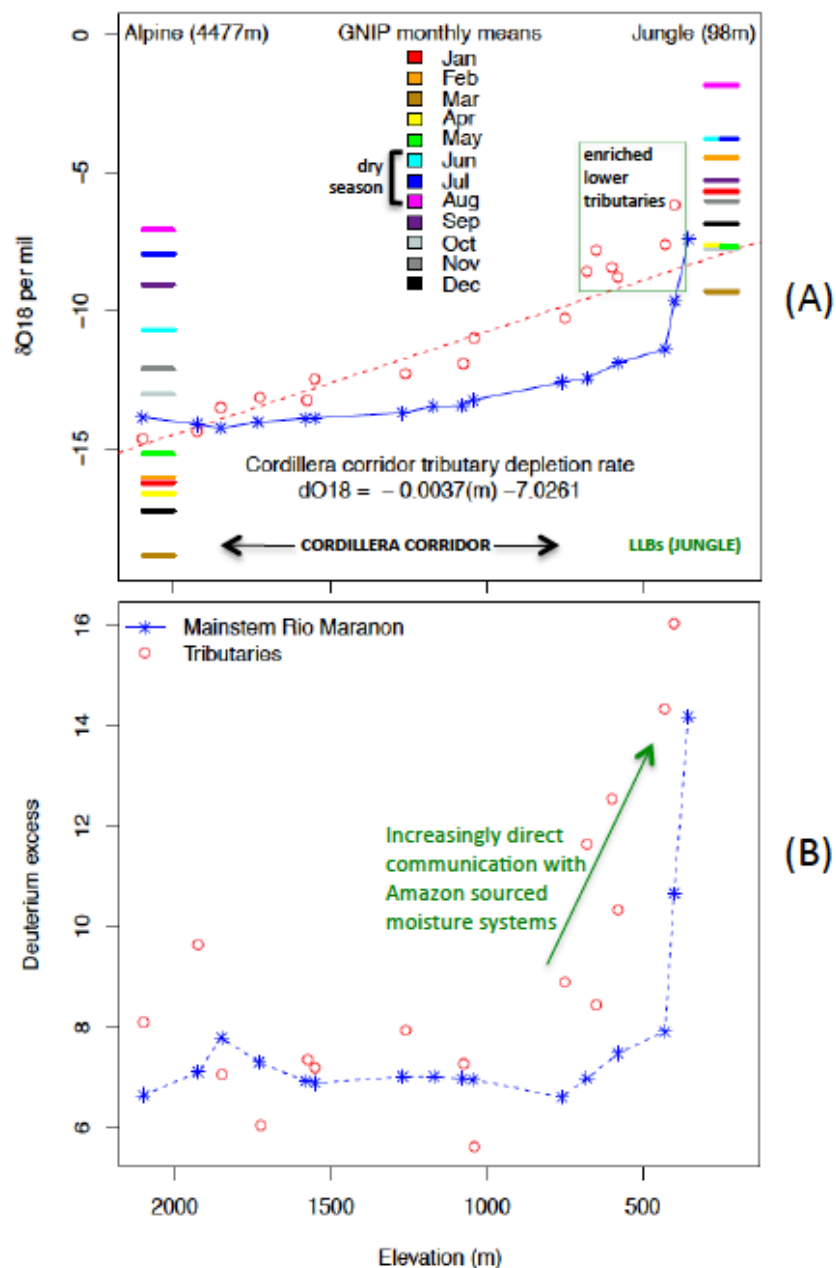


Figure 4.7: Stable isotope and deuterium excess progression across the study domain. (A) Stable isotope enrichment and (B) increasing Deuterium excess are related inversely to elevation. A clear influence of the high-discharge rain-fed basins below 430m is observed. In (A), Global Network of Isotopes in Precipitation (GNIP) monthly mean isotope values indicate a contrasting temporal variation of precipitation isotopes throughout the year between alpine (left edge) and jungle (right edge) records.

The isotopic character of the sub-basins' surface waters can be grouped into two regimes: the middle and upper sub-basins have confining slopes adjacent to the river (hereafter referred to as the Cordillera corridor), and the LLBs are rain-fed jungle tributaries with catchments more directly accessed by Amazon moisture systems. The Cordillera corridor tributaries show a gradual  $\delta\text{O}^{18}$  isotopic enrichment with decreasing elevation from -14.67‰ to -10.31‰. Enrichment of  $\delta\text{O}^{18}$  in the mainstem is observed with mixing of progressively enriched tributary inputs from below the confluence of the Putschka River at 1,850 m (-14.25‰) to the final sampling point at Montenegro (-7.41‰). The smaller tributaries in the upper reaches result in a gradual, incremental enrichment of the mainstem Marañón. In contrast, the abrupt isotopic enrichment of Marañón water downstream of the Chamaya confluence at 430 m ASL (Fig. 4.7A) is consistent with large-discharge, Amazonian sourced inputs from the isotopically enriched Chamaya, Chinchipe and Utcubamba tributaries (LLBs, Fig. 4.11).

Downstream enrichment through the Cordillera corridor suggests the elevation effect (Dansgaard, 1964) is a contributing factor to the isotopic gradient of Marañón waters (Fig. 4.7A). Precipitation isotopic signatures affected by altitude are the result of squeezing out of moisture from an air mass as air is adiabatically cooled while rising to greater elevations (Gat, 1996). In precipitation, heavier isotopes (e.g.,  $\text{O}^{18}$ ) are removed preferentially over lighter isotopes (e.g.,  $\text{O}^{16}$ ), leaving behind water vapor that is progressively more depleted by heavier isotopes as it moves up in elevation.

Previous Andean studies have shown spatial variability of isotopes is dominated by the elevation effect, with an range of depletion rates reported from -0.17‰ per 100m (Garcia et al., 1998) to -0.24‰ per 100m (Gonfiantini et al., 2001). Indeed these rates are similar to the globally established lapse rate of -0.28‰/100m (Poage & Chamberlain, 2001). In the Cordillera corridor

of the Marañón the  $\delta^{18}\text{O}$  depletion rate with elevation can be described by a linear fit correlating to an isotopic depletion rate of  $-0.37\text{‰}$  per 100m:

$$\delta^{18}\text{O} = [-0.0037(\text{meters}) - 7.0261] \quad R^2 = 0.92 \quad (8)$$

Using the above Andean depletion rates, over the 1,520m elevation change in the Cordillera corridor from the Putchka River (highest tributary at 2,100m ASL) to the Silaco River (580m ASL) the elevation change results in a depletion of  $-2.58$  to  $-3.64\text{‰}$   $\delta^{18}\text{O}$ . The actual change observed between these tributaries,  $-5.87\text{‰}$   $\delta^{18}\text{O}$ , suggests that additional factors, probably related to hypsographic effects within individual basins, contribute to the isotopic transition observed over the study domain. In addition to topographic effects, vegetation transpiration, evaporation or sublimation effects on alpine melt waters and standing water storage in the punas may affect isotopic signatures of surface waters.

Deuterium excess (D-excess), relative to the meteoric-water line, in tributary waters is significantly related to mean snow probability across sub-basins ( $p=0.01$ ,  $R^2=0.31$ ), with higher mean snow probabilities having greater Deuterium excess. This contrasts an alternative expectation of lower D-excess values in basins with higher evaporation and sublimation rates (Froehlich et al., 2001) expected from post-deposition processes in the snowier and more glaciated sub-basins. This result instead suggests the strong relationship between D-excess and snow probability is a factor of precipitation amount, moisture source and possibly water use by vegetation, but not related to post-deposition snowpack processes and this is logical given the far greater magnitude of water recirculation through the Amazon moisture systems as compared to the snow volumes associated with the tropical cryosphere. The increase in D-excess in

precipitation (indicated as the y-intercept of  $\delta^{18}\text{O}$ - $\delta\text{D}$  regressions in Fig. 8) of the LMWLs relative to the Global Meteoric Water Line (GMWL) reflects moisture recycling in Amazonia as systems travel across several thousand kilometers of humid, forested regions (Friedman, 1977; Salati et al., 1979). The Amazonian moisture system influence on precipitation D-excess is mirrored in surface waters receiving these rain inputs, as demonstrated by the rapid D-excess increase in LLB tributaries (Fig. 4.7B).

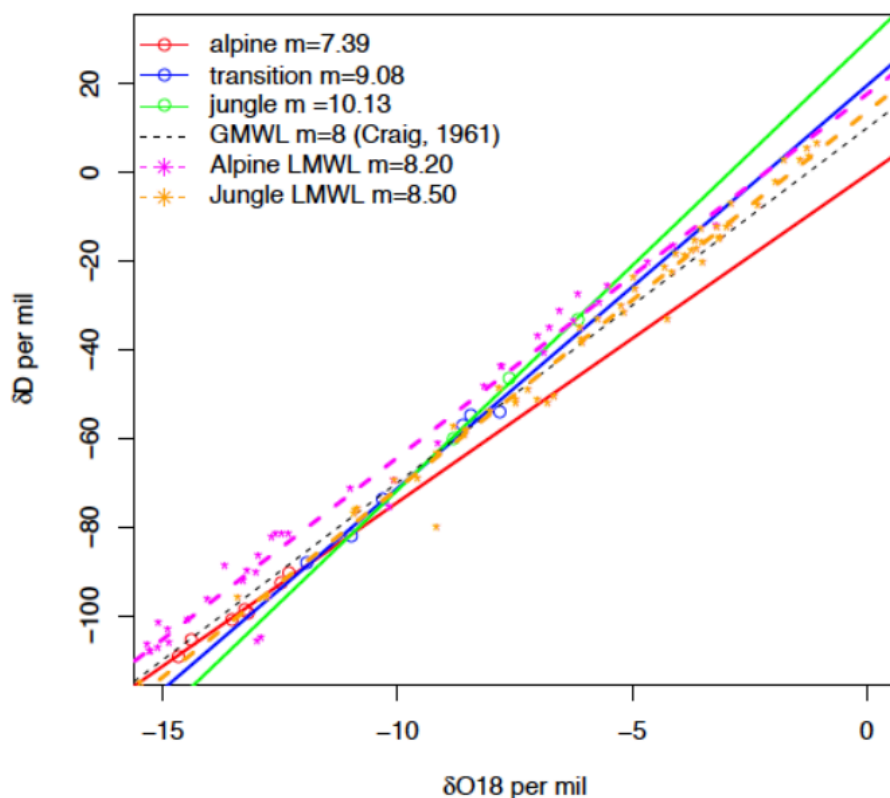


Figure 4.8:  $\delta^{18}\text{O}$  -  $\delta\text{D}$  relationship of Marañón surface waters. Data are grouped into three elevation zones (Fig. 2c), and compared to the Global Meteoric Water Line (GMWL) and the Local Meteoric Water Lines (LMWL) derived from GNIP records at high and low elevation stations. The lower slope of the  $\delta^{18}\text{O}$  -  $\delta\text{D}$  alpine tributaries as compared to the alpine LMWL indicate evaporative processes may be affecting the water signature in the upper basin, whereas this is not the case for jungle and transitional tributaries. That the LMWLs and GMWL are parallel indicate higher D excess in the LMWL, likely from moisture recycling of air masses moving across the Amazon basin.

The  $\delta^{18}\text{O}$ - $\delta^2\text{H}$  bi-plot (Fig. 4.8) also sheds light on the impact of evaporation or sublimation fluxes to the watershed because oxygen isotopes fractionate at a higher rate during evaporation and sublimation than hydrogen isotopes thereby changing the slope of the relation. The influence of evaporation and sublimation on water surfaces in the tropical Andes appears to be highly site-specific, with some studies in the region reporting a high evaporation signal (M. Williams et al., 2001) while others do not (Baraer et al., 2015; Stichler et al., 2001). Some evaporative effect is observed in the alpine samples ( $m=7.39$ ) relative to the LMWL ( $m=8.2$ ), suggesting possible importance to surface water of snow, ice, or ponded (puna) water in the alpine reach, whereas effects from transpiration are expected to be minimal due to limited vegetation in the alpine zone.

#### 4.4.3 Hydrochemistry

Ion concentrations in the mainstem Marañón generally increase as the river progresses downstream through the Cordillera corridor (Fig. 4.9) but are highly variable across sub-basins in the study domain indicating the diverse geology of the area (Appendix 4.1). Tributaries Yanomayo, Shuve, Conjun, Chamaya and Chinchipe are lower in  $\text{Ca}^{2+}$  than the mainstem, while all other tributaries are more concentrated, some by nearly a factor of two (e.g, Rupac = 3,206  $\mu\text{eq/L Ca}^{2+}$ ; Cresnejas = 3,371  $\mu\text{eq/L Ca}^{2+}$ ; Magdalena = 3,289  $\mu\text{eq/L Ca}^{2+}$ ).

A drastic dilution of the mainstem Marañón occurs with the inputs of the Chamaya and Chinchipe tributaries (Fig. 4.11), demonstrating lower solute concentrations combined with considerable volume as compared to the mainstem. Alkalinity,  $\text{SO}_4^{2-}$ , and  $\text{Ca}^{2+}$  dominate the constituents of Marañón waters (Fig. 4.9, Appendix 4.2). Jungle tributaries have a higher dominance of carbonate hardness than alpine or transitional tributaries that are balanced by other

anions other than the carbonates (Piper, 1944). Highly enriched stream waters are observed in the tufa stream at Rio Magdalena, which is also a distinct outlier in the Piper diagram (Appendix 4.2).

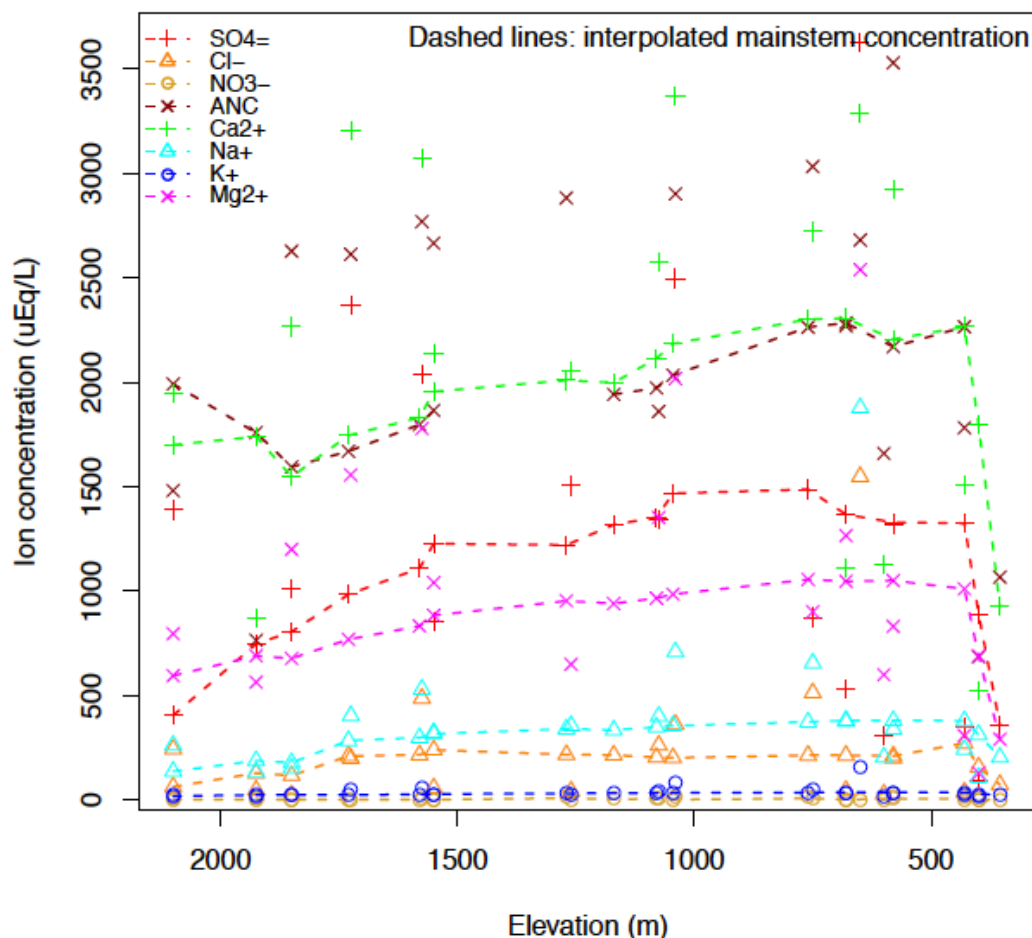


Figure 4.9: Variation of ion concentrations in tributaries and the mainstem throughout the study domain. Major ions gradually increase along the Marañón corridor with alpine and transition zone tributaries. The influx of major low-concentration tributaries in the jungle zone (Fig. 4.11) dilute ion concentrations of the Marañón below 430m ASL. Gaps in the mainstem alkalinity interpolation are due to insufficient sample quantities for lab analysis.

#### 4.4.4 Principal component analysis (PCA)

PCA consolidates multi-variable geochemical data into a data representation, capturing most of the variation of the original data with fewer degrees of freedom (the principal



components) (Christophersen & Hooper, 1992). PCA can be used to identify hydrochemical controls of the system (Fig. 4.10). Two principal components explain 74.2% of the variability in the data with the third PC adding only 8.7% additional explanation. PC1 explains 47.2% of the variability and is associated with chemical weathering products and an additional influence from evaporate deposits (Stallard and Edmond, 1983). The PC2 explains 31.0% of variability and is associated with the isotopic variables and silica. Water samples plotted on the PCA bi-plot show that controls of hydrochemical signatures vary over the different zones (Figs. 4.2C, 4.10). The 95% PCA confidence ellipses for the mean of each zone show that the alpine and jungle zones are well discriminated. As is evident, the alpine zone is highly dependent on PC1 which is related to geochemical weathering products of the catchment, whereas it is rather independent of PC2, isotopic variables. This is not surprising given the disproportionately high contribution of suspended sediments and geochemical constituents contributed to Amazon waters by the high relief areas of the Amazon basin (Gibbs, 1967; Stallard & Edmond, 1983). Geochemical weathering controls in the alpine may also indicate the importance of groundwater for sustaining dry-season baseflow. In contrast, the confidence ellipse for the jungle samples incorporating the LLBs plots along the 45-degree axis indicating this zone is affected by both components and thus weathering products, and a defined isotopic source-water signature (associated with the influence of Amazon moisture systems as discussed above), are both influential. The transition zone lies in between.

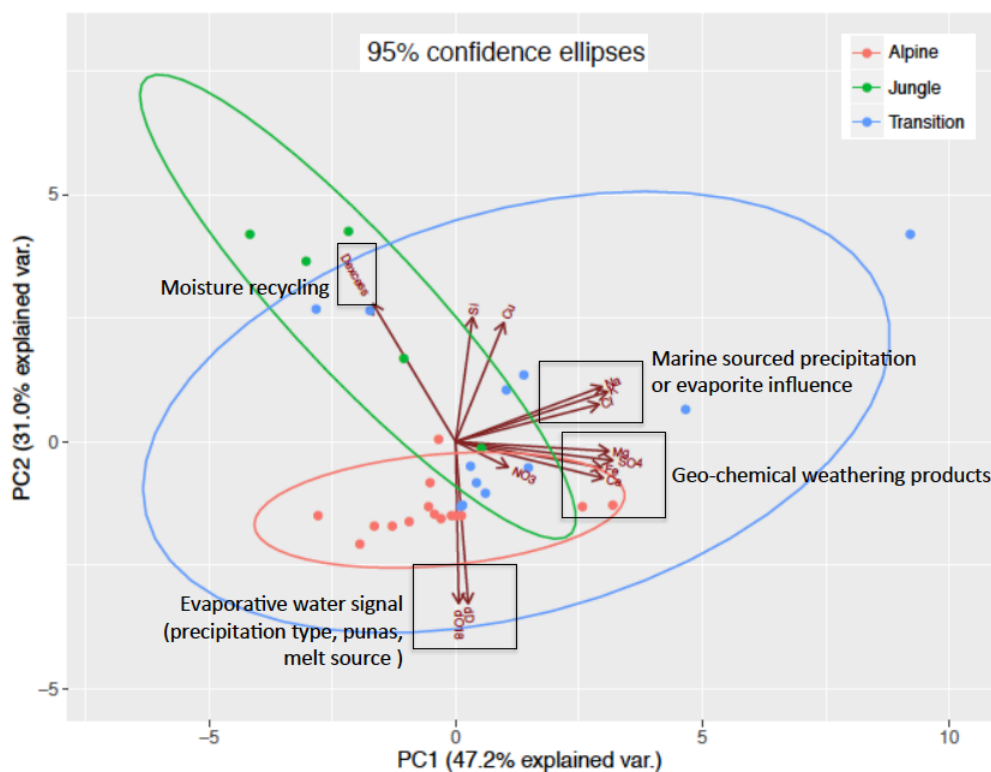


Figure 4.10: Principal component analysis indicates that controlling factors of hydrochemistry differs across zones. Principal component 1 (PC1) is described by geo-chemical weathering products and evaporates or marine sourced precipitations whereas Principal component 1 (PC2) depends on variables affecting isotopic composition (evaporative influence, type of precipitation, etc.) as well as Si. The confidence ellipses are shown for each zone and represent the 95% confidence region that the mean for each zone will be located within the ellipse.

#### 4.4.5 Tributary volumes

Using a two end-member mixing model, relative tributary volumes are calculated using a suite of conservative tracers. The error-weighted mean (EWM) of mixing model results for each tributary are shown in Figure 4.11 and Table 4.1, with less than 2% total mixing fraction error for all tributaries (0.84% mean error). Of the Cordillera corridor tributaries the Putchka, Yanomayo and San Miguel rivers contribute the most discharge to the Marañón relative to mainstem discharge at their confluence (35%, 22%, 20%, respectively). This is not entirely unsurprising given that the Putchka and Yanomayo sub-basins make up a relatively large

proportion of total basin area given their location high in the catchment. Also, the Putchka and Yanomayo sub-basins are glacierized whereas the San Miguel receives year round water from Laguna Piaz, a substantial lake 3km upstream of the Marañón confluence. The natural reservoirs (glacier ice and lake) in these sub-basins provide dry-season flow inputs absent in other tributaries. An especially significant mixing fraction result is that the Chamaya and Chinchipe rivers are major dry season inputs to the mainstem Marañón, with the discharge of each tributary nearly equaling or exceeding the discharge of the Marañón mainstem, upstream of the confluence (Fig. 4.11). The 67% discharge contribution calculated for the Chinchipe also includes the important, but unsampled, Utcubamba River flowing in from the right bank 2km upstream of the Chinchipe confluence.

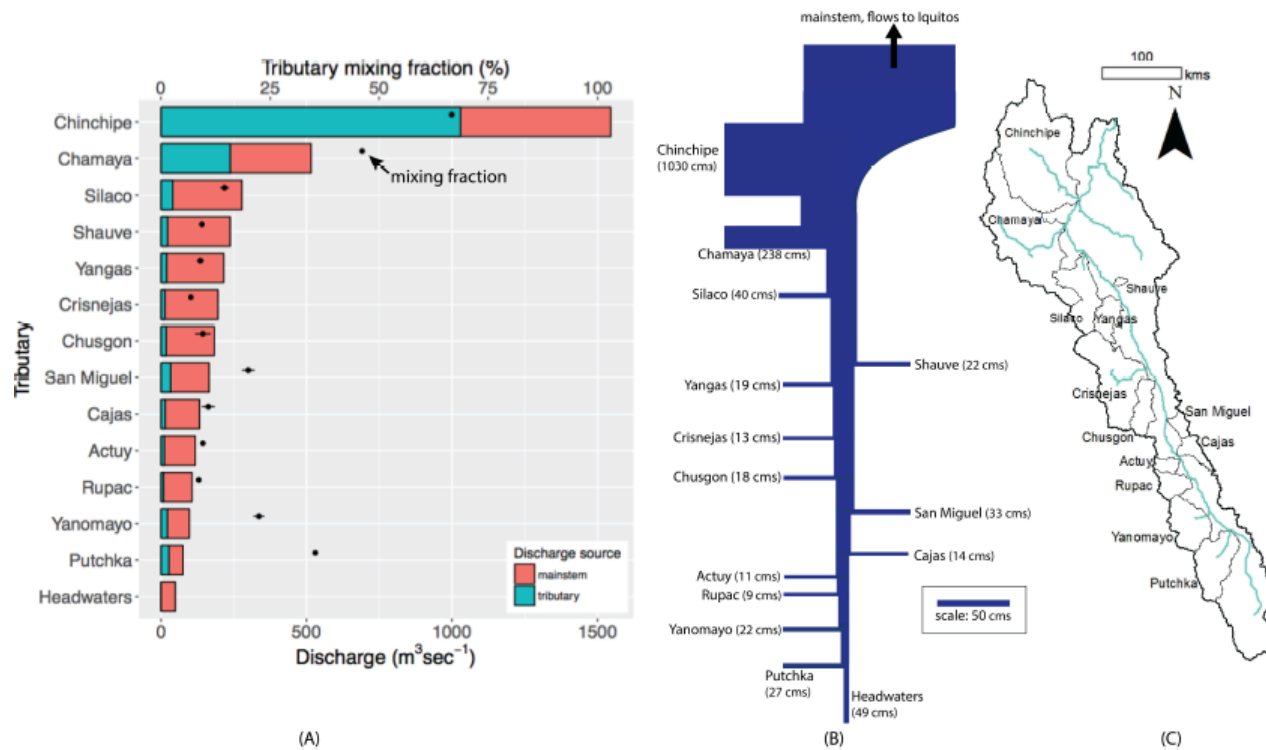


Figure 4.11: Mixing model results for tributary discharge contributions at their confluence with the Marañón. (A) Error weighted mean mixing fraction of tributaries (dots) indicates the relative proportion of flow the sub-basin provides relative to the mainstem. Whiskers identify the total propagated error to the mixing fraction. The stacked bars show approximate discharge for the mainstem and tributary flows based on the EWM mixing fraction solution and the propagated observed discharge at Balsas flow gage at the time of sampling. Although Lagrangian sampling minimizes errors, time variations of discharge cannot be captured. Moreover, tributary discharges include the named tributary plus tributaries of similar composition. Likewise, the mainstem discharge includes waters from tributaries that are similar to the mainstem in composition. The errors in Table 1 in part reflect inputs from tributaries with compositions that are dissimilar from the named tributary or the mainstem. (B) Conceptual flow diagram of the study domain demonstrating the LLB discharge dominance of the mainstem. (C) Sub-basins on map approximately aligned with vertical placement of tributaries in (A) and (B).

Table 4.1: Error-weighted mean mixing model results for tributary mixing fraction, total propagated error, and discharge results.

<b>Tributary</b>	<b>Tributary mixing model fraction (EWM)</b>	<b>Total error on mixing fraction</b>	<b>Estimated tributary discharge (<math>\text{m}^3\text{s}^{-1}</math>)<sup>a</sup></b>	<b>Mainstem discharge downstream of tributary confluence (<math>\text{m}^3\text{s}^{-1}</math>)<sup>a</sup></b>
<b>Headwaters</b>	n/a	n/a	n/a	49
<b>Putchka</b>	35.3%	0.42%	27	76
<b>Yanomayo</b>	22.4%	1.25%	22	97
<b>Rupac</b>	8.6%	0.42%	9	107
<b>Actuy</b>	9.6%	0.53%	11	118
<b>Cajas</b>	10.8%	1.47%	14	132
<b>San Miguel</b>	20.0%	1.45%	33	165
<b>Chusgon</b>	9.6%	1.81%	18	183
<b>Crisnejas</b>	6.8%	0.56%	13	196
<b>Yangas</b>	9.0%	0.84%	19	215
<b>Shauve</b>	9.4%	0.64%	22	238
<b>Silaco</b>	14.6%	1.02%	40	278
<b>Chamaya</b>	46.1%	0.35%	238	516
<b>Chinchipe</b>	66.6%	0.19%	1030	1546

<sup>a</sup> Discharge estimates propagated from flow observed ( $196 \text{ m}^3\text{s}^{-1}$ ) when passing Balsas gage on August 3, 2015.

Discharge volumes for tributaries and the mainstem at each sampled sub-basin (Table 4.1) demonstrate the similar order of magnitude of inputs provided from the Cordillera Corridor sub-basins in contrast to the LLBs. Mainstem discharge reconstructions at the historical gage locations of CQ ( $516 \text{ m}^3\text{s}^{-1}$ ) and Rentema ( $1546 \text{ m}^3\text{s}^{-1}$ ) are similar to the historical average flows at those locations in July which are estimated to be  $600 \text{ m}^3\text{s}^{-1}$  and  $1100 \text{ m}^3\text{s}^{-1}$ , respectively (Figure 4.5). The higher flow calculated at the Rentema gage site may be due to the timing of Chinchipe sampling, which occurred shortly after a precipitation event in the Chinchipe headwaters. This would result in a temporary pulse in Chinchipe discharge and a higher overall mainstem discharge at the Rentema gage site as compared to the historical July average. Notably,

the mainstem discharge increases by a factor of 31 across the domain, demonstrating the scale of hydrologic variation observed in this study.

Constituents that most influenced the EWM result varied depending on the tributary.  $\text{SO}_4^{2-}$ ,  $\text{Ca}^{2+}$ ,  $\text{Mg}^{2+}$  and  $\text{Cl}^-$  were common influential ions among most sub-basins as calculated by the influence metric (Table 4.2a). Isotopic variables,  $\delta\text{O}18$  and  $\delta\text{D}$ , were important to the EWM calculation outside of the four high-elevation sub-basins.

Table 4.2: Evaluating the impact of uncertainty on mixing fraction and EWM calculation. Greyed values indicate low influence (<5%) on the error weighted mean due to high constituent uncertainty. See Section 3, equations 2-6 for in-depth explanation.

*a: Influential analyte indicator, the percent influence imposed by the analyte on the EWM.*

Tributary	Ca <sup>+2</sup>	K <sup>+</sup>	Mg <sup>+2</sup>	Na <sup>+</sup>	Cl <sup>-</sup>	ANC	SO <sub>4</sub> <sup>-2</sup>	δD	δ18O
Putchka	0.4%	0.9%	1.3%	3.5%	7.2%	0.2%	86.1%	0.3%	0.3%
Yanomayo	59.9%	1.7%	3.8%	5.4%	13.0%	5.4%	10.8%	0.0%	0.3%
Rupac	13.3%	3.1%	11.7%	1.1%	0.0%	0.5%	70.0%	0.4%	0.3%
Actuy	14.4%	6.1%	23.4%	5.8%	6.9%	0.7%	42.2%	0.5%	0.2%
Cajas	2.4%	1.0%	5.1%	0.0%	25.4%	1.1%	44.9%	20.0%	9.8%
SanMiguel	0.0%	0.5%	14.9%	0.2%	29.1%		30.3%	24.9%	11.2%
Chusgon	18.7%	3.4%	35.1%	2.7%	4.2%	0.0%	0.0%	35.8%	17.7%
Crisnejas	10.4%	11.3%	22.3%	10.5%	3.2%	0.5%	33.9%	7.8%	4.7%
Yangas	2.6%	2.1%	1.0%	13.7%	22.4%	0.7%	34.6%	22.9%	9.2%
Shauve	13.6%	0.2%	1.2%	0.0%	4.2%	0.0%	35.1%	45.8%	17.6%
Silaco	12.6%	0.0%	3.7%	0.4%	0.0%	3.5%	0.0%	79.8%	31.9%
Chamaya	3.6%	0.6%	11.4%	1.2%	5.7%		43.1%	34.4%	10.5%
Chinchipe	11.2%	0.2%	12.8%	1.8%	2.8%		52.4%	18.9%	4.5%

*b: 2-component mixing model tributary fraction results across analytes.*

Tributary	Ca <sup>+2</sup>	K <sup>+</sup>	Mg <sup>+2</sup>	Na <sup>+</sup>	Cl <sup>-</sup>	ANC	SO <sub>4</sub> <sup>-2</sup>	δD	δ18O
Putchka	15.8%	52.3%	47.4%	40.7%	36.3%	45.7%	34.8%	30.3%	30.6%
Yanomayo	22.0%	1.3%	9.9%	18.4%	14.3%	16.5%	47.4%	-149.4%	49.8%
Rupac	5.9%	9.9%	8.1%	11.7%	-53.7%	13.5%	9.1%	11.8%	15.0%
Actuy	10.0%	7.1%	5.4%	7.8%	8.6%	7.0%	12.7%	0.5%	1.4%
Cajas	30.0%	-42.2%	44.3%	352.9%	12.1%	127.1%	1.7%	14.9%	14.2%
SanMiguel	242.8%	-32.1%	-4.2%	54.7%	7.7%		46.7%	16.9%	18.7%
Chusgon	15.2%	14.5%	4.9%	12.8%	-3.5%	-54.3%	-978.4%	12.1%	12.6%
Crisnejas	9.9%	3.7%	6.8%	5.0%	7.6%	26.5%	1.9%	29.2%	29.0%
Yangas	1.2%	8.3%	5.2%	2.7%	-0.2%	2.6%	19.7%	6.8%	5.6%
Shauve	8.4%	1.2%	1.4%	19.8%	1.7%	853.7%	4.5%	14.3%	14.9%
Silaco	8.3%	512.5%	17.9%	2.5%	-550.5%	7.0%	33.9%	15.8%	15.9%
Chamaya	62.1%	45.2%	45.8%	48.0%	49.1%		44.4%	46.1%	46.8%
Chinchipe	68.5%	64.6%	71.1%	53.1%	59.3%		66.9%	64.2%	64.0%

*c: Constituent contributions for EWM calculation.*

Tributary	Ca <sup>+2</sup>	K <sup>+</sup>	Mg <sup>+2</sup>	Na <sup>+</sup>	Cl <sup>-</sup>	ANC	SO <sub>4</sub> <sup>-2</sup>	δD	δ18O
Putchka	0.1%	0.5%	0.6%	1.4%	2.6%	0.1%	30.0%	0.1%	0.1%
Yanomayo	13.2%	0.0%	0.4%	1.0%	1.9%	0.9%	5.1%	0.0%	0.1%
Rupac	0.8%	0.3%	1.0%	0.1%	0.0%	0.1%	6.4%	0.0%	0.0%
Actuy	1.4%	0.4%	1.3%	0.5%	0.6%	0.0%	5.3%	0.0%	0.0%
Cajas	0.7%	-0.4%	2.2%	0.0%	3.1%	1.5%	0.8%	3.0%	1.4%
SanMiguel	0.1%	-0.2%	-0.6%	0.1%	2.2%		14.1%	4.2%	2.1%
Chusgon	2.8%	0.5%	1.7%	0.3%	-0.1%	0.0%	0.0%	4.3%	2.2%
Crisnejas	1.0%	0.4%	1.5%	0.5%	0.2%	0.1%	0.7%	2.3%	1.4%
Yangas	0.0%	0.2%	0.1%	0.4%	0.0%	0.0%	6.8%	1.6%	0.5%
Shauve	1.1%	0.0%	0.0%	0.0%	0.1%	0.0%	1.6%	6.6%	2.6%
Silaco	1.0%	0.0%	0.7%	0.0%	0.0%	0.2%	0.0%	12.6%	5.1%
Chamaya	2.3%	0.3%	5.2%	0.6%	2.8%		19.1%	15.9%	4.9%
Chinchipe	7.7%	0.1%	9.1%	0.9%	1.7%		35.0%	12.1%	2.9%

*Blank entries = mixing model results unavailable..*

Mixing-model performance was evaluated by way of comparing the mainstem concentrations using the EWM mixing fraction result with the observed concentrations in water samples (Fig. 4.12A). The modeled versus observed comparison demonstrates very good model performance ( $m=1.02$ ,  $b=4.96$ ,  $R^2=0.99$ ). The sample below the Cajas River confluence is an obvious Acid Neutralizing Capacity (ANC) outlier as marked in Figure 4.12A. In this instance the mixing model result is affected by an unsolvable 2-component mixing model problem whereby both the Cajas tributary and upstream Cajas ANC observations (the two end members) are smaller than the downstream Cajas sample (mixed sample result). This mathematically infeasible mixing situation suggests an additional but unmeasured chemical input to the Marañón between the mainstem samples collected upstream and downstream of the Cajas confluence. The EWM approach somewhat ameliorates the effect of this outlier on the final mixing fraction result by reducing the influence of highly uncertain mixing models like this one on the EWM.

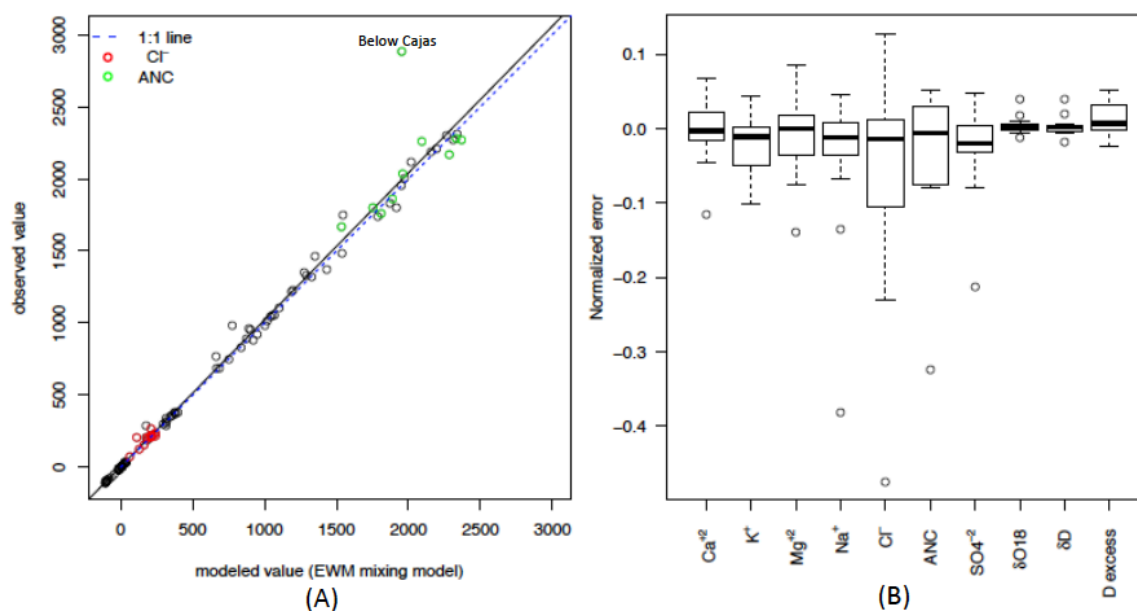


Figure 4.12: Error analysis of mixing model results indicate good agreement between modeled and observed constituent values. (A) Mainstem mixing-model concentration reconstructions of the modeled streamflow using the EWM mixing model results as compared to the observed concentrations. Negative values are isotopes reported as  $\delta$  (per mil) ratio to VSMOW (equation



1). (B) Normalized errors for mainstem-mixing-model results across analytes. Boxes relate to interquartile range, with whiskers identifying data falling within 1.5 times the interquartile range.

Normalized errors for all analytes are shown in Figure 4.12B. The median error is near zero for all analytes, with a tight interquartile spread for all but  $\text{Cl}^-$  and ANC which are highlighted as red and green points, respectively, in Figure 4.12A. All other constituent values are shown as black points.

The mismatch between modeled and observed concentrations for the ‘Below Cajas’ ANC sample increases the magnitude of normalized error for ANC. Consideration of the overall magnitude of  $\text{Cl}^-$  concentrations is important for interpreting chlorine’s larger normalized error values. Because  $\text{Cl}^-$  concentrations are low (ie, generally on the order of 100-200  $\mu\text{eq/L}$ ), a small difference between modeled and observed values results in a high normalized error as compared to higher magnitude concentration constituents with concentrations  $>1,000 \mu\text{eq/L}$ .

Of note, the modeled isotope ( $\delta\text{O}18$ ,  $\delta\text{D}$ ) performance is especially good even though their low magnitude values make them prone to being heavily influenced by even small analytic laboratory error. This strong result indicates that they are reliable tracers for use in mixing models.

#### **4.4.6 Errors due to low sample density over a large domain**

A core assumption in this approach is that the chemistry of each tributary may represent inputs from additional tributaries of a similar composition. Errors arise when non-sampled inputs of markedly different composition enter the mainstem between the tributary confluence and the downstream sample point assumed to represent a fully mixed mainstem sample (Fig. 4.3). An example of this effect is discussed in relation the Cajas River mixing model solution in the

section above. Drawbacks of using the minimal-sampling approach for efficient characterization are also demonstrated in the spread in mixing fraction results across analytes for a given tributary (Table 4.2b). This problem, which we deem minor, would have been further reduced if we had had the capacity to take additional samples once the river became well mixed downstream closer to tributary confluences.

Unmeasured inputs with unusual chemical concentrations, for example from point sources or geologically anomalous sub-basins, can sometimes be anticipated. For example in the case of San Miguel River, several notable inputs occur between the upstream (end member) and downstream (fully mixed) sample including wastewater byproducts associated with the town of Chagual, riverside Vijus mine's discharge, and major in-channel earthworks associated with a bridge construction site. More constrained mixing model results with lower variability across constituents (Table 4.2b, e.g., Chamaya, Chinchipe tributaries) have few potentially anomalous inputs, with upstream and downstream sampling sites located much closer together.

The EWM approach to mixing model fractions constrains the spread observed in mixing model results, collapsing the suite of results into an average value influenced proportionally by constituent-specific uncertainties. This approach provides a metric for identifying influential constituents in the EWM calculation, those with lower associated uncertainties. As is evident by equation 3, uncertainty values increase rapidly as the difference in concentrations,  $\Delta C$ , between end members (tributary and upstream sample, in this case) approach 0. Conversely, end members with high  $\Delta C$  have smaller uncertainties. The constituents that are found to be heavily influential (low uncertainty) in this study (Table 4.2a, e.g.,  $\text{SO}_4^{2-}$ ), are those with concentrations that oscillate from high to low, providing continually large  $\Delta C$  as the river progresses down river. This suggests that the presence of  $\text{SO}_4^{2-}$  is highly variable across the domain, whereas  $\text{Na}^+$  or  $\text{K}^+$

are more constrained, consistently present at high concentrations yielding higher uncertainty in mixing model calculations and thus less influence to the EWM.

The suite of constituents that influence the EWM changes across the domain. Isotopic variables are non-influential to EWM in the higher basins when isotopic levels across sub-basins are comparatively homogenous. In contrast, isotopes consistently influence EWM at mid- and lower- basins when isotopic composition changes rapidly with elevation (refer slope changes in Fig. 4.7A). In summary, the ‘influence metric’ highlights constituent variability within the system, and high constituent variability generally relates to lower 2-component mixing model fraction uncertainty yielding greater influence on the EWM. Table 4.2 demonstrates this result visually. The greyed values in Table 4.2a, b and c are those with less than 5% influence on the error weighted mean calculation. These low-influence constituents (Table 4.2a) in most cases correlate to the outlier mixing model results (Table 4.2b) as is expected since constituents with high uncertainty (low influence) produce mixing fractions with higher deviation. Tables 4.2a and 4.2b combine in Table 4.2c to determine each constituent’s contribution to the EWM. The small total error (Table 4.1) is a result of having relatively few dominant constituents influencing the EWM.

## **4.5 Discussion**

### **4.5.1 Hydrologic controls on discharge**

Discharge in the upper Marañón River is not driven by the headwater hydrologic system. Instead, our mixing model results show that much of the discharge is derived from the low lying Chamaya, Chinchipe and Utcubamba basins (Fig. 4.11). (The Utcubamba was not sampled for logistical reasons, but a similar regime to the Chinchipe is expected given precipitation mapping

results and topography. Refer hatched pattern sub-basin shown in Figure 4.1, 4.2C, 4.5A.) At these sub-basin confluences, Marañón discharges are controlled by high-precipitation inputs to the LLBs with more direct access to Amazon moisture systems. Moisture recycling (re-evaporation cycles) also leads to increases in D-excess as observed in the Chamaya (D excess = 14.34) and Chinchipe (D excess = 16.05) tributaries, and this is reiterated in our PCA results showing moisture recycling variables having strong influence on jungle water hydrochemistry.

Given the Amazon moisture-movement patterns, the LLBs are the first sub-basins of the study domain to intercept the wet air masses from the east. As these masses hit the topography of the Andes, considerable new precipitation falls in the LLBs even during the dry winter season, as evidenced by greener vegetation (Fig. 4.2A) and more snow (Fig. 4.6). In contrast, sub-basins in the Cordillera corridor are flanked on both banks by high peaks and lie in a rain shadow imposed from both the east and west. The bulk of the precipitation in the Cordillera corridor comes in March and April, synchronized with the end of the Amazonian rainy season when occasional Antarctic storms reach the Amazon (Friedman, 1977). These fronts can be especially moisture rich and able to overcome the initial orographic rain-out effect. Additionally, a subtle east-west snow cover trend is observed in the Cordillera corridor with snow cover probabilities higher on the eastern ridges (Fig. 4.5), suggesting some Amazonian moisture spillover to the eastern flanks of the Marañón corridor during the colder winter months.

Precipitation falling as snow is also more prevalent in the LLBs, where more abundant precipitation meets sub-freezing temperatures on the LLBs' ridgelines and mountain tops as high as 3,934 m. While the Marañón headwaters are higher and colder, they lack critical winter precipitation inputs needed to generate substantial snow. The majority of precipitation to the high-elevation catchments comes during the warmer wet season months of January through

March when most precipitation falls as rain, as demonstrated by the flashy wet season hydrograph at Balsas (Fig. 4.5B). The low snow cover to the upper basins implies low probability for glacier regeneration, supporting observations of rapidly wasting glacier systems across the Cordillera Blanca region (Racoviteanu et al., 2008). Remotely sensed products have not yet quantified the total snow-water equivalence in the Marañón basin, but even in the snowier LLBs, snow water inputs are dwarfed by those from rain.

We had initially assumed, based on naming and length expectations, that the largest water contribution would be from the highest elevation Marañón headwaters and its tributaries, that is, the river has a mainstem dominance. Our finding that the Marañón mainstem dry-season discharge is decidedly dominated by the high-runoff LLB sub-basins (Fig. 4.11) contradicts a general expectation that rivers are named for the tributary that controls annual discharge. Moreover, this finding shows another example that river length may not be a critical variable from which to anticipate relative discharge of continental-scale river systems. Instead, tributaries coming from northwestern Peru and Ecuador, the LLBs, drive the discharge. This would be expected throughout the year based on the discharge records (Fig. 4.5).

#### **4.5.2 Discharge sensitivity to climate**

A key question for this research revolved around the role that snow and ice play in the hydrology of the Marañón because of their high sensitivity to a warming climate (Barnett et al., 2005). This in turn raises questions about long-term discharge sustainability, an important consideration for viable hydropower development. The direct role of snow and ice melt as a dry-season river source (i.e., melt water's direct translation to open channel flow) appears to be

limited due to a) lower snow probability and limited glacier coverage in the headwaters (Fig. 4.6) and b) the dominance of rain over snow in the snowier LLBs (Fig. 4.4).

Flow vulnerabilities in the Cordillera corridor – the site of many of the proposed hydropower projects – is more likely impacted from indirect consequences of changes to water inputs especially regarding the substantial baseflow that provides water throughout the corridor during the dry winter season. The questions become, where does that baseflow come from and what is the character of the large base-flow reservoirs? Four possible reservoirs include glacial ice, seasonal snowpacks, groundwater, and puna (alpine wetland) storage.

The glacier area is small and snow probabilities are low in the upper sub-basins limiting the likelihood these reservoirs provide a substantial source for dry season river discharge. Size and geochemical data indicate that groundwater reservoirs must dominate baseflow. The importance of geochemical products (a sign of subsurface flow) in defining the chemistry of the alpine reach (Fig. 4.10) add evidence to support groundwater's important role in the corridor. Given this, the next logical question is what recharges groundwater?

Although groundwater samples were not acquired directly, baseflow samples can serve as a proxy for groundwater hydrochemistry. Baseflow isotopic results in the Cordillera corridor show an increasingly depleted isotopic signature at higher elevation tributaries owing to both elevation effect and additional fractionation processes as discussed above, likely evaporation or sublimation on alpine melt waters (snow and ice) or standing water in punas prior to soil infiltration. After infiltration to groundwater, fractionation largely stops. These fractionation effects are a plausible explanation for the high isotope depletion observed in baseflow, but still it does not differentiate between cryospheric water or puna water as recharge sources.

Melt-sourced groundwater has been shown to be critical for river flow in the alpine areas of the Cordillera Blanca (Baraer et al., 2015) but data presented here shows baseflow isotopic values are bracketed by wet season high elevation precipitation isotopes (Fig. 4.7A), suggesting that wet season rain dominates groundwater recharge. This finding indicates soil water and groundwater in the Cordillera Blanca may not be directly sensitive to glacier inputs but that the Marañón's substantial baseflow likely relies on some other storage reservoir.

Punas and puna-like ecosystems called páramo regulate extreme weather patterns (prolonged wet periods) through significant soil storage capacity, releasing water gradually during dry seasons to provide sustained baseflow to rivers (Balslev & Luteyn, 1992; Buytaert et al., 2007). Puna water storage functions are well known to provide large volume water storage as ecosystem services, including serving the majority of municipal water supplies to major centers including Quito and Bogata (Borrelli et al., 2015; Buytaert et al., 2006). Indeed, basins with water reservoirs have been shown to produce substantially more runoff than basins without these ecosystems at least partially due to low levels of evapo-transpiration and the high storage capacity afforded by highly organic soils (Buytaert et al., 2006, 2007). These distinct natural wetland reservoirs likely serve as critical wet season rain storage role to the Marañón. Pondered wet season rain present in puna ecosystems also more likely explains the increased fractionation signal observed in baseflow.

However, groundwater-surface water interactions in this region are complex and shifts in these interactions are possible due to secondary effects from glacial recession (Gordon et al., 2015). Upward vegetation expansion into melt-out areas (Young et al., 2017) may increase evapo-transpiration and decrease available alpine groundwater reserves, although this effect may not be noticeable given its magnitude relative to the apparently massive groundwater volumes

present in the Marañón basin. Increasing fragmentation and changes to the spatial distribution of water-controlled ecosystems such as punas and wetlands are thought to be caused by compromises to subsurface connectivity due to lessening meltwater inputs (Polk, 2016; Young, 2015). In this way glacier recession and resulting changes to meltwater generation may indirectly affect baseflow by way of impacting groundwater-surface water interactions and subsurface water storage reservoirs in the Marañón, eventually affecting the character of baseflow.

In sum, water resource sensitivity to climate is complex in the Marañón basin. The massive natural, gravity-fed subsurface and puna reservoirs appear to provide ample storage of wet season rain to service substantial dry season baseflow through the Cordillera corridor. Puna's hydrologic regulation function is compromised by anthropogenic disturbance (Ochoa-Tocachi et al., 2016), and conservation strategies are needed to protect these central ecosystem services. Long term climate effects on baseflow may be more far-reaching and convoluted, and require further study. In contrast, in the high-runoff LLBs, long-term discharge variation due to climate changes would likely be caused by changes in precipitation patterns (timing and amount).

#### **4.6 Conclusions**

This case study demonstrates the need for a multipronged approach to the characterization of remote rivers such as the Marañón. Baseline information is critical to provide a quantitative and objective evaluation mechanism for development projects. Yet, mobilizing and conducting studies over large regions and in compressed timeframes is a challenging prospect. Using a combination of processing of remotely sensed imagery and mapping can yield targeted, efficient field studies and be used to represent hydrologic settings in ways that are not obvious in



the field or from a literature review. In a sense, chemical analyses of stream-water samples effectively represents remote sensing of this upstream watershed and provides information not available through satellite imagery alone.

Dry-season discharge volume in the Marañón River, before its turn east to enter the amazon lowlands, is controlled by low elevation basins receiving large precipitation amounts from Amazonian moisture masses, and is not strongly controlled by discharge volume in the mainstem Marañón itself. In the upper basin the substantial dry season baseflow in the Cordillera corridor appears to rely on the drip feeding of wet season rain from massive natural storage reservoirs present in the higher elevations of the basin. Together, these high- and low-elevation sub-basins define the dry season response that the Marañón River will have to major hydropower development in terms of the long-term reliability of water supply.

Numerous remote mountain river systems, especially those in the Andes and across the Hindu Kush Himalaya, are poorly understood but are targeted for large-scale development as our global energy demands rise. Mountain rivers serve as the connecting conduit across elevations and ecosystems that maintain the continuum of material and nutrient transport, with far-reaching environmental, social and economic consequences. There is an urgent need for the environmental science community to act creatively to utilize remote sensing data together with basic *in situ* observations as demonstrated here to efficiently characterize large scale systems under development pressure. Understanding hydrologic controls and baseline conditions allow evaluation of the upstream-downstream affects of development decisions before actions are taken, possibly resulting in irreversible effects to some of the most important and bio-diverse ecosystems on the planet.

#### 4.7 Acknowledgments

The success of the Marañón Project is due in no small part to the 16-person team of river runners who paddled 620km of the Marañon River and assisted with the study presented here. Sincere thanks to James “Rocky” Contos, Tomas Binimelis, Pedro Peña, Ben Griffin, Jen-ai Stokesbary, Nate Mack, Nancy Moore and Christian Martin for tireless coordination, risk management and logistics to get this month long remote river trip on the water and down the river safely. Thank you also to Henry Worobec for his recording efforts, and to the suite of scientists who shared the motivation to initiate this baseline data set: Jaime Ruth Goode, Natalie Kramer Anderson, Jorge Peralta, Stephanie Gustavson, Diana Silva and Florencia Trama. Thank you to Lily Jackson for navigating geologic data sources, guidance on geologic mapping and grouping of rock types. Much gratitude goes to Holly Miller and her staff in the INSTAAR wet chemistry lab and Fred Luiszer at the University of Colorado Geological Sciences Department’s Laboratory for Environmental and Geological Sciences (LEGS) for the high quality lab analysis of all water samples.

The Marañon Project was partially funded by National Geographic Committee for Science and Exploration grant # 9752-15 awarded to Natalie Kramer Anderson (PI), and by generous friends and family who supported The Marañón Project crowd-funding campaign. Robert Stallard has been funded by the National Research Program for Water at the U.S. Geological Survey. Publication of this article was funded by the University of Colorado Boulder Libraries Open Access Fund.

## 4.8 Appendices

### 4.8.1 Appendix 4.1: Geologic map of the Marañón basin.

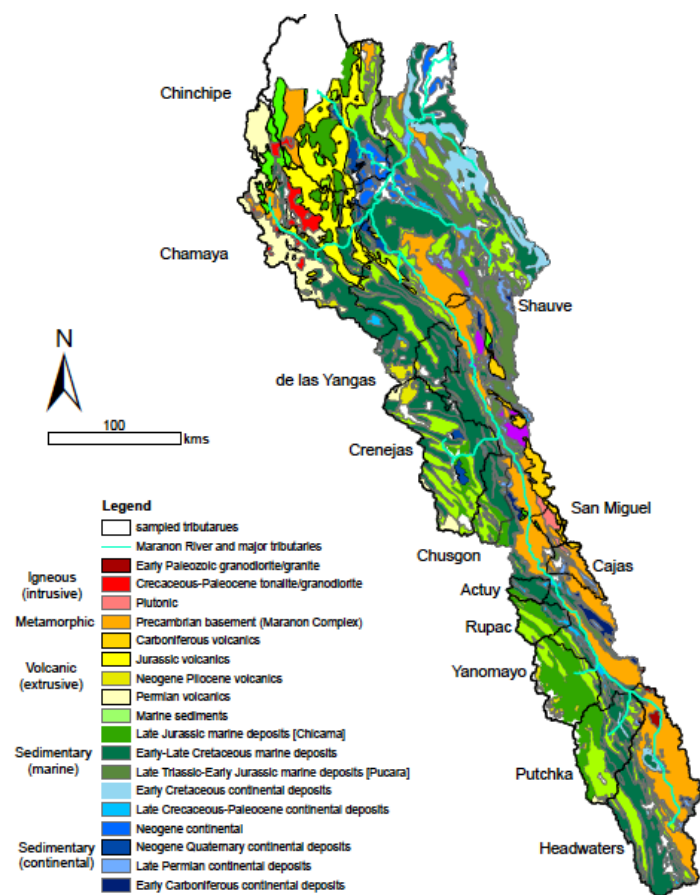


Figure 4.13: Geologic map of the Marañón basin. Geologic units are a simplified categorization of the 1999 1:100,000 scale Peruvian Geology map (Instituto Geológico, Minero y Metalúrgico (INGEMMET), 1999) where similar rock types were grouped together to consolidate classes. Continental deposits classes include clastic sediments (sandstones, river conglomerate, facies and soils). Marine sediments refer to limestones and chemical sedimentary rocks generally high in calcium carbonate.

#### 4.8.2 Appendix 4.2: Piper diagram for all water samples.

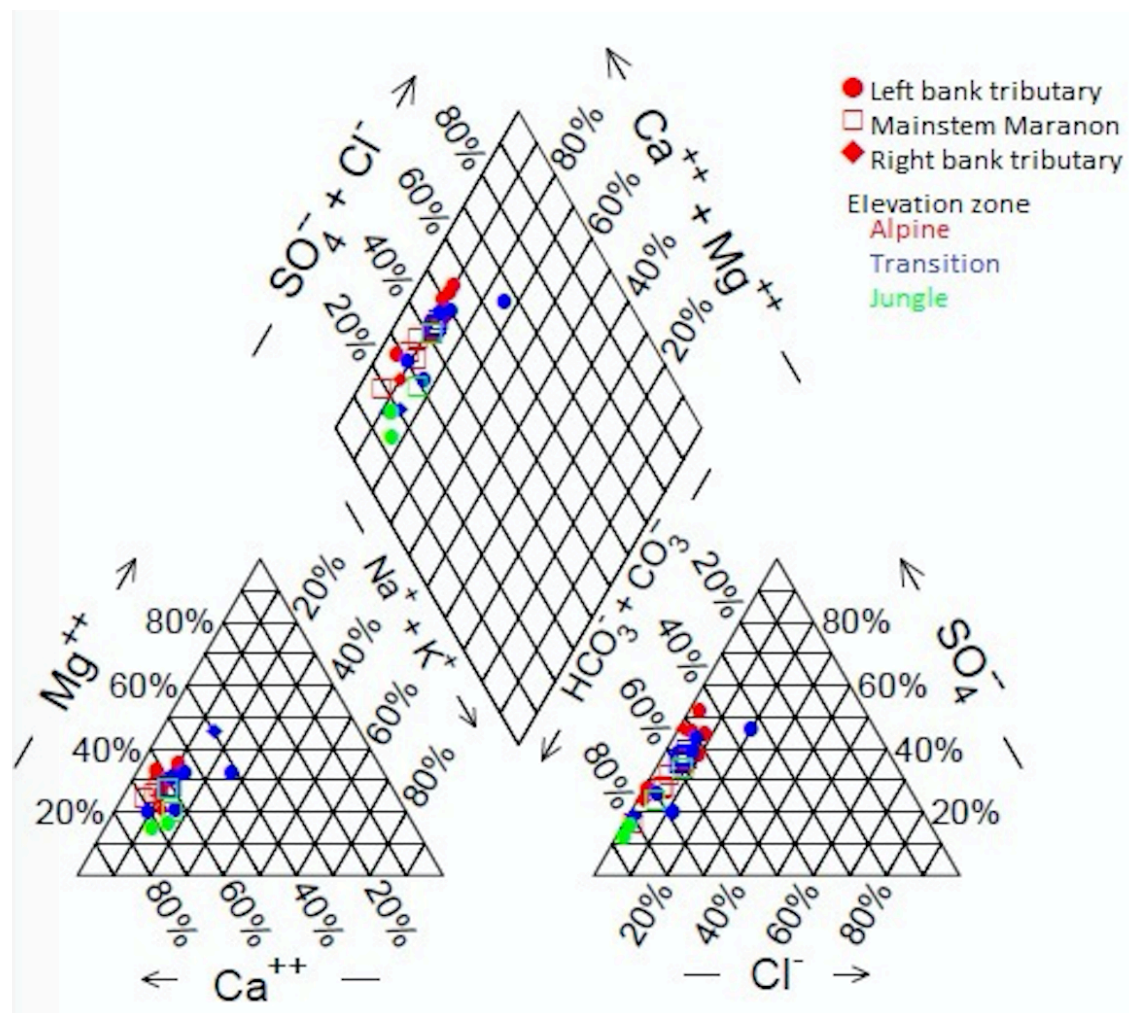


Figure 4.14: Alkalinity,  $\text{SO}_4^{2-}$ , and  $\text{Ca}^{2+}$  dominate the constituents of Marañón waters. Jungle tributaries have a higher dominance of carbonate hardness than alpine or transitional tributaries that are balanced by other anion sources.

### 4.8.3 Appendix 4.3: Sampled sub-basin attributes

Table 4.3: Sampled sub-basin topographic, climatic and geologic attributes.

Sub-basin	Drainage area (km <sup>2</sup> )	Elevation zone (Fig. 2)	Min elevation (m ASL)	Max elevation (m ASL)	Mean elevation (m ASL)	Mean slope (deg)	Mean snow prob	Avg July (dry season) precip (mm)	Avg March (wet season) precipitation (mm)	Avg annual precip (mm)	Dominant geologies <sup>b,c,d</sup>
<b>Headwaters</b>	6160	Alpine	2204	6418	4032	18.5	5%	10	143	750	Precambrian basement (Maranon complex)
											Early Cretaceous continental deposits
											Early-Late Cretaceous marine deposits
<b>Putchka</b>	2673	Alpine	2126	6258	3994	22.9	5%	6	138	783	Late Jurassic marine deposits (Chicama)
											Early Cretaceous continental deposits
											Early-Late Cretaceous marine deposits
<b>Yanomayo</b>	2168	Alpine	1974	6243	3846	22.3	11%	5	132	748	Early Cretaceous continental deposits
											Early-Late Cretaceous marine deposits
											Late Jurassic marine deposits (Chicama)
<b>Rupac</b>	926	Alpine	1764	4584	3498	21.3	0%	7	116	665	Early Cretaceous continental deposits
											Late Triassic-Early Jurassic marine deposits (Pucara)
											Early-Late Cretaceous marine deposits
<b>Actuy</b>	438	Alpine	1668	4672	3638	21.9	0%	10	139	798	Early Carboniferous continental deposits
											Precambrian basement (Maranon complex)
<b>Cajas</b>	719	Alpine	1595	4696	3545	23.1	8%	15	146	901	Early Carboniferous continental deposits
											Early Paleozoic granodiorite/granite
											Precambrian basement (Maranon complex)
<b>San Miguel</b>	455	Alpine	1302	4579	3386	26.3	15%	19	162	997	Early Carboniferous continental deposits
											Late Triassic-Early Jurassic marine deposits (Pucara)
											Late Jurassic marine deposits (Chicama)
<b>Chusgon</b>	1267	Transition	1083	4667	3206	21.1	0%	17	167	982	Early Cretaceous continental deposits
											Early-Late Cretaceous marine deposits
											Late Jurassic marine deposits (Chicama)
<b>Crisnejas</b>	4693	Transition	1002	4702	3118	15.7	0%	16	160	939	Early Cretaceous continental deposits
											Early-Late Cretaceous marine deposits
											Early Cretaceous continental deposits
<b>Yangas</b>	1188	Transition	768	4250	2993	18.8	1%	28	154	1022	Early-Late Cretaceous marine deposits
<b>Shauve</b>	110	Transition	737	3811	2213	25.6	8%	28	119	819	Precambrian basement (Maranon complex)
<b>Silaco</b>	2433	Transition	520	4232	2800	17.8	2%	30	141	978	Neogene Quaternary continental deposits
											Early Cretaceous continental deposits
											Early-Late Cretaceous marine deposits
<b>Chamaya</b>	7730	Jungle	425	4049	2202	21.1	7%	28	138	811	Late Jurassic marine deposits (Chicama)
											Late Triassic-Early Jurassic marine deposits (Pucara)
											Early Cretaceous continental deposits

												Late Jurassic marine deposits (Chicama)
												Late Triassic-Early Jurassic marine deposits (Pucara)
												Neogene Quaternary continental deposits
												Neogene Pliocene volcanics
												Precambrian basement (Maranon complex)
												Early Cretaceous continental deposits
												Early-Late Cretaceous marine deposits
<b>Chinchi</b>	7812	Jungle	353	3934	1692	20.1	20%	63	165	1199		

<sup>a</sup>Geology classifications derived from 1:100,000 scale Peruvian Geology map (INGEMMET, 1999).

<sup>b</sup>Continental deposits generally refer to clastic sediments (sandstones, river conglomerate facies, soils).

<sup>c</sup>Marine sediments typical include limestones and calcium carbonate sedimentary formations, with some clastics.

<sup>d</sup>The Maranon complex is highly metamorphosed at deep levels and thus can be highly crystalline.

#### 4.8.4 Appendix 4.4: Water sample data and mixing model components

Table 4.4: Water chemistry and isotopic data, water sample meta data, and mixing model components

Date sampled	Sample description, mixing model end member roles	Sample elev (m ASL)	River distance (km)	Elevation zone (Fig. 2)	$m^3 s^{-1}$			all ion concentrations in $\mu Eq L^{-1}$						
					Discharge	Latitude	Longitude	Ca <sup>+2</sup>	K <sup>+</sup>	Mg <sup>+2</sup>	Na <sup>+</sup>	Cl <sup>-</sup>	SO <sub>4</sub> <sup>-2</sup>	ANC
7/17/15	Upstream Putchka	2302	0	Alpine		-9.073493°	-76.938222°	1701.0	18.4	595.4	137.5	63.3	404.8	1991.9
7/17/15	Putchka tributary	2186	2	Alpine	44	-9.078115°	-76.945142°	1946.5	30.1	796.1	262.7	244.4	1388.6	1481.6
7/18/15	Downstream Putchka, upstream Yanomayo	1938	39	Alpine	81	-8.895251°	-77.149132°	1739.7	24.5	690.5	188.4	129.0	747.0	1758.8
7/18/15	Yanomayo tributary	1937	40.5	Alpine	36	-8.902606°	-77.161485°	868.9	18.6	564.4	134.6	47.2	871.9	764.8
7/20/15	Downstream Yanomayo, Upstream Huaylas	1872	58	Alpine	126	-8.779101°	-77.217443°	1548.3	24.5	678.0	178.5	117.3	806.2	1594.9
7/20/15	Huaylas tributary	1870	59	Alpine	<sup>b</sup> Not calculated	-8.771704°	-77.221419°	2266.5	28.3	1200.1	153.0	23.6	1012.3	2628.1
7/21/15	Downstream Huaylas, upstream Rupac	1741	101	Alpine	calculated	-8.511584°	-77.359443°	1745.8	24.4	769.1	284.8	210.6	983.8	1669.9
7/21/15	Rupac tributary	1750	102	Alpine	15	-8.508563°	-77.366396°	3206.2	48.9	1557.0	404.6	199.9	2367.7	2613.0
7/22/15	Downstream Rupac, upstream Actuy	1602	131	Alpine	162	-8.321838°	-77.473847°	1831.4	26.9	833.2	298.7	216.3	1109.9	1797.6
7/22/15	Actuy tributary	1605	132	Alpine	19	-8.318808°	-77.475659°	3076.0	56.5	1778.6	530.4	487.2	2039.2	2769.7
7/23/15	Downstream Actuy, upstream Cajas	1612	138	Alpine	177	-8.275496°	-77.504101°	1956.0	29.0	884.0	316.8	239.7	1227.7	1865.5
7/23/15	Cajas tributary	1582	138.5	Alpine	21	-8.272440°	-77.505267°	2135.6	22.9	1040.9	323.6	57.6	851.6	2666.4
7/27/15	Downstream Cajas, upstream San Miguel	1256	200	Alpine	196	-7.885920°	-77.634223°	2009.9	31.5	953.5	340.6	217.6	1221.2	2883.5
7/27/15	San Miguel tributary	1272	201	Alpine	39	-7.882844°	-77.629097°	2052.9	27.2	650.3	356.5	42.5	1504.6	QNS <sup>a</sup>
7/30/15	Downstream San Miguel, upstream Chusgon	1093	256.5	Transition	235	-7.485927°	-77.743442°	2114.4	32.9	966.3	349.3	204.2	1353.6	1973.1
7/30/15	Chusgon tributary	1082	257	Transition	23	-7.479037°	-77.751896°	2575.5	40.5	1352.6	401.1	262.4	1341.9	1861.1
8/1/15	Downstream Chusgon, upstream Cresnejas	1047	277	Transition	258	-7.366996°	-77.822635°	2184.6	34.0	985.4	355.9	202.2	1467.9	2033.9
8/1/15	Cresnejas tributary	1040	278	Transition	18	-7.347826°	-77.833402°	3371.1	82.4	2017.5	710.0	362.4	2497.0	2902.2
8/6/15	Downstream Cresnejas, upstream Yangas	761	395	Transition	275	-6.609696°	-78.114522°	2302.1	35.8	1055.6	373.7	214.4	1487.7	2263.9
8/6/15	Yangas tributary	769	396	Transition	25	-6.603928°	-78.118031°	2721.9	50.0	901.5	655.6	513.2	875.2	3033.2
8/8/15	Downstream Yangas, upstream Shuve	710	424	Transition	300	-6.458188°	-78.199172°	2307.0	37.0	1047.5	381.5	214.0	1366.9	2284.0
8/8/15	Shuve tributary	708	425	Transition	28	-6.455567°	-78.206824°	1109.1	30.5	1265.7	376.4	45.9	534.9	2270.7
8/11/15	Downstream Shuve, upstream Silaco	537	487	Transition	328	-6.087641°	-78.505627°	2206.6	36.9	1050.5	380.5	211.1	1329.6	2170.1
8/11/15	Silaco tributary	531	488	Transition	48	-6.087924°	-78.508466°	2923.9	36.7	831.0	339.2	200.0	1316.6	3529.6
8/12/15	Downstream Silaco, upstream Chamaya	431	538.5	Jungle	376	-5.798495°	-78.705474°	2266.2	35.8	1011.2	379.4	272.3	1325.2	2265.9
8/12/15	Chamaya tributary	425	539	Jungle	173	-5.785582°	-78.704206°	1508.5	23.3	308.4	242.5	38.3	345.9	1782.1
8/13/15	Downstream Chamaya, upstream Chinchipe	364	582	Jungle	549	-5.535312°	-78.563920°	1795.8	30.2	689.2	313.7	157.5	890.5	QNS <sup>a</sup>
8/13/15	Chinchipe tributary	353	583	Jungle	366	-5.516203°	-78.553260°	525.7	20.5	129.5	108.6	15.9	94.4	686.0
8/14/15	Downstream Chinchipe at Montenegro	326	618	Jungle	915	-5.311663°	-78.431333°	925.8	23.9	291.3	204.8	73.5	358.2	1067.3
7/29/15	Not an end member; mainstem downstream Vijus mine waste outlet	1165	225	Alpine		-7.721448°	-77.667828°	1998.7	32.5	940.9	335.0	215.1	1318.3	1942.0
8/8/15	Not an end member; Magdalena creek, tufa stream	638	437	Transition		-6.389930°	-78.281343°	3289.2	160.3	2540.0	1878.4	1549.0	3626.3	2681.1
8/9/15	Not an end member; right bank tributary, Conjun River	540	458	Transition		-6.266168°	-78.369008°	1128.1	19.1	600.0	206.0	28.5	305.1	1659.9

<sup>a</sup>QNS = Sample quantity not sufficient for analysis.

<sup>b</sup>Not calculated due to anomolous inputs observed in vicinity of Huaylas tributary

Date sampled	Sample description, mixing model end member roles	ppb			pH	$\mu\text{S}$ L-1	D excess	parts per mil	
		Si	Cu	Fe				$\delta^{18}\text{O}$	$\delta\text{D}$
7/17/15	Upstream Putchka	3001.0	0.14	681	7.75	242.1	6.65	-13.87	-104.28
7/17/15	Putchka tributary	2999.8	0.65	758	7.53	326.4	8.09	-14.67	-109.26
7/18/15	Downstream Putchka, upstream Yanomayo	3098.5	0.38	695	7.75	270.3	7.11	-14.11	-105.79
7/18/15	Yanomayo tributary	2813.1	0.20	330	7.44	169.8	9.65	-14.39	-105.49
7/20/15	Downstream Yanomayo, Upstream Huaylas	3052.7	0.27	601	7.68	424.0	7.79	-14.25	-106.22
7/20/15	Huaylas tributary	5202.6	0.10	930	7.79	364.8	7.07	-13.53	-101.20
7/21/15	Downstream Huaylas, upstream Rupac	3175.3	0.31	717	7.78	299.2	7.3	-14.04	-105.03
7/21/15	Rupac tributary	4685.6	0.41	1323	7.96	564.9	6.06	-13.18	-99.41
7/22/15	Downstream Rupac, upstream Actuy	3360.8	0.52	758	7.70	324.8	6.93	-13.91	-104.37
7/22/15	Actuy tributary	3890.7	0.35	1300	8.04	586.6	7.36	-13.25	-98.65
7/23/15	Downstream Actuy, upstream Cajas	3357.4	0.35	818	7.79	342.8	6.89	-13.90	-104.34
7/23/15	Cajas tributary	4480.9	0.32	904	7.83	357.6	7.21	-12.48	-92.61
7/27/15	Downstream Cajas, upstream San Miguel	3555.2	0.36	839	7.84	350.0	7.02	-13.70	-102.60
7/27/15	San Miguel tributary	4534.1	0.77	849	7.52	325.5	7.95	-12.31	-90.49
7/30/15	Downstream San Miguel, upstream Chusgon	3710.5	0.38	869	7.78	364.4	6.98	-13.44	-100.55
7/30/15	Chusgon tributary	4500.3	0.51	1067	7.99	437.6	7.28	-11.93	-88.13
8/1/15	Downstream Chusgon, upstream Cresnejas	3841.6	0.29	873	7.81	377.6	6.96	-13.25	-99.04
8/1/15	Cresnejas tributary	6165.0	0.81	1444	8.06	653.1	5.63	-10.98	-82.19
8/6/15	Downstream Cresnejas, upstream Yangas	4016.1	0.37	936	7.94	412.8	6.61	-12.59	-94.12
8/6/15	Yangas tributary	5812.2	0.55	1147	7.98	452.5	8.89	-10.31	-73.61
8/8/15	Downstream Yangas, upstream Shuve	4149.4	0.35	970	7.72	406.8	6.98	-12.46	-92.73
8/8/15	Shuve tributary	7449.9	0.32	464	7.76	273.3	11.64	-8.60	-57.15
8/11/15	Downstream Shuve, upstream Silaco	4439.1	0.31	934	7.91	384.8	7.48	-11.89	-87.63
8/11/15	Silaco tributary	4487.3	0.53	1212	7.93	438.0	10.34	-8.80	-60.06
8/12/15	Downstream Silaco, upstream Chamaya	4544.3	0.39	999	7.93	396.4	7.91	-11.40	-83.28
8/12/15	Chamaya tributary	6794.2	1.13	746	7.56	203.4	14.34	-7.62	-46.66
8/13/15	Downstream Chamaya, upstream Chinchipe	5109.7	0.63	760	7.66	293.7	10.67	-9.63	-66.40
8/13/15	Chinchipe tributary	4357.6	0.82	236	7.33	80.0	16.05	-6.16	-33.22
8/14/15	Downstream Chinchipe at Montenegro	5109.8	0.87	417	7.43	150.6	14.18	-7.41	-45.11
7/29/15	Not an end member; mainstem downstream Vijus mine waste outlet	3645.1	0.32	841	7.88	367.6	7.02	-13.47	-100.70
8/8/15	Not an end member; Magdalena creek, tufa stream	5592.6	1.11	1355	7.87	883.0	8.44	-7.82	-54.13
8/9/15	Not an end member; right bank tributary, Conjun River	7751.8	0.19	491	7.70	192.8	12.54	-8.44	-54.96

<sup>a</sup>QNS = Sample quantity not sufficient for analysis.

<sup>b</sup>Not calculated due to anomolous inputs observed in vicinity of Huaylas tributary



#### 4.8.5 Appendix 4.5: Laboratory equipment specifications

Table 4.5: Laboratory analysis instruments, methods, precision, and detection limits for water chemistry parameters.

Analyte	Ca <sup>+2</sup>	K <sup>+</sup>	Mg <sup>+2</sup>	Na <sup>+</sup>	Si	Cu	Fe	Cl <sup>-</sup>	SO <sub>4</sub> <sup>-2</sup>	ANC	δD	δ18O
<b>Instrument/method</b>	Inductively Coupled Plasma Mass Spectrometer (ICP-MS)							Metrohm 840 Compact IC		Manual gran titration	Picarro L2130-i	
<b>Lab precision (% RSD)</b>	0.24%	0.59%	0.31%	0.43%	unknown			0.62%	0.17%	0.87%	0.10%	0.13%
<b>Analysis detection limit (µeq/L unless otherwise noted)</b>	0.49	0.09	0.11	0.1	0.183 ppb	0.008 ppb	0.010 ppb	0.17	0.06	n/a	n/a	n/a

## CHAPTER 5

### 5: FINAL THOUGHTS

#### 5.1 Synthesis of Results

The primary goals of this research were to clarify the role of melt water in river and groundwater systems of mountain basins, and to develop and test a method for rapidly identifying hydrologic controls in areas facing imminent change. To achieve these objectives, I utilized three studies with progressively larger study domains and progressively less data availability. Some hydrology-related datasets (snow cover, ice area, rain inputs, vegetation presence) were interpreted from processed remote sensing data products in geographical information systems. Hydrochemistry and isotope data from field water samples were collected and analyzed to drive various mixing model methods that determined streamflow partitioning.

Results of the case studies demonstrate the complex and varied role of meltwater across scales and sites. Meltwater plays a critical role in surface flow and groundwater recharge in arid mountain areas like Colorado and Central Asia where snow makes up the vast majority of inputs. In the more hydro-climatically variable Andes and Amazon, melt play a much lesser direct role in river flow. At regional (non-headwater) scales, the role of melt in surface flow diminishes with elevation and/or with distance from the glacier coincident with decreasing percent of snow and ice cover of the total basin area. Groundwater, too, relies on melt for recharge, but both deep and shallow paths are influenced by the geology, topography and melt rate. The mechanisms

involved with this process are varied and complex, with an apparent direct connection between melt and groundwater in the Saddle, Martinelli and Naryn basins but an indirect, melt connection in the Marañón where high storage capacity in alpine wetlands serve as an intermediary between melt and river flow.

The Rapid Hydrologic Assessment approach was designed to respond to the time-sensitive needs for understanding key controls of the remote, data scarce mountain basins. Two flavors of RHA were tested via two case studies: 1) the Naryn River draining the Tien Shan mountains of Kyrgyzstan and 2) the Andean headwater stem to the Amazon River, the Marañón. These case studies each presented unique and interesting facets to eliciting hydrologic function across the system. The importance of groundwater flow paths for melt in the Naryn basin complicated end member designation because of the many variations to groundwater's chemical fingerprint across a 4,000m elevation gradient. In the Marañón, the inability to sample alpine end members required an even more streamlined approach to sampling and data interpretation, utilizing only surface water samples and an error-weighted mean 2-part mixing model method to differentiate upstream and downstream flow controls. While these study aspects were unexpected, they are opportune examples of how a mountain hydrologist can modify the overall RHA 'satellite+field' approach to suit the specific limitations of the site, dataset or study. This makes RHA more widely applicable to myriad conditions present across mountain environments.

## **5.2 Implications for future research**

The case studies presented here are a very small drop in the bucket of major, unstudied river systems under-going or under pressure of hydrologic change, with the potential for wide application of RHA to mountain basins worldwide. While the RHA method demonstrated here

provides an initial baseline hydrologic understanding *prior* to change, just as importantly, RHA can also be appropriately adopted for implementation *after* major disturbance has occurred. This allows for evaluation of hydrologic implications from that disturbance, for example post-fire, post-earthquake, post-storm, among others. In these cases, evolving conditions from  $t=0$  after disturbance requires immediate response and quick collection to capture the essence of change. The predictive quality assumed by a traditional hydrologic modeling frameworks may not apply in disturbance-based studies, highlighting the applicability and importance of the ‘satellite+field’ data collection technique to capture anomalous or unpredictable behaviors.

## REFERENCES

- Abbott, M. D., Lini, A., & Bierman, P. R. (2000).  $\delta^{18}\text{O}$ ,  $\delta\text{D}$  and  $^3\text{H}$  measurements constrain groundwater recharge patterns in an upland fractured bedrock aquifer, Vermont, USA. *Journal of Hydrology*, 228(1–2), 101–112. [https://doi.org/10.1016/S0022-1694\(00\)00149-9](https://doi.org/10.1016/S0022-1694(00)00149-9)
- Balslev, H. (ed ), & Luteyn, J. L. (ed ). (1992). Paramo, an Andean ecosystem under human influence. Retrieved from <http://agris.fao.org/agris-search/search.do?recordID=XF2015011387>
- Baraer, M., McKenzie, J., Mark, B. G., Gordon, R., Bury, J., Condom, T., ... Fortner, S. K. (2015). Contribution of groundwater to the outflow from ungauged glacierized catchments: a multi-site study in the tropical Cordillera Blanca, Peru. *Hydrological Processes*, 29(11), 2561–2581. <https://doi.org/10.1002/hyp.10386>
- Baraer, M., Mark, B. G., McKenzie, J. M., Condom, T., Bury, J., Huh, K.-I., ... Rathay, S. (2012). Glacier recession and water resources in Peru's Cordillera Blanca. *Journal of Glaciology*, 58(207), 134–150. <https://doi.org/10.3189/2012JoG11J186>
- Barnett, T. P., Adam, J. C., & Lettenmaier, D. P. (2005). Potential impacts of a warming climate on water availability in snow-dominated regions. *Nature*, 438(7066), 303–309. <https://doi.org/10.1038/nature04141>
- Barnhart, T. B., Molotch, N. P., Livneh, B., Harpold, A. A., Knowles, J. F., & Schneider, D. (2016). Snowmelt rate dictates streamflow. *Geophysical Research Letters*, 43(15), 2016GL069690. <https://doi.org/10.1002/2016GL069690>
- Belling, M. (2016). Grandes hidroeléctricas en las selva no están en agenda del Gobierno. *Proactivo*. Retrieved from <http://proactivo.com.pe/grandes-hidroelectricas-en-las-selva-no-estan-en-agenda-del-gobierno/>
- Blasch, K. W., & Bryson, J. R. (2007). Distinguishing Sources of Ground Water Recharge by Using H and O isotopes. *Ground Water*, 45(3), 294–308. <https://doi.org/10.1111/j.1745-6584.2006.00289.x>
- Borrelli, P., Armenteras, D., Panagos, P., Modugno, S., & Schütt, B. (2015). The Implications of Fire Management in the Andean Paramo: A Preliminary Assessment Using Satellite Remote Sensing. *Remote Sensing*, 7(9), 11061–11082. <https://doi.org/10.3390/rs70911061>

- Bremer, L. L., Auerbach, D. A., Goldstein, J. H., Vogl, A. L., Shemie, D., Kroeger, T., ... Tiepolo, G. (2016). One size does not fit all: Natural infrastructure investments within the Latin American Water Funds Partnership. *Ecosystem Services*, *17*, 217–236. <https://doi.org/10.1016/j.ecoser.2015.12.006>
- Brismar, A. (2004). Attention to impact pathways in EISs of large dam projects. *Environmental Impact Assessment Review*, *24*(1), 59–87. [https://doi.org/10.1016/S0195-9255\(03\)00162-8](https://doi.org/10.1016/S0195-9255(03)00162-8)
- Bruno, M. C., & Siviglia, A. (2012). Assessing Impacts of Dam Operations - Interdisciplinary Approaches for Sustainable Regulated River Management. *River Research and Applications*, *28*(6), 675–677. <https://doi.org/10.1002/rra.1616>
- Burns, D. A., McDonnell, J. J., Hooper, R. P., Peters, N. E., Freer, J. E., Kendall, C., & Beven, K. (2001). Quantifying contributions to storm runoff through end-member mixing analysis and hydrologic measurements at the Panola Mountain Research Watershed (Georgia, USA). *Hydrological Processes*, *15*(10), 1903–1924. <https://doi.org/10.1002/hyp.246>
- Bury, J., Mark, B. G., Carey, M., Young, K. R., McKenzie, J. M., Baraer, M., ... Polk, M. H. (2013). New Geographies of Water and Climate Change in Peru: Coupled Natural and Social Transformations in the Santa River Watershed. *Annals of the Association of American Geographers*, *103*(2), 363–374. <https://doi.org/10.1080/00045608.2013.754665>
- Buytaert, W., Iñiguez, V., & Bièvre, B. D. (2007). The effects of afforestation and cultivation on water yield in the Andean páramo. *Forest Ecology and Management*, *251*(1), 22–30. <https://doi.org/10.1016/j.foreco.2007.06.035>
- Buytaert, W., Céleri, R., De Bièvre, B., Cisneros, F., Wyseure, G., Deckers, J., & Hofstede, R. (2006). Human impact on the hydrology of the Andean páramos. *Earth-Science Reviews*, *79*(1–2), 53–72. <https://doi.org/10.1016/j.earscirev.2006.06.002>
- Caine, N. (1989). Hydrograph separation in a small alpine basin based on inorganic solute concentrations. *Journal of Hydrology*, *112*(1), 89–101.
- Carey, M., Molden, O. C., Rasmussen, M. B., Jackson, M., Nolin, A. W., & Mark, B. G. (2017). Impacts of Glacier Recession and Declining Meltwater on Mountain Societies. *Annals of the American Association of Geographers*, *107*(2), 350–359. <https://doi.org/10.1080/24694452.2016.1243039>
- Casey, N., & Zarate, A. (2017). Corruption Scandals With Brazilian Roots Cascade Across Latin America. *New York Times*. Retrieved from <https://www.nytimes.com/2017/02/13/world/americas/peru-colombia-venezuela-brazil-odebrecht-scandal.html>

- Castello, L., & Macedo, M. N. (2016). Large-scale degradation of Amazonian freshwater ecosystems. *Global Change Biology*, 22(3), 990–1007. <https://doi.org/10.1111/gcb.13173>
- Cayan, D. R., Das, T., Pierce, D. W., Barnett, T. P., Tyree, M., & Gershunov, A. (2010). Future dryness in the southwest US and the hydrology of the early 21st century drought. *Proceedings of the National Academy of Sciences*, 107(50), 21271–21276. <https://doi.org/10.1073/pnas.0912391107>
- Chang, A. T. C., Foster, J. L., Gloersen, P., Campbell, W. J., Josberger, E. G., Rango, A., & Danes, Z. F. (1987). Estimating snowpack parameters in the Colorado River basin. In *Large-Scale Effects of Seasonal Snow Cover* (pp. 343–352). IAHS Publication 166.
- Chang, A. T. C., Foster, J. L., & Hall, D. K. (1996). Effects of Forest on the Snow Parameters Derived from Microwave Measurements During the Boreas Winter Field Campaign. *Hydrological Processes*, 10(12), 1565–1574. [https://doi.org/10.1002/\(SICI\)1099-1085\(199612\)10:12<1565::AID-HYP501>3.0.CO;2-5](https://doi.org/10.1002/(SICI)1099-1085(199612)10:12<1565::AID-HYP501>3.0.CO;2-5)
- Cholan, W. (2015). Odebrecht suspende temporalmente proyecto Chadín II. *Kaosenlared*. Retrieved from <http://kaosenlared.net/peru-odebrecht-suspende-temporalmente-proyecto-chadin-ii/>
- Christophersen, N., Neal, C., Hooper, R. P., Vogt, R. D., & Andersen, S. (1990). Modelling streamwater chemistry as a mixture of soilwater end-members — A step towards second-generation acidification models. *Journal of Hydrology*, 116(1–4), 307–320. [https://doi.org/10.1016/0022-1694\(90\)90130-P](https://doi.org/10.1016/0022-1694(90)90130-P)
- Christophersen, N., & Hooper, R. P. (1992). Multivariate analysis of stream water chemical data: The use of principal components analysis for the end-member mixing problem. *Water Resources Research*, 28(1), 99–107. <https://doi.org/10.1029/91WR02518>
- Clow, D. W., Schrott, L., Webb, R., Campbell, D. H., Torizzo, A., & Dornblaser, M. (2003). Ground water occurrence and contributions to streamflow in an alpine catchment, Colorado Front Range. *Groundwater*, 41(7), 937–950.
- Cogley, J. G. (submitter), Sharp, M., Nukes, E., Kienholz, C., & Wyatt, F. (analysts). (2015). GLIMS Glacier Database, Version 1. Analysis IDs 309559-312362. Accessed 1/17/2017, GLIMS, National Snow and Ice Data Center, Boulder, Colorado. <https://doi.org/http://dx.doi.org/10.7265/N5V98602>
- Cowie, R. M., Knowles, J. F., Dailey, K. R., Williams, M. W., Mills, T. J., & Molotch, N. P. (2017). Sources of streamflow along a headwater catchment elevational gradient. *Journal of Hydrology*. <https://doi.org/10.1016/j.jhydrol.2017.03.044>
- Cuffey, K. M., & Paterson, W. S. B. (2010). *The Physics of Glaciers*. Academic Press.

- Dansgaard, W. (1964). Stable isotopes in precipitation. *Tellus*, 16(4), 436–468.  
<https://doi.org/10.1111/j.2153-3490.1964.tb00181.x>
- Dozier, J. (1989). Spectral signature of alpine snow cover from the landsat thematic mapper. *Remote Sensing of Environment*, 28, 9–22. [https://doi.org/10.1016/0034-4257\(89\)90101-6](https://doi.org/10.1016/0034-4257(89)90101-6)
- EurasiaNet. (2016). "Kyrgyzstan: Russia Pushing to Get Dam Money Back." Retrieved from <http://www.eurasianet.org/node/80181>
- Fearnside, P. M. (2002). Greenhouse Gas Emissions from a Hydroelectric Reservoir (Brazil's Tucuruí Dam) and the Energy Policy Implications. *Water, Air, and Soil Pollution*, 133(1–4), 69–96. <https://doi.org/10.1023/A:1012971715668>
- Finer, M., & Jenkins, C. N. (2012). Proliferation of Hydroelectric Dams in the Andean Amazon and Implications for Andes-Amazon Connectivity. *PLOS ONE*, 7(4), e35126. <https://doi.org/10.1371/journal.pone.0035126>
- Forsberg, B. R., Melack, J. M., Dunne, T., Barthem, R. B., Goulding, M., Paiva, R. C. D., ... Weisser, S. (2017). The potential impact of new Andean dams on Amazon fluvial ecosystems. *PLOS ONE*, 12(8), e0182254. <https://doi.org/10.1371/journal.pone.0182254>
- Foster, J. L., Chang, A. T. C., & Hall, D. K. (1997). Comparison of snow mass estimates from a prototype passive microwave snow algorithm, a revised algorithm and a snow depth climatology. *Remote Sensing of Environment*, 62(2), 132–142. [https://doi.org/10.1016/S0034-4257\(97\)00085-0](https://doi.org/10.1016/S0034-4257(97)00085-0)
- Friedman, I. (1977). The Amazon Basin, Another Sahel? *Science*, 197(4298), 7–7. <https://doi.org/10.1126/science.197.4298.7>
- Frisbee, M. D., Phillips, F. M., Campbell, A. R., Liu, F., & Sanchez, S. A. (2011). Streamflow generation in a large, alpine watershed in the southern Rocky Mountains of Colorado: Is streamflow generation simply the aggregation of hillslope runoff responses? *Water Resources Research*, 47(6). <https://doi.org/10.1029/2010WR009391>
- Froehlich, K., Gibson, J., & Aggarwal, P. (2001). Deuterium excess in precipitation and its climatological significance. *International Atomic Energy Agency, C&S Papers Series*, 13, 54–66.
- Garcia, M., Villalba, F., Araguas-Araguas, L., & Rozanski, K. (1998). The role of atmospheric circulation patterns in controlling the regional distribution of stable isotope contents in precipitation: Preliminary results from two transects in the Ecuadorian Andes. In *Isotope techniques in the study of environmental change*. Vienna, Austria: IAEA. Retrieved from [http://inis.iaea.org/Search/search.aspx?orig\\_q=RN:29044418](http://inis.iaea.org/Search/search.aspx?orig_q=RN:29044418)



- Gat, J. R. (1996). Oxygen and Hydrogen Isotopes in the Hydrologic Cycle. *Annual Review of Earth and Planetary Sciences*, 24(1), 225–262. <https://doi.org/10.1146/annurev.earth.24.1.225>
- Gibbs, R. J. (1967). The Geochemistry of the Amazon River System: Part I. The Factors that Control the Salinity and the Composition and Concentration of the Suspended Solids. *Geological Society of America Bulletin*, 78(10), 1203–1232. [https://doi.org/10.1130/0016-7606\(1967\)78\[1203:TGOTAR\]2.0.CO;2](https://doi.org/10.1130/0016-7606(1967)78[1203:TGOTAR]2.0.CO;2)
- Gleick, P. H., & Heberger, M. (2014). Water Conflict Chronology. In D. P. H. Gleick (Ed.), *The World's Water* (pp. 173–219). Island Press/Center for Resource Economics.
- Gonfiantini, R., Roche, M.-A., Olivry, J.-C., Fontes, J.-C., & Zuppi, G. M. (2001). The altitude effect on the isotopic composition of tropical rains. *Chemical Geology*, 181(1–4), 147–167. [https://doi.org/10.1016/S0009-2541\(01\)00279-0](https://doi.org/10.1016/S0009-2541(01)00279-0)
- Gordon, R. P., Lautz, L. K., McKenzie, J. M., Mark, B. G., Chavez, D., & Baraer, M. (2015). Sources and pathways of stream generation in tropical proglacial valleys of the Cordillera Blanca, Peru. *Journal of Hydrology*, 522, 628–644. <https://doi.org/10.1016/j.jhydrol.2015.01.013>
- Goulden, M. L., & Bales, R. C. (2014). Mountain runoff vulnerability to increased evapotranspiration with vegetation expansion. *Proceedings of the National Academy of Sciences*, 111(39), 14071–14075. <https://doi.org/10.1073/pnas.1319316111>
- Greenland, D. (1989). The Climate of Niwot Ridge, Front Range, Colorado, U.S.A. *Arctic and Alpine Research*, 21(4), 380–391. <https://doi.org/10.2307/1551647>
- Griffin, D., & Anchukaitis, K. J. (2014). How unusual is the 2012–2014 California drought? *Geophysical Research Letters*, 41(24), 2014GL062433. <https://doi.org/10.1002/2014GL062433>
- Groll, M., Opp, C., Kulmatov, R., Ikramova, M., & Normatov, I. (2015). Water quality, potential conflicts and solutions—an upstream–downstream analysis of the transnational Zarafshan River (Tajikistan, Uzbekistan). *Environmental Earth Sciences*, 73(2), 743–763. <https://doi.org/10.1007/s12665-013-2988-5>
- Groves, C. R., Game, E. T., Anderson, M. G., Cross, M., Enquist, C., Ferdaña, Z., ... Shafer, S. L. (2012). Incorporating climate change into systematic conservation planning. *Biodiversity and Conservation*, 21(7), 1651–1671. <https://doi.org/10.1007/s10531-012-0269-3>
- Hall, J. S., Asbjornsen, H., Aguirre, N., Berry, Z. C., Lebrija, E., Martínez-Ramos, M., & van Breugel, M. (2015). Understanding Natural Capital: Ecosystem Patterns and Processes. In *Managing Watersheds for Ecosystem Services in the Steepland Neotropics* (pp. 44–48). Inter-American Development Bank (Infrastructure and Environment Sector).

- Environment, Rural Development Disaster Risk Management Division); IDB-MG-340. Retrieved from <http://lacer.lacea.org/handle/11319/7233>
- Hamlet, A. F., Mote, P. W., Clark, M. P., & Lettenmaier, D. P. (2005). Effects of Temperature and Precipitation Variability on Snowpack Trends in the Western United States\*. *Journal of Climate*, 18(21), 4545–4561. <https://doi.org/10.1175/JCLI3538.1>
- Hanmann, H. B. (2002). The ionic pulse, snowmelt flowpaths, and surface water chemistry in two alpine basins, Colorado Rocky Mountains, United States. Doctoral Dissertation, University of Colorado at Boulder, Boulder, CO.
- Harte, P. T. (1996). Factors affecting recharge to crystalline rock in the Mirror Lake area, Grafton County, New Hampshire. *USGS Professional Paper*.
- Hartmann, J., Harrison, D., Oppermann, J., & Gill, R. (2013). The New Frontier of Hydropower Sustainability: Planning at the System Scale. The Nature Conservancy for Inter-American Development Bank Environmental Safeguards Unit.
- Hijmans, R. J., Cameron, S. E., Parra, J. L., Jones, P. G., & Jarvis, A. (2005). Very high resolution interpolated climate surfaces for global land areas. *International Journal of Climatology*, 25(15), 1965–1978. <https://doi.org/10.1002/joc.1276>
- Hill, D. (2015). Peru's mega-dam projects threaten Amazon River source and ecosystem collapse. *Mongabay*. Retrieved from <https://news.mongabay.com/2015/04/perus-mega-dam-projects-threaten-amazon-river-source-and-ecosystem-collapse/>
- Hill, D. (2016). Hitler Rojas - the Peruvian farmer killed for opposing a mega-dam? *The Guardian*. Retrieved from <https://www.theguardian.com/environment/andes-to-the-amazon/2016/jan/25/hitler-rojas-peruvian-killed-mega-dam>
- Hood, E., Williams, M., & Cline, D. (1999). Sublimation from a seasonal snowpack at a continental, mid-latitude alpine site. *Hydrological Processes*, 13(1213), 1781–1797.
- Hooper, R. P. (2003a). Diagnostic tools for mixing models of stream water chemistry. *Water Resources Research*, 39(3), n/a–n/a. <https://doi.org/10.1029/2002WR001528>
- Hooper, R. P. (2003b). Diagnostic tools for mixing models of stream water chemistry. *Water Resources Research*, 39(3). <https://doi.org/10.1029/2002WR001528>
- Hooper, R. P., Christophersen, N., & Peters, N. E. (1990). Modelling streamwater chemistry as a mixture of soilwater end-members — An application to the Panola Mountain catchment, Georgia, U.S.A. *Journal of Hydrology*, 116(1–4), 321–343. [https://doi.org/10.1016/0022-1694\(90\)90131-G](https://doi.org/10.1016/0022-1694(90)90131-G)
- Humphries, H. C., Bourgeron, P. S., & Mujica-Crapanzano, L. R. (2008). Tree spatial patterns and environmental relationships in the forest–alpine tundra ecotone at Niwot Ridge,

- Colorado, USA. *Ecological Research*, 23(3), 589–605. <https://doi.org/10.1007/s11284-007-0413-9>
- IAEA/WMO. (2016). Global Network of Isotopes in Precipitation. The GNIP Database. Accessible at: <http://www.iaea.org/water>.
- Immerzeel, W. W., Beek, L. P. H. van, & Bierkens, M. F. P. (2010). Climate Change Will Affect the Asian Water Towers. *Science*, 328(5984), 1382–1385. <https://doi.org/10.1126/science.1183188>
- Instituto Geologico, Minero y Metalurgico (INGEMMET). (1999). National Geologic Map of Peru. Retrieved from <http://www.ingemmet.gob.pe/carta-geologica-nacional>
- Jamasmie, C. (2016, April 18). Community opposition forces Newmont to abandon Conga project in Peru. Retrieved March 29, 2017, from <http://www.mining.com/community-opposition-forces-newmont-abandon-conga-project-peru/>
- Jansson, P., Hock, R., & Schneider, T. (2003). The concept of glacier storage: a review. *Journal of Hydrology*, 282(1–4), 116–129. [https://doi.org/10.1016/S0022-1694\(03\)00258-0](https://doi.org/10.1016/S0022-1694(03)00258-0)
- Justice, C. O., Vermote, E., Townshend, J. R. G., Defries, R., Roy, D. P., Hall, D. K., ... Barnsley, M. J. (1998). The Moderate Resolution Imaging Spectroradiometer (MODIS): land remote sensing for global change research. *IEEE Transactions on Geoscience and Remote Sensing*, 36(4), 1228–1249. <https://doi.org/10.1109/36.701075>
- Kaser, G. (1999). A review of the modern fluctuations of tropical glaciers. *Global and Planetary Change*, 22(1–4), 93–103. [https://doi.org/10.1016/S0921-8181\(99\)00028-4](https://doi.org/10.1016/S0921-8181(99)00028-4)
- Kaser, G., & Osmaston, H. (2002). *Tropical Glaciers*. Cambridge University Press.
- King, J. (2012). Characterization of the shallow hydrogeology with estimates of recharge at a high-altitude mountainous site, Niwot Ridge, Front Range, Colorado. Master's thesis. University of Colorado.
- Knowles, J. F., Blanken, P. D., Williams, M. W., & Chowanski, K. M. (2012). Energy and surface moisture seasonally limit evaporation and sublimation from snow-free alpine tundra. *Agricultural and Forest Meteorology*, 157, 106–115. <https://doi.org/10.1016/j.agrformet.2012.01.017>
- Knowles, N., Dettinger, M. D., & Cayan, D. R. (2006). Trends in Snowfall versus Rainfall in the Western United States. *Journal of Climate*, 19(18), 4545–4559. <https://doi.org/10.1175/JCLI3850.1>
- Konrad, C. P., Warner, A., & Higgins, J. V. (2012). Evaluating Dam Re-Operation for Freshwater Conservation in the Sustainable Rivers Project. *River Research and Applications*, 28(6), 777–792. <https://doi.org/10.1002/rra.1524>

- Kundzewicz, Z. W., Nohara, D., Tong, J., Oki, T., Buda, S., & Takeuchi, K. (2009). Discharge of large Asian rivers – Observations and projections. *Quaternary International*, 208(1–2), 4–10. <https://doi.org/10.1016/j.quaint.2009.01.011>
- Lee, J. J. (2014). Where Does the Amazon River Begin? Retrieved December 28, 2016, from <http://news.nationalgeographic.com/news/2014/02/140213-amazon-river-length-source-maps-science/>
- Leopold, M., Dethier, D., Völkel, J., Raab, T., Rikert, T., & Caine, N. (2008). Using Geophysical Methods to Study the Shallow Subsurface of a Sensitive Alpine Environment, Niwot Ridge, Colorado Front Range, U. S. A. *Arctic, Antarctic, and Alpine Research*, 40(3), 519–530. [https://doi.org/10.1657/1523-0430\(06-124\)\[LEOPOLD\]2.0.CO;2](https://doi.org/10.1657/1523-0430(06-124)[LEOPOLD]2.0.CO;2)
- Liu, F., Parmenter, R., Brooks, P. D., Conklin, M. H., & Bales, R. C. (2008). Seasonal and interannual variation of streamflow pathways and biogeochemical implications in semi-arid, forested catchments in Valles Caldera, New Mexico. *Ecohydrology*, 1(3), 239–252. <https://doi.org/10.1002/eco.22>
- Liu, F., Williams, M. W., & Caine, N. (2004). Source waters and flow paths in an alpine catchment, Colorado Front Range, United States. *Water Resources Research*, 40(9). <https://doi.org/10.1029/2004WR003076>
- Liu, F., Conklin, M. H., & Shaw, G. D. (2017). Insights into hydrologic and hydrochemical processes based on concentration-discharge and end-member mixing analyses in the mid-Merced River Basin, Sierra Nevada, California. *Water Resources Research*, 53(1), 832–850. <https://doi.org/10.1002/2016WR019437>
- Lo Lau, J. (2016). El río que no se deja llevar por la corriente. *Mongabay*. Retrieved from [https://es.mongabay.com/2016/09/hidroelectricas-conflictos-amazonia-medio\\_ambiente-peru/](https://es.mongabay.com/2016/09/hidroelectricas-conflictos-amazonia-medio_ambiente-peru/)
- Mark, B. G., McKenzie, J. M., & Gómez, J. (2005). Hydrochemical evaluation of changing glacier meltwater contribution to stream discharge: Callejon de Huaylas, Peru / Evaluation hydrochimique de la contribution évolutive de la fonte glaciaire à l'écoulement fluvial: Callejon de Huaylas, Pérou. *Hydrological Sciences Journal*, 50(6), null-987. <https://doi.org/10.1623/hysj.2005.50.6.975>
- Mark, B. G., & Mckenzie, J. M. (2007). Tracing Increasing Tropical Andean Glacier Melt with Stable Isotopes in Water. *Environmental Science & Technology*, 41(20), 6955–6960. <https://doi.org/10.1021/es071099d>
- Mast, M. A., Drever, J. I., & Baron, J. (1990). Chemical weathering in the Loch Vale watershed, Rocky Mountain National Park, Colorado. *Water Resources Research*, 26(12), 2971–2978.

- Maule, C. P., Chanasyk, D. S., & Muehlenbachs, K. (1994). Isotopic determination of snow-water contribution to soil water and groundwater. *Journal of Hydrology*, 155(1–2), 73–91. [https://doi.org/10.1016/0022-1694\(94\)90159-7](https://doi.org/10.1016/0022-1694(94)90159-7)
- Moody, J. A. (1993). Evaluation of the Lagrangian scheme for sampling the Mississippi River during 1987-90 (USGS Numbered Series No. 93–4042). U.S. Geological Survey : Earth Science Information Center, Open-File Reports Section. Retrieved from <http://pubs.er.usgs.gov/publication/wri934042>
- Mote, P. W. (2003). Trends in snow water equivalent in the Pacific Northwest and their climatic causes. *Geophysical Research Letters*, 30(12), <https://doi.org/10.1029/2003GL017258>
- Mote, P. W., Hamlet, A. F., Clark, M. P., & Lettenmaier, D. P. (2005). Declining mountain snowpack in western North America. <https://doi.org/10.1175/BAMS-86-1-39>
- Musselman, K. N., Clark, M. P., Liu, C., Ikeda, K., & Rasmussen, R. (2017). Slower snowmelt in a warmer world. *Nature Climate Change*, 7(3), 214–219. <https://doi.org/10.1038/nclimate3225>
- Nolin, A. W., Dozier, J., & Mertes, L. A. (1993). Mapping alpine snow using a spectral mixture modeling technique. *Annals of Glaciology*, 17(1), 121–124.
- Ochoa-Tocachi, B. F., Buytaert, W., De Bièvre, B., Céleri, R., Crespo, P., Villacís, M., Arias, S. (2016). Impacts of land use on the hydrological response of tropical Andean catchments. *Hydrological Processes*, 30(22), 4074–4089. <https://doi.org/10.1002/hyp.10980>
- O’Driscoll, M. A., DeWalle, D. R., McGuire, K. J., & Gburek, W. J. (2005). Seasonal 18O variations and groundwater recharge for three landscape types in central Pennsylvania, USA. *Journal of Hydrology*, 303(1–4), 108–124. <https://doi.org/10.1016/j.jhydrol.2004.08.020>
- Oxtobee, J. P. A., & Novakowski, K. (2002). A field investigation of groundwater/surface water interaction in a fractured bedrock environment. *Journal of Hydrology*, 269(3–4), 169–193. [https://doi.org/10.1016/S0022-1694\(02\)00213-5](https://doi.org/10.1016/S0022-1694(02)00213-5)
- Painter, T. H., Rittger, K., McKenzie, C., Slaughter, P., Davis, R. E., & Dozier, J. (2009). Retrieval of subpixel snow covered area, grain size, and albedo from MODIS. *Remote Sensing of Environment*, 113(4), 868–879. <https://doi.org/10.1016/j.rse.2009.01.001>
- Pearson, R. C., & Johnson, G. (1980). Mineral resources of the Indian Peaks Study Area, Boulder and Grand counties, Colorado, with a section on interpretation of aeromagnetic data (USGS Numbered Series No. 1463). U.S. Govt. Print. Off., Retrieved from <http://pubs.er.usgs.gov/publication/b1463>

- Pfeffer, W. T., Arendt, A. A., Bliss, A., Bolch, T., Cogley, J. G., Gardner, A. S., ... Sharp, M. J. (2014). The Randolph Glacier Inventory: a globally complete inventory of glaciers. *Journal of Glaciology*, 60(221), 537–552. <https://doi.org/10.3189/2014JoG13J176>
- Piper, A. (1944). A graphic procedure in the geochemical interpretation of water-analysis. *American Geophysical Union Transactions*, 914–923.
- Poage, M. A., & Chamberlain, C. P. (2001). Empirical Relationships Between Elevation and the Stable Isotope Composition of Precipitation and Surface Waters: Considerations for Studies of Paleoelevation Change. *American Journal of Science*, 301(1), 1–15. <https://doi.org/10.2475/ajs.301.1.1>
- Polk, M. H. (2016). They Are Drying Out: Social-Ecological Consequences of Glacier Recession on Mountain Peatlands in Huascarán National Park, Peru. Dissertation submitted to University of Texas-Austin.
- Poulenard, J., Podwojewski, P., Janeau, J.-L., & Collinet, J. (2001). Runoff and soil erosion under rainfall simulation of Andisols from the Ecuadorian Páramo: effect of tillage and burning. *CATENA*, 45(3), 185–207. [https://doi.org/10.1016/S0341-8162\(01\)00148-5](https://doi.org/10.1016/S0341-8162(01)00148-5)
- Praamsma, T., Novakowski, K., Kyser, K., & Hall, K. (2009). Using stable isotopes and hydraulic head data to investigate groundwater recharge and discharge in a fractured rock aquifer. *Journal of Hydrology*, 366(1–4), 35–45. <https://doi.org/10.1016/j.jhydrol.2008.12.011>
- Racoviteanu, A. E., Arnaud, Y., Williams, M. W., & Ordoñez, J. (2008). Decadal changes in glacier parameters in the Cordillera Blanca, Peru, derived from remote sensing. *Journal of Glaciology*, 54(186), 499–510. <https://doi.org/10.3189/002214308785836922>
- Racoviteanu, A. E., Armstrong, R., & Williams, M. W. (2013). Evaluation of an ice ablation model to estimate the contribution of melting glacier ice to annual discharge in the Nepal Himalaya. *Water Resources Research*, 49(9), 5117–5133. <https://doi.org/10.1002/wrcr.20370>
- Racoviteanu, A. (submitter, analyst). (2007). GLIMS Glacier Database, Version 1. Analysis IDs 60827-61235. Accessed 1/17/2017, GLIMS, National Snow and Ice Data Center, Boulder, Colorado. <https://doi.org/http://dx.doi.org/10.7265/N5V98602>
- Raimondi, A. (1879). Resolución del problema: Cuál de los ríos que forman el Amazonas puede ser el río madre? (Vol. 3). Lima, Perú: Impreta del Estado, El Perú.
- Raup, B., Racoviteanu, A., Khalsa, S. J. S., Helm, C., Armstrong, R., & Arnaud, Y. (2007). The GLIMS geospatial glacier database: A new tool for studying glacier change. *Global and Planetary Change*, 56(1–2), 101–110. <https://doi.org/10.1016/j.gloplacha.2006.07.018>

- Regonda, S. K., Rajagopalan, B., Clark, M., & Pitlick, J. (2005). Seasonal Cycle Shifts in Hydroclimatology over the Western United States. *Journal of Climate*, *18*(2), 372–384. <https://doi.org/10.1175/JCLI-3272.1>
- Rittger, K., Painter, T. H., & Dozier, J. (2013). Assessment of methods for mapping snow cover from MODIS. *Advances in Water Resources*, *51*, 367–380. <https://doi.org/10.1016/j.advwatres.2012.03.002>
- Rosenthal, W., & Dozier, J. (1996). Automated Mapping of Montane Snow Cover at Subpixel Resolution from the Landsat Thematic Mapper. *Water Resources Research*, *32*(1), 115–130. <https://doi.org/10.1029/95WR02718>
- Sadler, B. (2000). World Commission on Dams report: Environmental and social assessment for large dams. Earthscan Publications Ltd. Retrieved from [http://www.unep.org/dams/WCD/report/WCD\\_DAMS%20report.pdf](http://www.unep.org/dams/WCD/report/WCD_DAMS%20report.pdf)
- Safeeq, M., Grant, G. E., Lewis, S. L., & Tague, C. L. (2013). Coupling snowpack and groundwater dynamics to interpret historical streamflow trends in the western United States. *Hydrological Processes*, *27*(5), 655–668. <https://doi.org/10.1002/hyp.9628>
- Salati, E., Dall'Olio, A., Matsui, E., & Gat, J. R. (1979). Recycling of water in the Amazon Basin: An isotopic study. *Water Resources Research*, *15*(5), 1250–1258. <https://doi.org/10.1029/WR015i005p01250>
- Schauwecker, S., Rohrer, M., Acuña, D., Cochachin, A., Dávila, L., Frey, H., ... Vuille, M. (2014). Climate trends and glacier retreat in the Cordillera Blanca, Peru, revisited. *Global and Planetary Change*, *119*, 85–97. <https://doi.org/10.1016/j.gloplacha.2014.05.005>
- Schmitt, R. J. P., Bizzi, S., & Castelletti, A. (2016). Tracking multiple sediment cascades at the river network scale identifies controls and emerging patterns of sediment connectivity. *Water Resources Research*, *52*(5), 3941–3965. <https://doi.org/10.1002/2015WR018097>
- Servicio Nacional de Meteorología e Hidrología del Perú (SENAMHI). (2015, July). Monitoreo Hidrológico Año 2014-2015.
- Stallard, R. F., & Edmond, J. M. (1983). Geochemistry of the Amazon: 2. The influence of geology and weathering environment on the dissolved load. *Journal of Geophysical Research: Oceans*, *88*(C14), 9671–9688. <https://doi.org/10.1029/JC088iC14p09671>
- Stichler, W., Schotterer, U., Frohlich, K., Ginot, P., Kull, C., Gaggeler, H., & Pouyaud, B. (2001). Influence of sublimation on stable isotope records recovered from high-altitude glaciers in the tropical Andes. *Journal of Geophysical Research-Atmospheres*, *106*.
- Tague, C., & Grant, G. E. (2009). Groundwater dynamics mediate low-flow response to global warming in snow-dominated alpine regions. *Water Resources Research*, *45*(7). <https://doi.org/10.1029/2008WR007179>

- Taylor, S., Feng, X., Kirchner, J. W., Osterhuber, R., Klaue, B., & Renshaw, C. E. (2001). Isotopic evolution of a seasonal snowpack and its melt. *Water Resources Research*, 37(3), 759–769.
- The Economist. (2013). Gold in the hills. *The Economist*. Retrieved from <http://www.economist.com/news/asia/21573615-attitudes-towards-foreign-investors-hold-troubled-country-back-gold-hills>
- The Economist. (2014). Mi CASA no es tu CASA. *The Economist*. Retrieved from <http://www.economist.com/news/asia/21608806-plan-export-electricity-looks-cursed-mi-casa-no-es-tu-casa>
- Toohey, R. C., Herman-Mercer, N. M., Schuster, P. F., Mutter, E. A., & Koch, J. C. (2016). Multidecadal increases in the Yukon River Basin of chemical fluxes as indicators of changing flowpaths, groundwater, and permafrost: YUKON RIVER BASIN CHEMICAL FLUXES. *Geophysical Research Letters*, 43(23), 12,120-12,130. <https://doi.org/10.1002/2016GL070817>
- Uhlenbrook, S., Frey, M., Leibundgut, C., & Maloszewski, P. (2002). Hydrograph separations in a mesoscale mountainous basin at event and seasonal timescales: HYDROGRAPH SEPARATIONS AT VARIOUS TIMESCALES. *Water Resources Research*, 38(6), 31-1-31–14. <https://doi.org/10.1029/2001WR000938>
- Vannote, R. L., Minshall, G. W., Cummins, K. W., Sedell, J. R., & Cushing, C. E. (1980). The River Continuum Concept. *Canadian Journal of Fisheries and Aquatic Sciences*, 37(1), 130–137. <https://doi.org/10.1139/f80-017>
- Viviroli, D., Weingartner, R., & Messerli, B. (2003). Assessing the Hydrological Significance of the World's Mountains. *Mountain Research and Development*, 23(1), 32–40. <https://doi.org/10.1659/0276-4741>
- Wagnon, P., Ribstein, P., Francou, B., & Pouyaud, B. (1999). Annual cycle of energy balance of Zongo Glacier, Cordillera Real, Bolivia. *Journal of Geophysical Research: Atmospheres*, 104(D4), 3907–3923. <https://doi.org/10.1029/1998JD200011>
- Williams, M., Hood, E., Ostberg, G., Francou, B., & Galarraga, R. (2001). Synoptic Survey of Surface Water Isotopes and Nutrient Concentrations, Paramo High-Elevation Region, Antisana Ecological Reserve, Ecuador. *Arctic, Antarctic, and Alpine Research*, 33(4), 397. <https://doi.org/10.2307/1552548>
- Williams, M. W., Cline, D., Hartman, M., & Bardsley, T. (1999). Data for snowmelt model development, calibration, and verification at an Alpine Site, Colorado Front Range. *Water Resources Research*, 35(10), 3205–3209. <https://doi.org/10.1029/1999WR900088>



- Williams, M. W., Knauf, M., Cory, R., Caine, N., & Liu, F. (2007). Nitrate content and potential microbial signature of rock glacier outflow, Colorado Front Range. *Earth Surface Processes and Landforms*, *32*(7), 1032–1047. <https://doi.org/10.1002/esp.1455>
- Williams, M. W., Bardsley, T., & Rikers, M. (1998). Overestimation of snow depth and inorganic nitrogen wetfall using NADP data, Niwot Ridge, Colorado. *Atmospheric Environment*, *32*(22), 3827–3833.
- Williams, M. W., Brooks, P., Mosier, A., & Tonnessen, K. (1996). Mineral nitrogen transformations in and under seasonal snow in a high-elevation catchment in the Rocky Mountains, United States. *Water Resources Research*, *32*(10), 3161–3171.
- Williams, M. W., Knauf, M., Caine, N., Liu, F., & Verplanck, P. L. (2006). Geochemistry and source waters of rock glacier outflow, Colorado Front Range. *Permafrost and Periglacial Processes*, *17*(1), 13–33. <https://doi.org/10.1002/ppp.535>
- Wilson, A., Williams, M. W., Kayastha, R. B., & Racoviteanu, A. (2016). Use of a hydrologic mixing model to examine the roles of meltwater, precipitation and groundwater in the Langtang River basin, Nepal. *Annals of Glaciology*. <https://doi.org/10.3189/2016AoG71A067>
- Wilson, A., Gladfelter, S., Williams, M. W., Shahi, S., Baral, P., Armstrong, R., & Racoviteanu, A. (2017). High Asia: The International Dynamics of Climate Change and Water Security. *Journal of Asian Studies*. <https://doi.org/10.1017/S0021911817000092>
- Windhorst, D., Waltz, T., Timbe, E., Frede, H.-G., & Breuer, L. (2013). Impact of elevation and weather patterns on the isotopic composition of precipitation in a tropical montane rainforest. *Hydrology and Earth System Sciences*, *17*(1), 409. <https://doi.org/http://dx.doi.org/10.5194/hess-17-409-2013>
- Winemiller, K. O., McIntyre, P. B., Castello, L., Fluet-Chouinard, E., Giarrizzo, T., Nam, S., ... Sáenz, L. (2016). Balancing hydropower and biodiversity in the Amazon, Congo, and Mekong. *Science*, *351*(6269), 128–129. <https://doi.org/10.1126/science.aac7082>
- Working Group II. (2007). Impacts, Adaptation and Vulnerability, 10.6.2 The Himalayan glaciers. In *IPCC Fourth Assessment Report: Climate Change 2007*. Retrieved from [https://www.ipcc.ch/publications\\_and\\_data/ar4/wg2/en/ch10s10-6-2.html](https://www.ipcc.ch/publications_and_data/ar4/wg2/en/ch10s10-6-2.html)
- Young, K. R. (2015). Ecosystem change in high tropical mountains. In *The high-mountain cryosphere: Environmental changes and human risks* (pp. 227–46). Cambridge, U.K.: Cambridge University Press.
- Young, K. R., Ponette-González, A. G., Polk, M. H., & Lipton, J. K. (2017). Snowlines and Treelines in the Tropical Andes. *Annals of the American Association of Geographers*, *107*(2), 429–440. <https://doi.org/10.1080/24694452.2016.1235479>